ACTIVE AND PASSIVE SEISMIC INVESTIGATION OF STRUCTURE OF OROGENIC LITHOSPHERE IN ASIA AND SOUTH AMERICA

A Dissertation

Presented to the Faculty of the Graduate School

of Cornell University

In Partial Fulfillment of the Requirements for the Degree of

Doctor of Philosophy

by

Chen Chen

January 2015

ACTIVE AND PASSIVE SEISMIC INVESTIGATION OF STRUCTURE OF OROGENIC LITHOSPHERE IN ASIA AND SOUTH AMERICA

Chen Chen, Ph. D.

Cornell University 2015

Asia and South America possess the two iconic orogenic belts – Himalayas and Andes and two largest and highest plateaus – Tibetan Plateau and Puna Plateau on the earth. Their lithospheres were formed under continental-continental collision and ocean-continent subduction regimes respectively. Seismic images of their current lithospheric structure provide key insights into the current stage in their evolutionary process. Lithospheric structure beneath the Tibetan Plateau has been studied using deep seismic reflection profiling since the beginning of the INDEPTH project in 1992. This international effort led by consortium of Chinese and western academic institutions, continued over 25 years in four different phases. Key features spanned by this megatransect include the Main Himalaya Thrust (MHT) at the southern margin of the plateau, crustal seismic bright spots in the south and central part of the plateau, Moho topography across the plateau and especially an abrupt step in the Moho beneath the northeastern margin of the Plateau beneath the Qaidam Basin. A recent reflection profile by the SINOPROBE Project across the Sichuan Basin located at the southeast edge of the Tibetan Plateau, reveals sub-crustal dipping reflectors which are very likely to result from Neo-Proterozoic subduction beneath the Sichuan Basin. The preservation of these features supports the interpretation that the Sichuan Basin represents at buttress against eastward deformation and crustal thickening of the Tibetan Plateau. Lithospheric structure beneath the Andean orogenic belt is here

studied with a novel seismic reflection technique, one which uses earthquakes below 100 km depth as sources to illuminate the overlying lithospheric structure. The application of this technique is based upon exploitation of USArray, a large scale, high density passive seismic array that has been moving across the continental US since 2003. Analysis of 124 earthquakes that occurred between 2003 to 2012 provides a) new estimates of crustal thickness in areas previously imaged by conventional techniques; b) the first estimates of Moho depth in areas inaccessible to conventional geophysical surveys, c) mapped regions with nonreflective Mohos and d) identified prominent crustal seismic reflectors that may mark magma chambers, large scale decollements, or intracrustal phase changes in various parts of the Andean system. Each of these new observations constitute significant new constraints for geodynamic models of the Andean tectonics.

BIOGRAPHICAL SKETCH

Chen Chen was born on August 25th, 1985 in Beijing, China. Because he was born in the morning, his parents named him after "morning" in Chinese ("Chen") and since then he has the same first and last names in English. He attended Fuwaiyixiao Elementary School, No. 35 Middle School, No. 8 High School. He won the award given by the Beijing Municipal Education Commission for being an excellent student leader in his high school.

He considers himself fortunate to get into Peking University, one of the top universities in China. Because of his love for geography and physics in high school, he chose geophysics as his major at Peking University. He has never regretted making this first big decision in his life and is so glad that his parents respected his choice. He studied the fault rupture for a M=6.2 earthquake near Beijing using D-InSAR and Coulomb stress modeling methods for his Bachelor's thesis. He dreamed of going to the United States or Europe for further education in his early years of college because he really wished to go out of his homeland and see other parts of the world. Four years later, this dream came true.

He also considers himself fortunate to be accepted for graduate study at Cornell University. He came to beautiful Ithaca in August 2007, and studied seismology in the Department of Earth and Atmospheric Sciences with Professor Larry Brown. During his PhD studies, he did field work on the Tibetan Plateau, a Caribbean Island, the Puna Plateau and various parts of the United States. He enjoyed all this field work and attending scientific conferences. He served as the President and Vice President of the Cornell student chapter of the American Association of Petroleum Geologists (AAPG), from 2008 to 2010. He received the Meyer Bender Memorial Scholarship for 2010-2011. This dissertation represents the results of the

research conducted during Chen Chen's six years as a graduate student.

After his PhD defense, Chen Chen moved to Houston, TX and where he has been working for Shell Oil Company ever since.

Chen Chen got married to Yuan during his PhD studies. While working on his PhD, they led a happy life in Ithaca as a family. Chen has been playing basketball since middle school and he had broken his arm, elbow, ankle and knee for his favorite sport. However many times he had to say "goodbye" to the hoops, he still came back to the court and had fun with his friends. Chen had a really bad fever for over a month due to Mono (Infectious mononucleosis) in 2012 but thanks to the great care from his wife he recovered. Through all of these, he kept smiling and appreciated his life more than ever. He felt he had been so lucky in many ways and has enjoyed whatever life brought him. On January 22nd, 2014, daughter Stefanie was born and Chen's life has totally been changed.

For Yuan and Stefanie.

ACKNOWLEDGMENTS

Xiaomin Zhou and Baohui Chen: his mother and father, for everything - for bringing him to the world and enjoying his life, for always being there.

Yuan: his wife, for loving me and supporting me so unconditionally, for considering, for taking care of him no matter what happened to him. He loves you.

Professor Larry Brown: for everything during his graduate study and life since then, for all help, all concerns, all supports - both financially and in spirit. All your projects were so fun to participate. You have always been considerate, patient and supportive during difficult times: absence of four months due to knee injury in Beijing, absence of two months due to MONO in Ithaca; when he doubted himself. The trust, confidence and optimism you extended to him meant a whole lot and has influenced his life ever since. The rigorousness you taught him about doing research also will benefit him for a life time. The art of interacting with people is engraved his mind.

Professor Muawia Barazangi: for your 100% dark chocolate love, even though it tastes bitter, it is also sweet, for all the snacks you fed him.

Professor Suzanne Kay: for supporting him, for your patience to guide him, for passing him key knowledge about geoscience.

Professor Matthew Pritchard and Professor David Hysell: for being his committee members, for helping him in classes, for making him view science from different perspectives.

Steve Gallow: Without you, his work would never be finished because of all the computer/software issues.

Professor Terry Jordan, Professor Rick Allmendinger, Professor Bob Kay, Professor Bryan Isacks, Professor Rowena Lohman, Professor Larry Cathles, Professor Warren Allmon, Professor Susan Riha, Professor Chris Andronicos, George Hade, Alexandra Moore, Mainak Mookherjee, Frank Horowitz, Mike Willis, Julie Elliott, Professor Jason Phipps-Morgan: for all your help and feedbacks to his research.

Amy Colvin, Savannah Sawyer, Judy Starr, Carol Armstrong, Linda Hall, Carolyn Spohn: for all your assistance for him to live in Ithaca so easily.

All his fellow graduate students, for making him live so joyfully in Ithaca and US:

Jennifer Jay: for your help with his research and his life.

Diego Quiros: for all the field work you and he have done together, for all the time you and he shared in the lab.

Andrew Melkonian: for all your aid on computer programming.

Scott Henderson: for all the joy during basketball, meals and parties.

Ji Cheng: for always being his best friend in Ithaca.

Chao Shi: for being like his big brother.

Chao An: for inspiring him in research and in life.

Bill Barnhart, Anastasija Cabolova, Veronica Prush, Felipe Aron, Chuanquan Yu, Tiffany Tchakirides, Peter Nester, Katie Tamulonis, Katrina Byerly, Danielle Wolf, Stephanie Devlin, Phil Nee, Tianqi Liu, Joseph Kato, Sander Hunter, Naomi Kirk-Lawlor, Han Yue, Hao Zhang

Thanks to all his collaborators and colleagues: **Professor Simon Klemperer, Marianne Karplus, Professor Rainer Kind, Professor Xiaohui Yuan, Professor Jim Mechie, Professor Rui Gao, Zhanwu Lu, Professor Wenjin Zhao, Professor Zhenhan Wu, Professor Shuwen Dong, Professor Patricia Alvarado, Professor Peter Molnar, Professor James Ni.**

Special thanks to his previous advisors and mentors at Peking University. Because of them, he was able to come to Cornell for graduate study: **Professor John(Yongshun) Chen, Professor Qiming Zeng, Zhuqi Zhang**.

Thanks to all his supervisors and colleagues in industry: **Brian Ruskin, Chris Willacy, Greg Hester, Ken Matson; Jim Dodge, Betsy Torrez, Steve Levine, Eva Roberts, Bill Babcock, Paul Basinski, Richard Chuchla, Laurie Green**.

Special thanks to all his hobbies: Basketball, LEGO, Twilight Struggle (board game), many other board games; and his favorite foods: Chongqing spicy chicken, Gongpao chicken from most of all Chinese restaurants, Kalbi box and California sunrise from "Plum Tree".

Special thanks to the NSF for funding to support his research, INDEPTH 4: EAS-0410155; Southern Puna Seismic Experiment: EAR-0538112; and pP precursor study using USArray: EAR-0944236; and to the Chinese Academy of Geological Sciences (CAGS) for supporting his field trip during SINOPROBE seismic acquisition on the Tibetan Plateau.

TABLE OF CONTENTS

LIST OF FIGURES

INTRODUCTION

The concept of dividing the earth's upper portions into a mechanically strong layer overlying a weak layer dates as least as far back as Barrell (1914), who introduced the terminology of "lithosphere" and "asthenosphere" to describe these two mechanically distinct layers. However, it was plate tectonics theory (Condie, 1997) that brought this terminology to the forefront of modern geoscience. Lithospheric structure and the nature of the lithosphere-asthenosphere boundary (LAB) remain very hot research topics to this day (Fischer et al., 2010). Many of the most powerful methods to study lithospheric structure derive from seismology. There are now a range of seismic methodologies in use to probe the lithosphere, with foci that reach from the base of the lithosphere to the very near surface. So-called "passive" techniques take advantage of natural energy sources such as earthquakes or ambient noise, while "active" techniques rely upon artificial or controlled sources such as explosives or vibratory equipment (e.g. vibroseis). All these seismic techniques represent elastic wave spotlights that illuminate the earth at depth. Seismic waves from these various sources serve to interrogate rock properties while they are travelling through the earth media at depth, then carry this critical information back to recording systems (seismometers) at the surface for processing, analysis and interpretation.

Perhaps the most ubiquitous feature within the lithosphere is the Moho, named after Andruja Mohorovicic who first proposed this prominent discontinuity from seismic refraction measurements in 1909 (Mohorovičić, 1909). The Moho is now universally interpreted as the boundary between the crust and upper mantle within the lithosphere. However, the Moho is also now recognized (e.g. (Oliver, 1988) to be

much more complicated than a simple first-order (zero-thickness) boundary and has been documented to vary significantly in different locations (Jarchow and Thompson, 1989).

We now understand that the Moho is just one of many seismically mappable features within the lithosphere (Prodehl and Mooney, 2012) whose nature continue to challenge the observers and interpreters alike. The work contained in this thesis represents several different approaches to the seismic detection, mapping and interpretation of lithospheric structure in two iconic regions of the earth, the Tibet-Himalayan zone of collision between two continental lithospheres and the Andes mountain range, the global archetype of orogeny by subduction of ocean lithosphere beneath continental lithosphere. This work exploits a range of seismic techniques, including the application of well-known multichannel, controlled-source seismic reflection methods to the study of the deep crust in Tibet to the development of a relatively novel method of using earthquakes to image the underside of lithospheric structure beneath the Andes with multichannel analysis techniques.

The Tibetan Plateau formed by collision between the Indian plate and the Eurasian plate and is regarded as the classic prototype of continental-continental collision in plate tectonic theory (Condie, 1997). The mechanism responsible for the uplift of the adjacent Tibetan Plateau, the world's largest, remains a topic of scientific contention.

Chapter 1 integrates several key deep controlled seismic reflection profiles collected over the past 20 years within the Tibetan Plateau to produce the first complete seismic reflection cross-section to span the plateau. This transect, which

draws heavily from the INDEPTH and SINOPROBE initiatives, extends from the Himalaya in the south to Qaidam basin to the north. This seismic "mega" section is the most comprehensive and coherent representation of these results yet produced for the Tibetan lithosphere. It provides the context for more detailed analyses of the data from the central part and northeastern part of transect, which were first processed as part of this study. These images contain new constraints for modern tectonic models purported to explain the mechanisms of plateau formation and evolution.

In Chapter 2, the importance of regions adjacent to the Tibetan Plateau to its evolution is addressed by analysis of a deep seismic reflection profile in the Sichuan basin recently acquired by the SINOPROBE initiative. These data were migrated to reveal an important band of dipping subcrustal reflectors, which are proposed to be the remnants of Neo-Proterozoic subduction along the northwestern margin of the Yangtze block. Their preservation to the present is evidence for the role of the Sichuan lithosphere as a mechanical "bulwark" which constrained the lateral growth of the Tibetan Plateau.

In Chapter 3, the seismic methodology at the core of the previous chapters is turned upside down, with earthquakes now serving in lieu of explosives as the seismic imaging source. In a study that represents a novel marriage of the recording capabilities of the USArray seismic network, the power of multichannel processing techniques developed for conventional seismic reflection surveying, and the fortuitous geometry of deep earthquakes, new seismic images of the internal structure of the lithosphere have been produced for key areas within the Andes mountain belt. In particular, new measurements of crustal thickness are derived for various parts of the

Andes, including remote areas not yet probed by conventional surface geophysical measurements. Key crustal structures are also mapped, and methodologies developed to not only enhance weak reflections but to discriminate true reflections of geological significance from seismic energy travelling more complex paths that might easily be misinterpreted as lithospheric structure.

REFERENCES

Barrell, J., 1914. The strength of the Earth's crust. J. Geol. 655–683.

Condie, K.C., 1997. Plate Tectonics. Butterworth-Heinemann.

Fischer, K.M., Ford, H.A., Abt, D.L., Rychert, C.A., 2010. The lithosphere-asthenosphere boundary. Annu. Rev. Earth Planet. Sci. 38, 551–575.

Jarchow, C.M., Thompson, G.A., 1989. The nature of the Mohorovicic discontinuity. Annu. Rev. Earth Planet. Sci. 17, 475.

Mohorovičić, A., 1909. Das Beben vom 8. Oktober 1910. Jahrb Meteorol Obs. Zagreb Für.

Oliver, J., 1988. Moho. Geology 16, 291.

Prodehl, C., Mooney, W.D., 2012. Exploring the Earth's crust: history and results of controlled-source seismology. Geological Society of America.

CHAPTER 1

A DEEP SEISMIC REFLECTION PROFILE SPANNING THE TIBETAN PLATEAU: INDEPTH AND SINOPROBE

1.0 ABSTRACT

Beginning in 1992, Project INDEPTH was formed as an international collaboration led by the Chinese Academy of Geological Sciences and Cornell University with the ambitious goal of collecting a lithospheric scale, multichannel seismic reflection profile across the Himalayas and Tibet Plateau. During the course of its subsequent field programs in 1994, 1996 and 2007 the INDEPTH Consortium expanded to include a diverse array of geophysical and geological surveys to probe the nature and evolution of the Plateau. In 2009-2010 the SINOPROBE initiative, inspired in part by the success of INDEPTH, collected its own deep seismic reflection profiles within and along the boundaries of the Tibet Plateau. Here we present the results of integrating the INDEPTH seismic reflection profiling with complementary results from the SINOPROBE-2 survey in central Tibet, providing a comprehensive view of the Tibetan lithosphere as represented by high resolution reflection profiling. Interpretation of this new representation is guided by critical complementary observations from passive seismology, magnetotelluric surveys and geologic mapping along this trans-Tibetan corridor. Highlights of this new image include the "thin-skinned" nature of crustal overthrusting in the Himalayas, the distribution of proposed partial melting zones in the Tibetan crust, the internal morphology of the Tibetan Moho, constraints on possible crustal flow within the Tibetan crust and a dramatic

Moho step at the northeastern edge of the plateau which contrasts radically with the geometry of collision along the Himalayan margin.

1.1 INTRODUCTION

Since the first seismic refraction survey was carried out on the Tibetan Plateau in 1958 by Chinese scientists in the Qaidam basin (Zeng and Gan, 1961), there have been many controlled source, refraction-style seismic experiments in various parts of the Tibetan plateau (Gao et al., 2005; Mechie et al., 2011; Mechie and Kind, 2013).

Project INDEPTH (INternational DEep Profiling of Tibet and the Himalaya) was the first initiative to apply the multichannel near-vertical reflection technique to probe the deep structure of the Himalayan collision zone (Figure 1-1). Due to the success of INDEPTH I in the Himalayas in 1992 (Zhao et al., 1993), three subsequent INDEPTH field studies probed crustal structure from the High Himalaya in the south to the Qaidam Basin in the north using both controlled and natural sources (Nelson et al., 1996; Alsdorf et al., 1998a; Zhao et al., 2001; Tilmann et al., 2003; Karplus et al., 2011). However, due in part to funding limitations, multichannel reflection profiling was not a significant component of INDEPTH III in the central portion of the plateau, although a short test survey indicated that it could be effective in probing the thickened crust there (Ross et al., 2004).

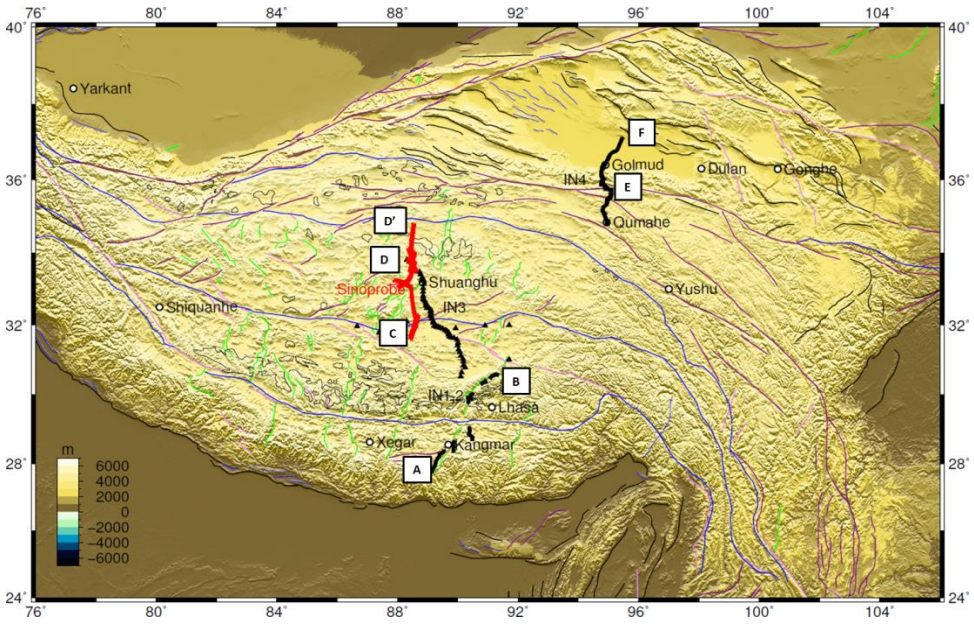

Figure 1-1 Regional topography map with active structures from Taylor and Yin (Taylor and Yin, 2009). Blue lines: sutures. Purple lines: left lateral strike-slip faults. Pink lines: right lateral strike-slip faults. Green lines: normal faults. Thin black lines: thrust faults. Thin blue lines: folds. Thinner black lines: distribution of Tibetan Cenozoic volcanism. Thick black lines: CMP locations of INDEPTH (IN) 1, 2 and 4 controlled source experiments. Black triangles: INDEPTH (IN) 3 broad band and short period seismic stations. Red line: CMP locations of SINOPROBE Qiangtang controlled source profile.

In 2008 Chinese scientists launched a national earth science project called SINOPROBE with the ambitious goal of probing the composition, structure and evolution of the continental lithosphere beneath all of China in an effort to better understand tectonic processes related to earthquakes and natural resources. A major component of SINOPROBE was the collection of deep seismic reflection and refraction data, a component designated SINOPROBE-2. In 2009 and 2010 SINOPROBE-2 collected a 350-km-long seismic reflection profile in the Tibetan Plateau across the boundary between the Lhasa block and the adjacent Qiangtang terrane. This deep reflection profile covers much of the same terrane as INDEPTH III, thus filling the gap in deep reflection coverage between INDEPTH I & II and INDEPTH IV. Here we merge the seismic reflection results from INDEPTH and

SINOPROBE to present the first complete seismic reflection image of the Tibetan Plateau, extending from the Himalayan megathrust in the south to the dramatic offset in the Moho that marks the edge of the Tibetan Plateau in the northeast.

1.2 DATA ACQUISTION

1.2.1 INDEPTH I and II (phase 1 and 2)

INDEPTH I, consisting of lines Tib1 and Tib2, was conducted in 1992, and was followed by INDEPTH II in 1994, during which seismic lines Tib3 through Tib11 were recorded (Figure 1-2). All of these profiles basically followed the Yadong-Gulu rift, which is one of the largest of the north-south trending extensional systems crossing the Himalaya and southern Tibetan plateau. This rift valley provided the only logistically feasible route for geophysical work at that time. Geologically, these profiles started in High Himalaya to the south, crossed the Tethyan Himalaya, Yarlung Zangbo Suture, Gandese Batholith and Linzizong Volcanics and ended in the southern Lhasa Terrane. Explosive sources of 50/200 kg sizes were spaced at 200 and 3000 m respectively. CMP spacing was 25 m for Tib1 and Tib2, and 12.5 m for Tib3-Tib11. All profiles had a nominal fold of 15. Data were recorded to 50s two way travel time using a 120 channel recording system in INDEPTH I and a 240 channel system during INDEPTH II(Alsdorf et al., 1998c).

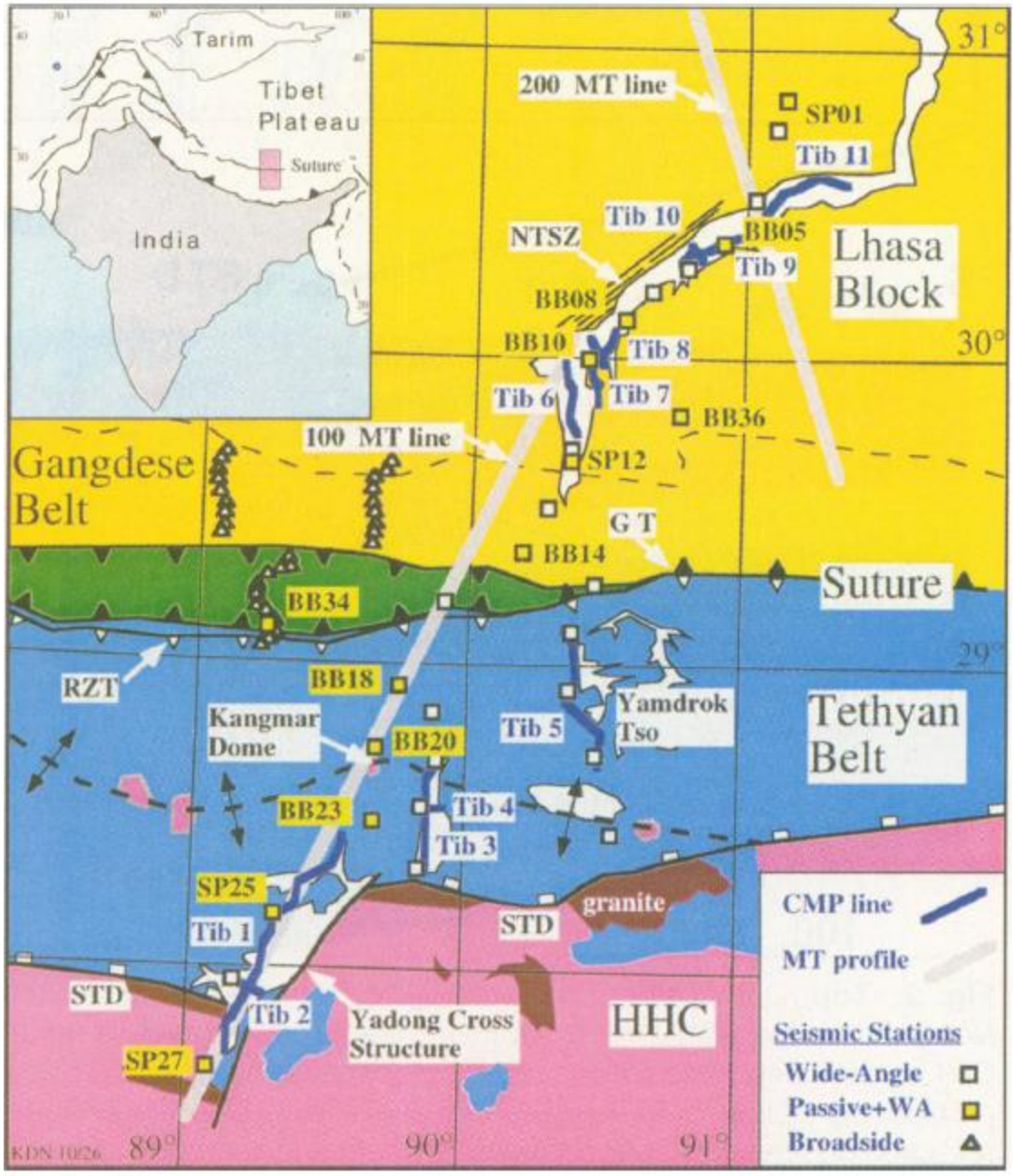

Figure 1-2 Figure 1 from (1996) INDEPTH I (Tib1, Tib2) and INDEPTH II (Tib3-Tib11) near-vertical seismic reflection profiles are shown.

1.2.2 SINOPROBE-2: Qiangtang

From October 2009 to May 2010, the SINOPROBE-2 Qiangtang deep seismic reflection profile was collected (Figure 1-3). It ran from west of Nam Co in

the northern Lhasa Block, crossed the Bangong-Nujiang Suture west of the Lumpola Basin, and extended to within 50 km of the Jinshang Suture within the Qiangtang Block.

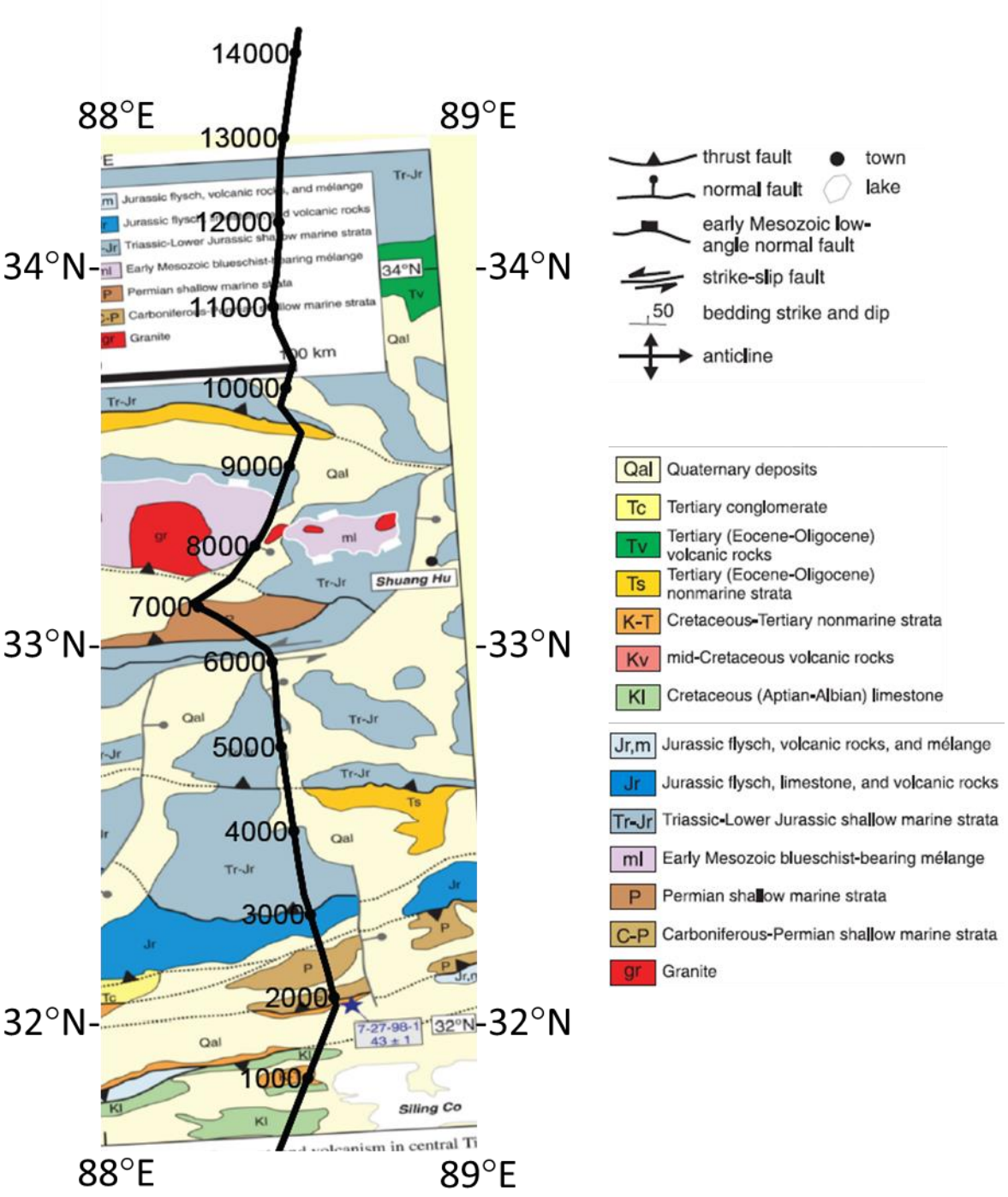

Figure 1-3 SINOPROBE CMP locations on geological map from figure 2 of Kapp et al. (2005)

The southern end of this profile lies on Cretaceous limestone and Cretaceous-Tertiary nonmarine strata. North of the Bangong-Nujiang Suture, it

crosses the Southern Qiangtang Block, which is mainly covered by Mesozoic strata. The central part of the profile traverses the central Qiangtang metamorphic belt, which consists mainly of early Mesozoic blueschist-bearing melange. The profile reaches well into the northern Qiangtang Block, which is covered by similar Mesozoic strata as Southern Qiangtang Block. The profile ends just south of the Jinsha Suture within Tertiary (Eocene-Oligocene) volcanic rocks (Figure 1-3).

The total length of the SINOPROBE profile was about 350 km. Explosive sources of various sizes were used: 1000 kg (50 km spacing), 200 kg (500 m spacing for northern part and 1 km for southern part) and 50 kg (250 m spacing for southern part). Vertical component geophones were used to record at a station spacing of 50 m, so the CMP spacing was 25 m. Data were recorded for 60s for big shots (1000 kg) and 30s for middle shots and small shots (200, 50 kg). A 720 channel recording system was used.

1.2.3 INDEPTH IV (phase 4):

In the summer of 2007, INDEPTH collected new data across the northeastern margin of the Tibetan Plateau (Figure 1-1). This seismic expedition included a controlled-source profile component (INDEPTH IV) and a passive source part, eventually designated as ASCENT (Array Seismology Collaborative Experiments in Northeastern Tibet), which continued recording until 2009. The N-S seismic reflection profile extends from the central Qaidam Basin in the north, passing the key city of Golmud, then crosses the Kunlun strike-slip fault onto the

Songpan-Ganzi terrane of the Tibetan plateau in the south (Zhao et al., 2008; Karplus et al., 2011).

The controlled-source component utilized 5 big shots (KS1 to KS5), consisting of 1000 to 2000 kg explosive charges roughly equally spaced along this 270 km crooked profile. There were also 100 small shots of 80 kg size within the central part of the profile between KS2 to KS4 at a nominal 1 km spacing (Figure 1-4).

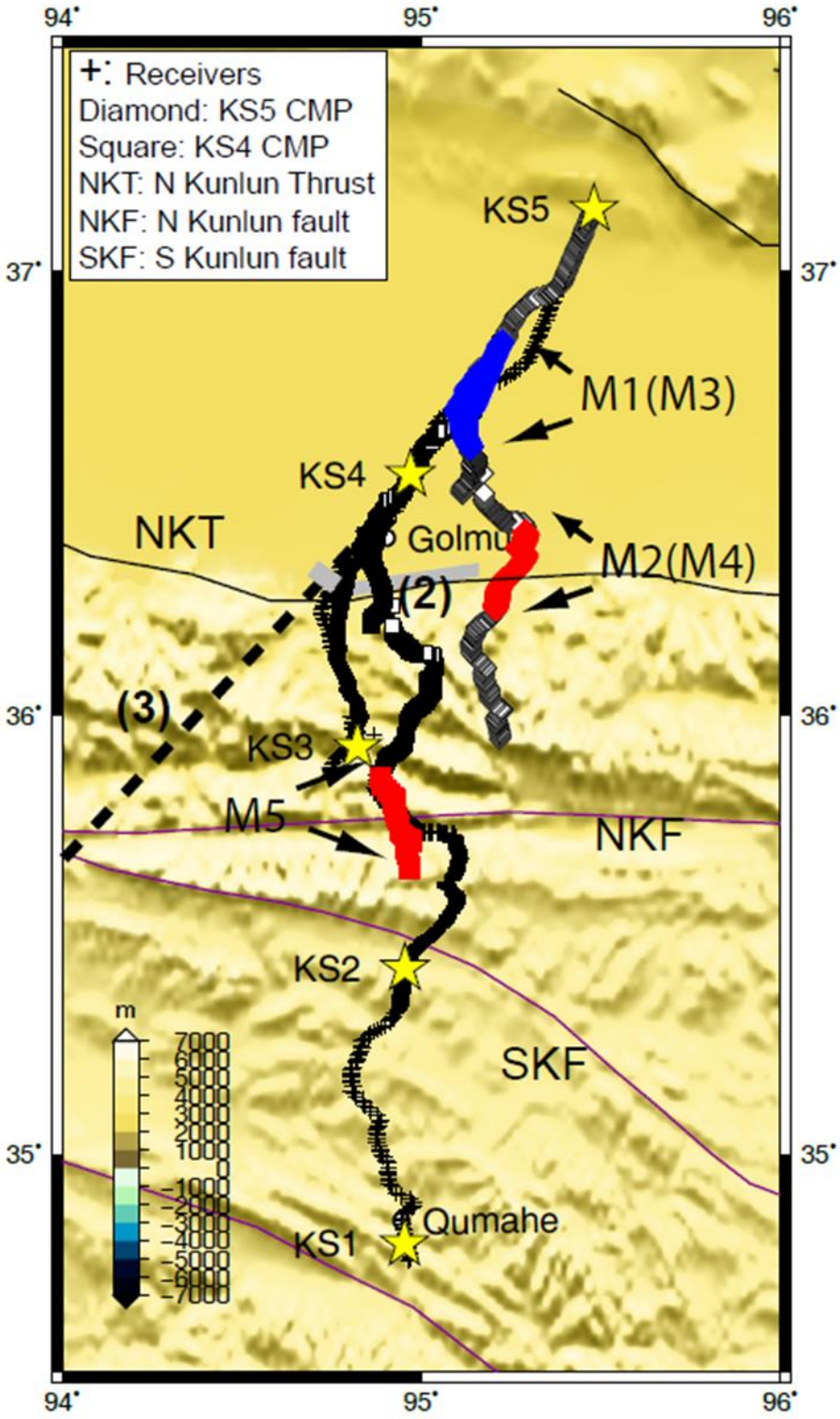
94°
95°
96°
37°
36°
35°
+: Receivers
Diamond: KS5 CMP
Square: KS4 CMP
NKT: N Kunlun Thrust
NKF: N Kunlun fault
SKF: S Kunlun fault
KS5
M1(M3)
KS4
NKT
Golmu
M2(M4)
(2)
(3)
KS3
M5
NKF
KS2
SKF
m
7000
6000
5000
4000
3000
2000
1000
0
−1000
−2000
−3000
−4000
−5000
−6000
−7000
Qumahe
KS1

Figure 1-4 INDEPTH IV profile. Red CMP: deep Moho beneath Tibetan Plateau, Blue CMP: shallow Moho beneath the Qaidam Basin. M1~M5: Moho reflection seen from shot gathers KS5 and KS4.

These shots were recorded by a multichannel reflection-style array consisting of a SERCEL 1000 channel cabled system, with 10 Hz geophones at 50 m spacing deployed between KS3 to KS4, and an complementary deployment of 950 Reftek RT125 ("Texan") recorders from the IRIS PASSCAL instrument pool. 655 Texans were deployed at 100 m spacing between KS2 to south of KS3, and another 295 were spaced about 600 m to 1 km from KS1 to KS5. The CMP spacing is about 25 m and 50 m for the central dense part and 300m-500m for the sparse southern part (Figure 1-4).

1.3 DATA PROCESSING

1.3.1 INDEPTH I & II:

The details of the original proocessing of the southern INDEPTH surveys are summarized by Alsdorf et al. (1996) and Alsdorf (1997). In this study, we apply two additional processing steps to those results to facilitate their display here: First, we computed the amplitude envelope of each CMP stacked trace using Hilbert transforms (Yilmaz, 2001). Subsequently we computed and display the signed square of the amplitude envelope. Both of these modifications were invoked to enhance the visibility of the reflection patterns when displayed at small scales (Figure 1-5, Figure 1-6).

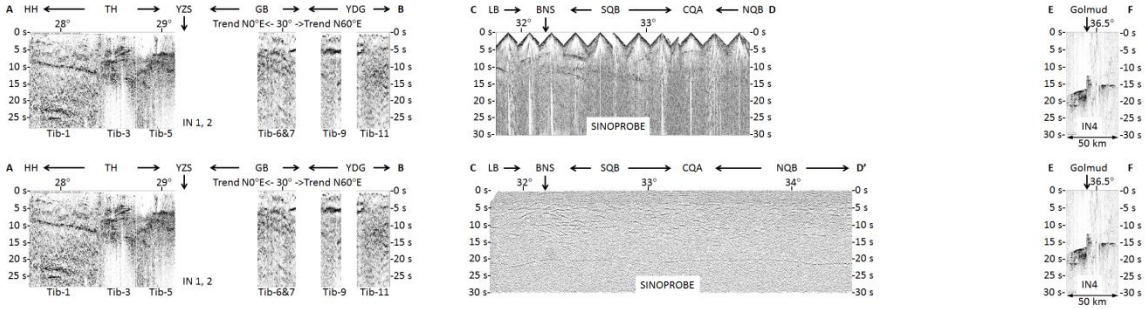

Figure 1-5 Multichannel CMP reflection profiles from INDEPTH I & II, SINOPROBE (upper: single fold, lower: multiple folds), INDEPTH IV (single fold). Data are plotted without vertical exaggeration (assuming Vp=6km/s) HH: High Himalaya. TH: Tethyan Himalaya. YZS: Yarlung Zangbo Suture. GB: Gandese Batholith. YDG: Yangbajain-Damxung Graben. LB: Lhasa Block. BNS: Bangong-Nujiang Suture. SQB: South Qiangtang Block. CQA: Central Qiangtang Anticlinorium. NQB: North Qiangtang Block.

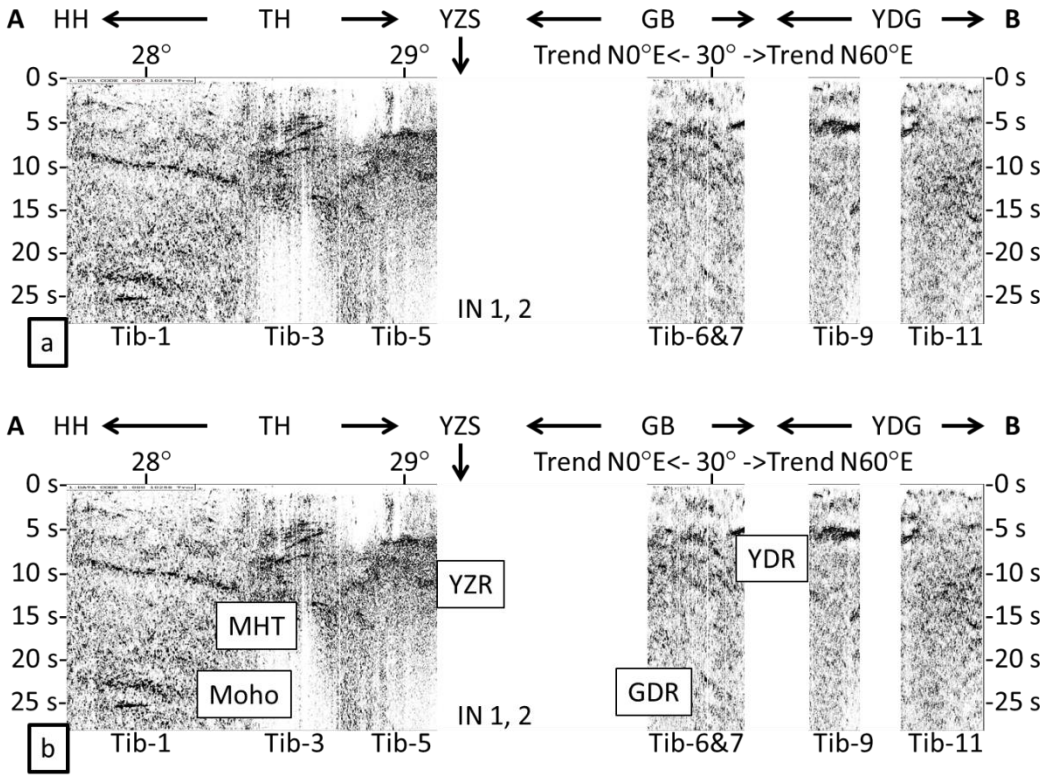

Figure 1-6 (a) Signal enhanced version of data corresponding to plate 1 of (Alsdorf et al., 1998b) with (b) interpretive identifications. Cross lines are not shown here. Tib1, Tib3, Tib5, Tib6, Tib7 are oriented ~N-S and were projected into an N-S direction. Tib9 and Tib11 trend N60°E and not projected. HH: High Himalaya. TH: Tethyan Himalaya. YZS: Yarlung Zangbo Suture. GB: Gandese Batholith. YDG: Yangbajain-Damxung Graben. MHT: Main Himalayan Thrust. GDR: Gangdese Deep Reflection. YDR: Yamdrok-Damxung Reflector. YZR: Yarlung-Zangbo Reflection.

1.3.2 SINOPROBE-2: Qiangtang

We here use two versions of the SINOPROBE Qiangtang reflection section. One is based on the fully processed, high fold section produced by the Beijing Petrosound company as discussed by Lu et al. (2013). The other is a single fold version of the data processed at Cornell. The Beijing version better images the weaker reflections along the profile, while the Cornell version better represents key amplitude variations within the profile (Figure 1-7).

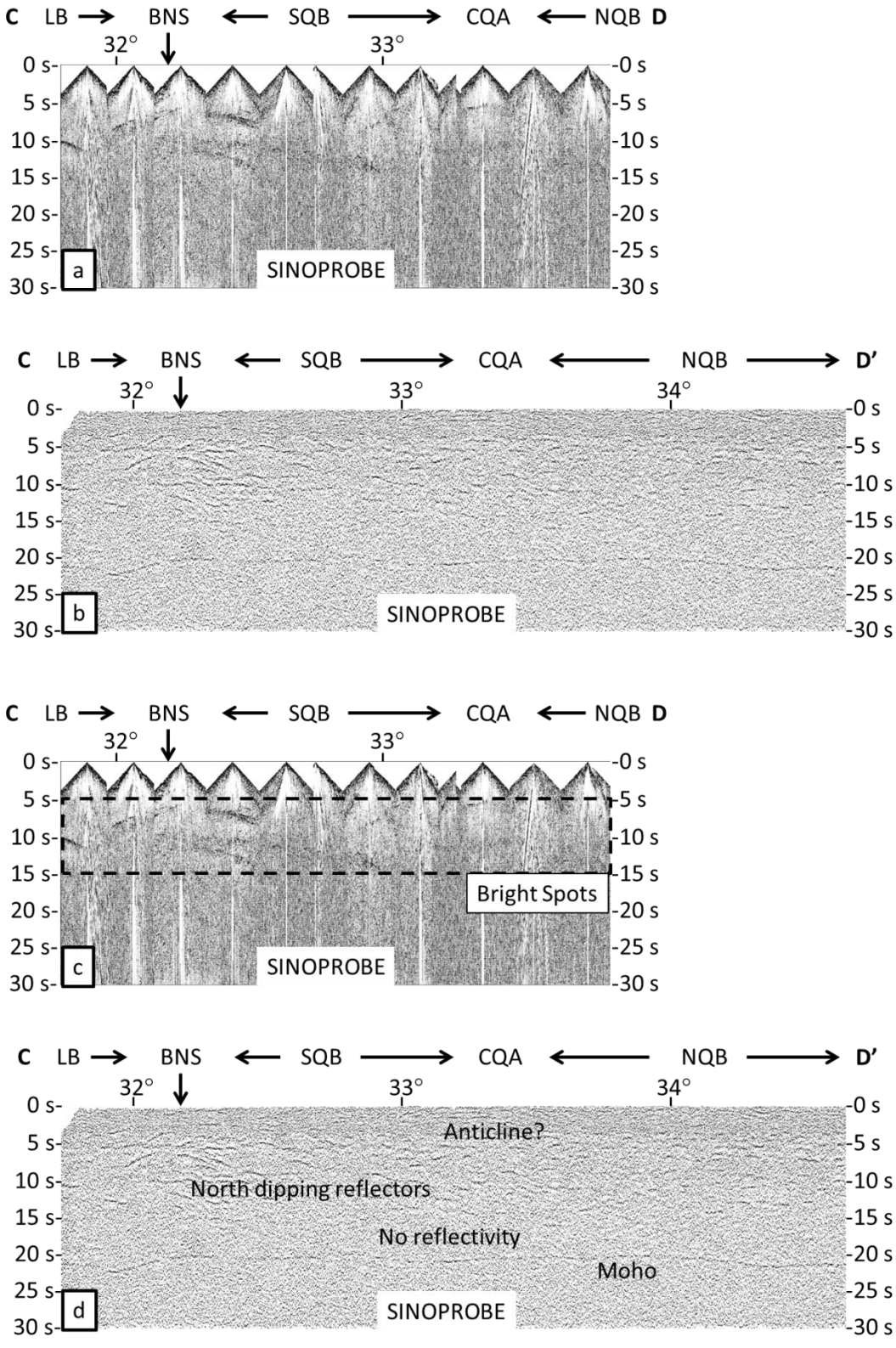
C
LB
BNS
SQB
CQA
NQB
D
32°
33°
34°
0 s
5 s
10 s
15 s
20 s
25 s
30 s
-0 s
-5 s
-10 s
-15 s
-20 s
-25 s
-30 s
a
SINOPROBE
D'
b
c
Bright Spots
d
Anticline?
North dipping reflectors
No reflectivity
Moho

Figure 1-7 SINOPROBE CMP section: (a) single fold, relative amplitudes preserved; (b) coherency enhanced stacked profile after migration, fold=72. Key events labeled on (c) several bright spots are observed between 5s and 15s; Key features labeled in (d) include (1) a distinct Moho without obvious offset but with variation of its depth ~2s (6km); (2) north dipping reflectors beneath BNS; (3) non-reflective lower crust, unlikely caused by energy penetration because of successful imaging of Moho; (4) an anticlinal structure beneath the CQA. LB: Lhasa Block. BNS: Bangong-Nujiang Suture. SQB: South Qiangtang Block. CQA: Central Qiangtang Anticlinorium. NQB: North Qiangtang Block. QB: Qiangtang Block.

1.3.2.1 Multi-fold stacked seismic section

The core processing of the SINOPROBE profile was done by a contractor – the Beijing Petrosound Geoservices Ltd. (http://petrosound.com/) using Grisys and CGG seismic processing software. Extensive, but mostly conventional, CMP processing (Lu et al. 2013) is used to enhance the reflection signal (average stacking fold about 72) and the resulting stack was migrated (Figure 1-7). In addition, higher resolution oil exploration data is used to tie deeper structure to surficial outcrop in the Qiangtang region.

One of the most critical differences between these two images is the relatively continuous reflection at 20-25 sec two way travel time (TWTT) that is interpreted as the Moho (Gao et al., 2013). We attribute this dramatic image to a proprietary processing algorithm called RELNOI (REmoval of the Linear NOIse before stacking) in the Grisys software package used by the Beijing Processing Center. This software appears to have been particularly effective at enhancing the weaker reflections on this survey, including the Moho (Jin et al., 2008). Figure 1-8 illustrates the impact of this particular signal enhancement routine as applied to unstacked shot gathers. Subsequent processing at the Beijing center included pre-stack migration and CMP stacking.

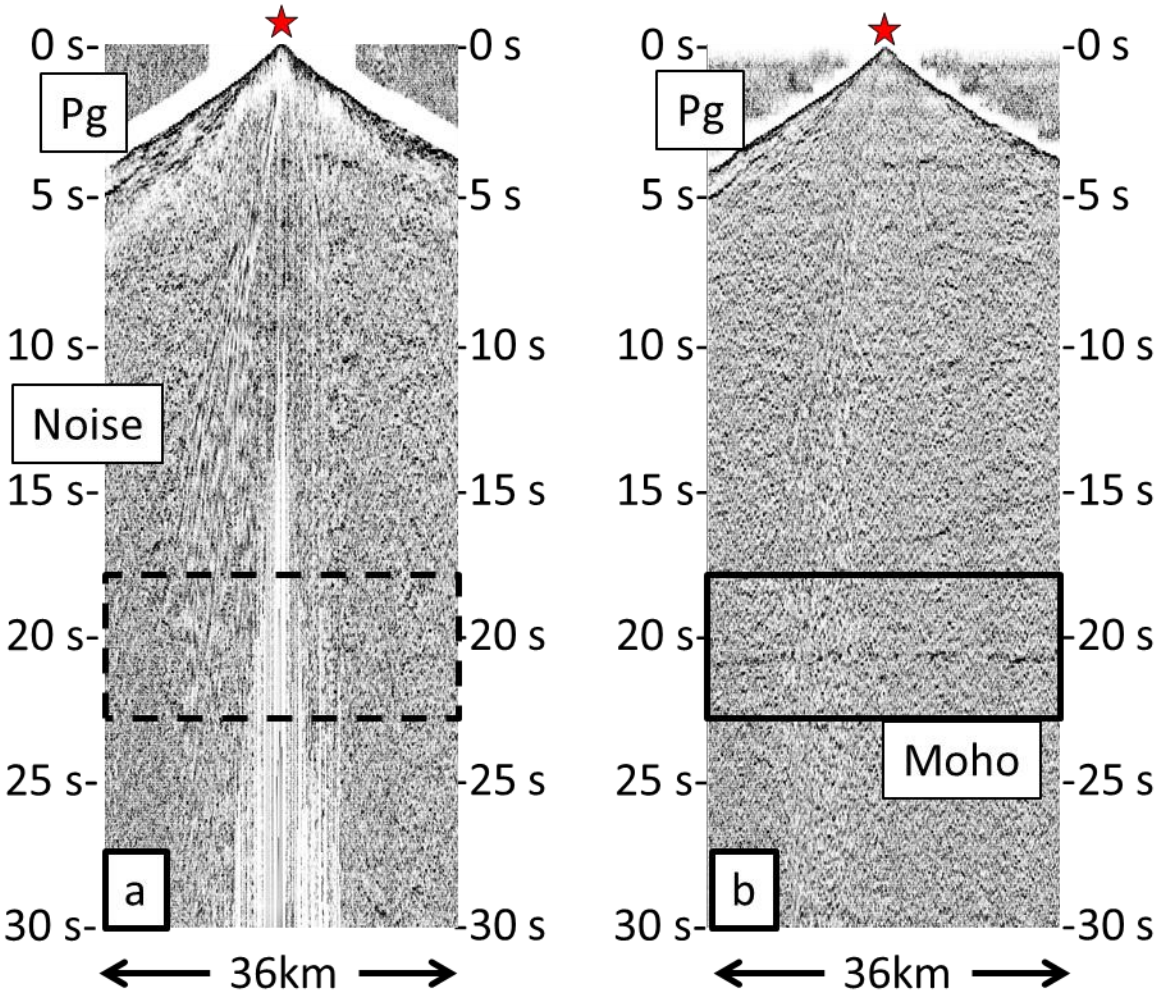

Figure 1-8 Shot gather from the southern part of the SINOPROBE profile (between CMP 1000 to 2000 on profile A). (a) Before processing. Notice the linear high amplitude noises (ground roll) which are steeper (lower velocity) than the direct P wave. No clear reflections are visible in the dashed box. (b) After processing with the RELNOI module. Notice that linear noise was largely removed and a Moho reflection is now visible at ca 21s.

The Beijing processed sections reveal a complex pattern of reflectivity in the upper crust and a remarkably continuous Moho reflection reflector. However, the coherency enhancement used to produce this section has muted some of the more dramatic amplitude variations that are apparent in the unprocessed recordings.

1.3.2.2 Single fold section

In particular, between CMP=1 (in the south) to CMP=9200 (in the north), several amplitude anomalies, i.e. bright spots, are evident on unprocessed shot gathers but are not prominent on the fully processed section because the amplitude balancing used in the latter (Figure 1-7). Therefore we produced a single fold version of the profile as a simple approach to retain the original amplitude relationships. 13 shots were selected to provide complete coverage from CMP 1 to CMP 9200, the section within which the bright spots are observed on the unstacked data. These CMP traces were NMO corrected using an average Vp=5.5 km/s, a value consistent with the velocities derived during the CMP processing.

1.3.3 INDEPTH IV (Phase 4):

Only direct P wave arrivals can be clearly seen from unprocessed recordings of the small shots collected as part of INDEPTH IV, and even this energy is poorly recorded by the entire receiver array for some shot locations. Few, if any, deep reflections are evident from any of the small shots. We suspect this due to the combination of poor source coupling, high attenuation and high noise levels from wind and nearby railway and highway.

Although deep near-vertical reflections are few, and largely uninterpretable on the conventional stacked sections, prominent reflection energy is present at depth on wide angle recordings of several of the large shots that were primarily intended for refraction analysis. These deep reflections, along with the direct P arrivals, form the basis of Karplus et al.'s (2011) velocity model across the Kunlun (Figure 1-9). Since a critical aspect of the refraction model is the nature of an apparently large offset of the

Moho at the boundary between the Tibetan Plateau and Qaidam Basin (Figure 1-9), we produced a reflection image using the wide angle recordings that mimics what would be expected from a near vertical profile.

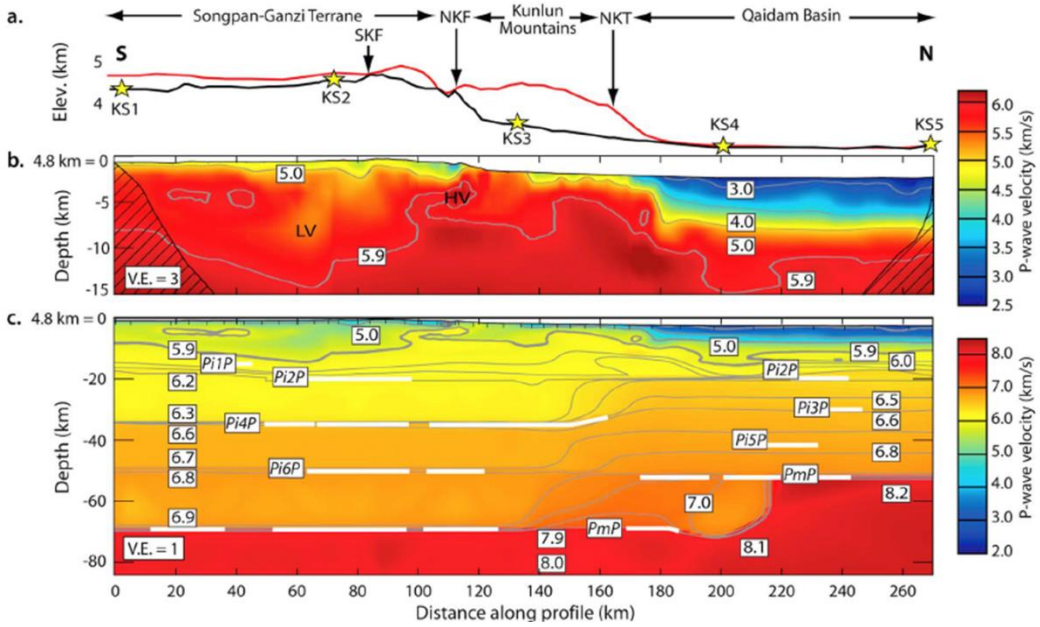

Figure 1-9 Figure 8 from Karplus et al. (2011). (a) Elevation along INDEPTH IV receivers (black curve) and elevation averaged over 2° between 94° to 96°E from TOPO1 (red). SKF, south Kunlun Fault; NKF, North Kunlun Fault; NKT, North Kunlun Thrust. (b) shallow velocity structure from first arrival tomography. Vertical exaggeration (V.E.) is 3. HV, high-velocity zone; LV, low-velocity zone. (c) composite shallow and deep crustal velocity model using ray tracing method. White lines: major reflectors. No vertical exaggeration.

The wide-angle reflection data were recorded by both the "SERCEL" and "Texan" arrays. We first resampled to 8 ms and applied DC bias removal to eliminate a prominent recording offset in the data. Obviously bad or extremely noisy traces, (fewer than 10 % of the total) were eliminated from the dataset. An Ormsby bandpass filter (0.5-1-4-8 Hz) was applied to improve the signal-to-noise ratio. This filter was selected based on empirical tests of various bandwidths, and on the observed spectra of the direct P arrival and reflected PmP arrivals.

A refraction static correction was applied to the shot gathers in the following manner: (1) direct P arrival times were picked manually for all traces (2) modeled direct P arrival times were derived from the Karplus et al. (2011) velocity model and shot and receiver locations; (3) traces were shifted according to the difference between (1) observed direct P time and (2) modeled direct P time with consideration of receiver and shot elevation (shot elevation was used as datum and Vp = 5km/s was assumed. By this means, variations in the direct P arrival time caused by receiver and source elevation changes were eliminated.

We then applied an unconventional version of the normal moveout (NMO) correction that only shifted the reflectors according to their offset (x), average velocity above (V) and intercepted time (t0) without stretching the waveform. This type of moveout is sometimes, referred to as a "block sum" normal moveout correction, BSNMO" (Rupert and Chun, 1975). V and t0 were calculated by the $x^2 - t^2$ method by manually picking our target reflector (Moho) times.

The formula is used to correct for the moveout is:

$$t_{correction} = \frac{\sqrt{x^2 + 4V{t_0}^2}}{V} - 2t_0$$

The advantage of using this simple one-time-shift calculation instead of the traditional shot gathers NMO correction is that it avoids a form of distortion known as NMO strectching, which is a stretching of the reflecton waveforms at wide angles by conventional NMO correction (Yilmaz, 2001). We subsequently applied bandpass filtering (0.5-1-4-8 Hz) to reduce noise and f-x deconvolution to enhance continuity. The recording from shot KS5 shot before and after our NMO correction is shown in

Figure 1-10 to Figure 1-13.

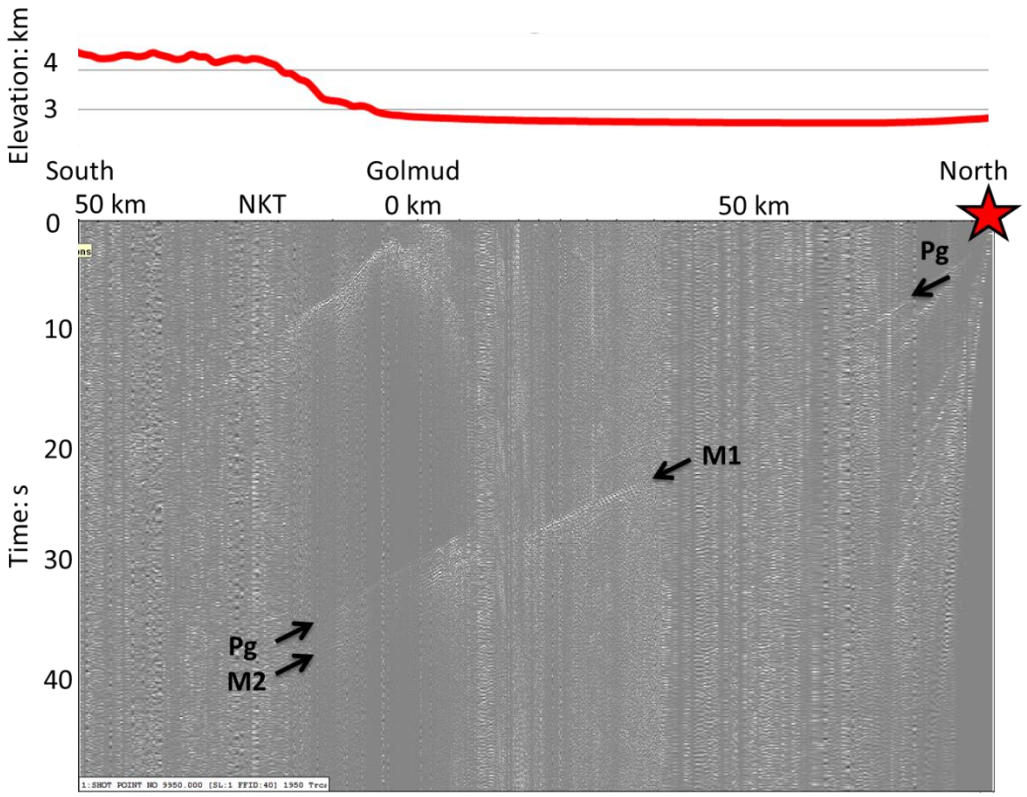

Figure 1-10 Shot gather for KS5 with Ormsby filter 0.5-1-4-8 Hz. Red star = shot. Red line = surface topography.

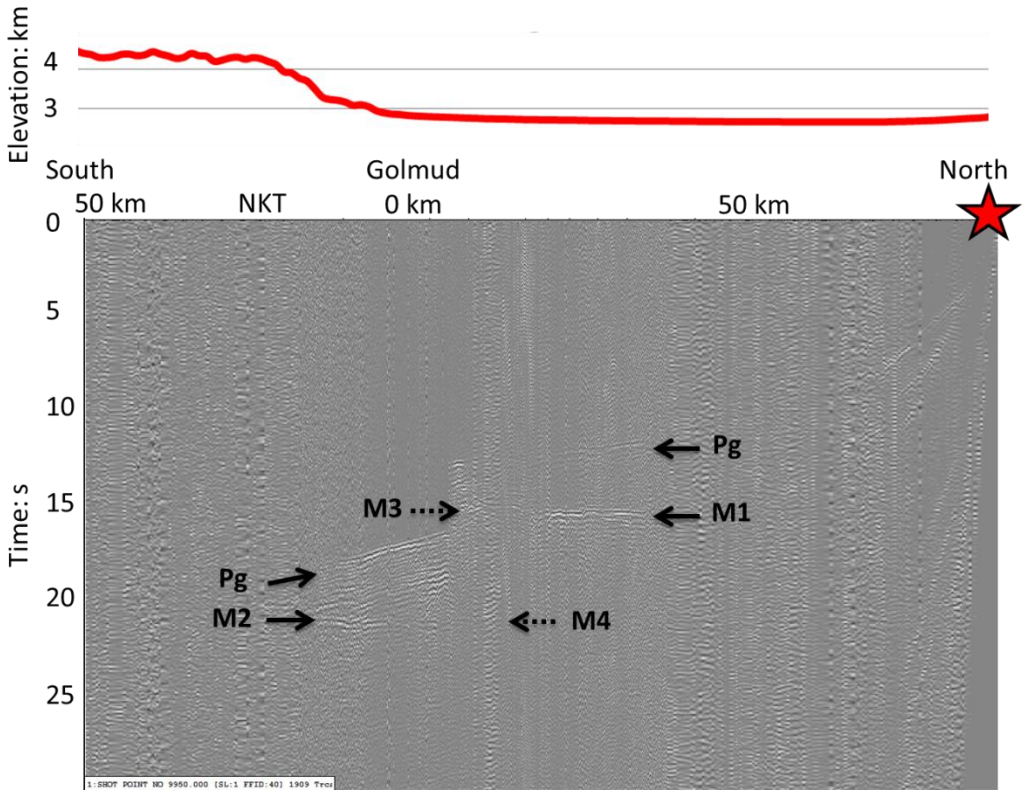

Figure 1-11 Figure 1-10 after BSNMO correction. Vertical exaggeration 1:1 for depth (assuming Vp= 6km/s) and horizontal distance.

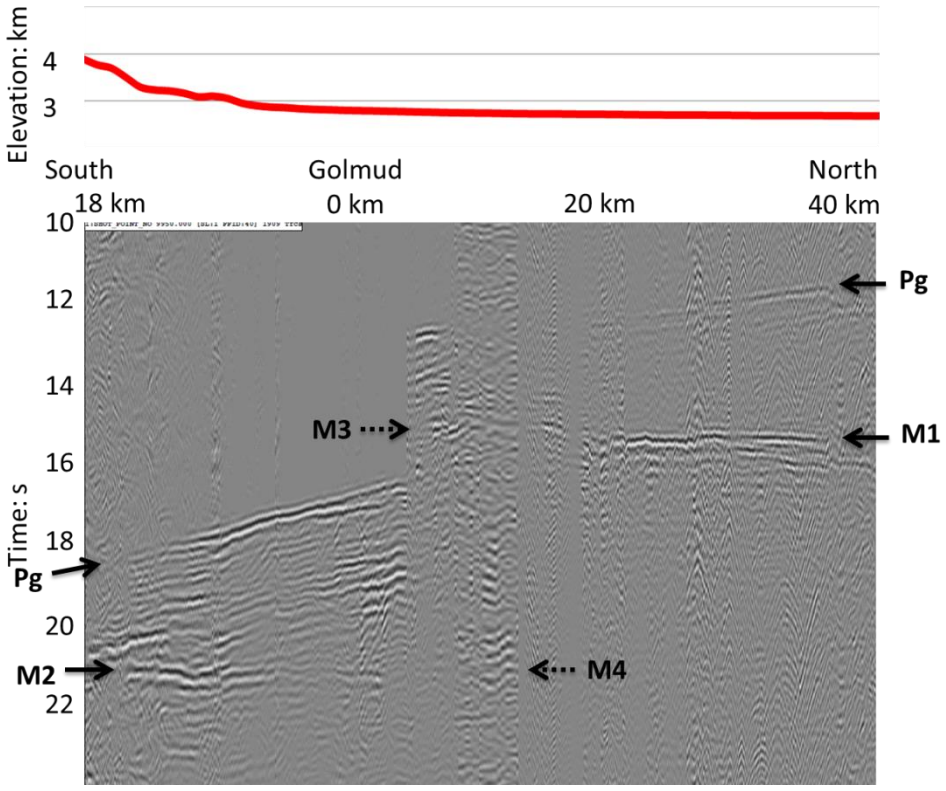

Figure 1-12 Shot gather for KS5 (blow up) after BSNMO correction and f-x deconvolution.

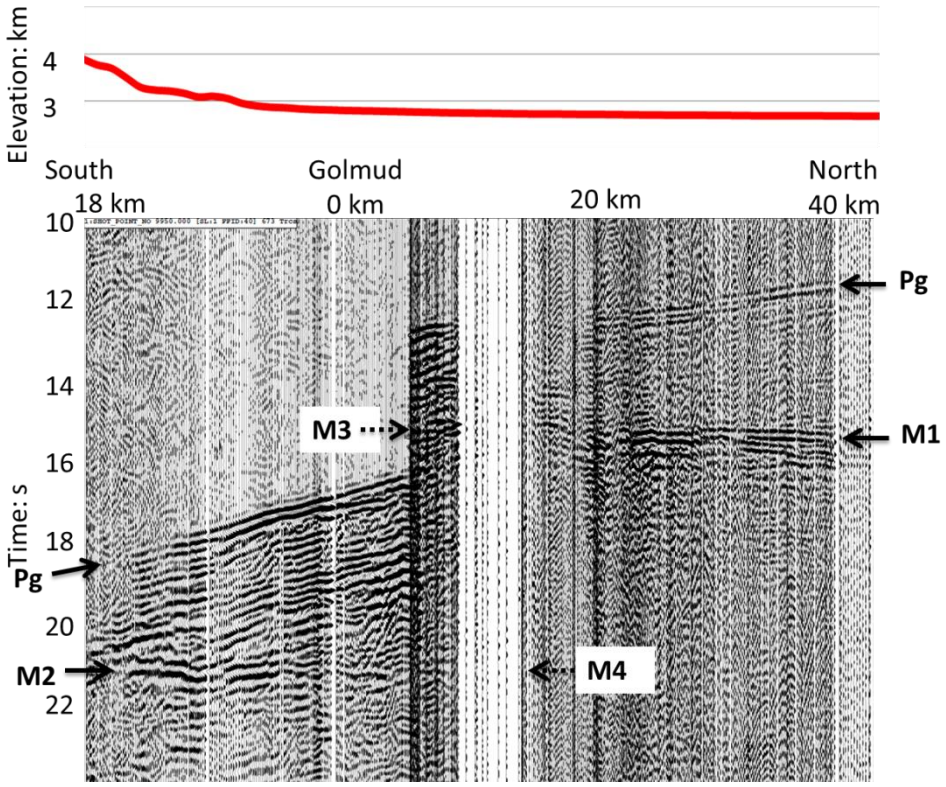

Figure 1-13 Wiggles trace display the data in Figure 1-12. For better rendering, we have here summed neighboring 2 (or 4) traces.

1.4 RESULTS AND DISCUSSION

Many of the most important lithospheric structures illuminated by INDEPTH and SINOPROBE are discussed in the papers reporting the original results. Here we briefly summary the key observations with a focus on those aspects for which this new comprehensive display provide fresh context.

1.4.1 Megathrusts:

1.4.1.1 MHT (Main Himalayan Thrust)

The most prominent result of INDEPTH I & II was its image of a mid-crustal north dipping reflector extending from around 8s (25km) to 14s (45km) beneath the TH (Tethyan Himalaya) (Figure 1-5, Figure 1-6). This reflector was named the MHT

(Main Himalayan Thrust) by Zhao et al. (1993). Subsequently it has also been observed on several natural source seismic surveys using receiver function techniques. Schulte-Pelkum et al. (2005) reported a decollement at 10- 20 km depth (the shallow segment of MHT) along a transect located a few hundred km to the west (86°E to 87°E) of INDEPTH I & II (88°E to 90°E). The HICLIMB profile reported by Nabelek et al. (2009) , located much further west (84°E to 85°E), also imaged the MHT. Strong anisotropy above the MHT (Schulte-Pelkum et al., 2005) and at the crust/mantle interface (Nábělek et al., 2009) was inferred from the receiver function transects. The one above the MHT was interpreted as a response to the shear stresses caused by slip from great earthquakes at shallower depths (Schulte-Pelkum et al., 2005). The one at the Indian Moho was attributed to the shearing process during its underthrusting (Nábělek et al., 2009).

The MHT marks the decollement beneath which Indian lithosphere underthrusts the Euroasian lithosphere. All of these results support, at least in part, the underthrusting model proposed by (Argand, 1924; Barazangi and Ni, 1982; Ni and Barazangi, 1984; Zhao and Morgan, 1987; Beghoul et al., 1993). However, the extent of understhrusting is still controversial. The Indian crust is interpreted to extend beneath the central Lhasa block at 31°N beneath the HICLIMB profile by (Nábělek et al., 2009). The extent of Indian lithospheric underthrusting appears to vary from west to east beneath Tibetan plateau according to both receiver function studies (Zhao et al., 2010, 2011) and tomography (Li et al., 2008). Most studies, including INDEPTH III (Tilmann et al., 2003) indicate that the Indian lithosphere extends to about the Bangong-Nujiang Suture at the longitude of the INDEPTH-SINOPROBE transect.

1.4.1.2 Crustal-scale thrusting at the Bangong Nujiang Suture

Kapp et al. (2003, 2005, 2007) proposed a subduction/underthrusting model in late Jurassic and early Cretaceous to explain the suturing of the Lhasa and Qiangtang terranes. As this model is analogous to the collision occuring today at the southern Tibetan Plateau, one might expect a major decollement or low angle thrust fault to mark underthrusting of the Lhasa terrane beneath the Qiangtang terrane. This older megathrust, if it exists, should exist beneath the BNS and extend to the north of it.

However, there is no clear, coherent reflector on the SINOPROBE profile comparable to the MHT (Figure 1-7). While it is possible that a Jurassic megathrust might have lost its reflectivity (e.g. post-collisional deformation, dewatering, metamorphism), or never juxtaposed sufficiently distinct materials to have even been reflective, it is also possible that this ancient collision evolved in a manner different from the modern Himalaya collision. This older collision may simply not have involved the degree of terrane overthrusting that is characteristic of the Himalayas, perhaps due to the different nature of the crustal blocks being sutured together.

1.4.1.3 Crustal scale thrusting beneath the Kunlun

A major north vergent thrust, the North Kunlun thrust (NKT) (Qaidam Border Fault in (Zhu and Helmberger, 1998) was first proposed by Burchfiel et al. (1989), even though there is no surface trace mapped because of quaternary fan deposits. It is located at the front of the Kunlun Mountain between the Qaidam Basin and the Tibetan Plateau. Some interpreters agree with the thrust mechanism of this fault but the direction and geometry of thrusting is controversial. Meyer et al. (1998) used fieldwork combined with SPOT image analysis to suggest as a north-directed, steeply

south-dipping fault, penetrating down to the upper mantle. Chen et al. (1999) inferred a intracrustal decollement dipping south beneath the Kunlun mountains from earthquake focal mechanisms, surface geology and shallow (~3s, <10km) seismic reflection data. A south dipping listric thrust at the Kunlun Qaidam Border was interpreted from seismic reflection data by Song and Wang (1993) and Bally et al. (1986).

In contrast, Yin et al. (2007, 2008) argued that the North Kunlun Thrust fault is a south-directed, north-dipping fault carrying the upper crust of the Qaidam basin over the high-elevation Eastern Kunlun Range by thrusting over a potential decollement in the middle crust level beneath the Kunlun Range and Qaidam Basin. However, the Yin et al. (2007, 2008) model is based primarily on the seismic reflection data between Qimen Tagh Mountains and Qaidam basin, which is about 400~500 km west of our study area and may not be appropriate for the Kunlun where the INDEPTH profile crosses.

Although the INDEPTH IV profile was deployed specifically to image any major, low angle crustal thrust faults within the Kunlun Mountain, there is little if any evidence of a coherent reflective interface within the crust from either the near-vertical or wide-angle data. Though absence of reflectivity is a weak basis for interpretation, the INDEPTH IV reflection data could be construed to favor a steeply dipping Kunlun fault (strike slip, reverse or even normal) over a moderately dipping fault of either vergence.

1.4.2 Moho topography and Moho offsets

The Moho depth, or the crustal thickness, is a critical constraint on

geodynamic models of the evolution of the Tibetan plateau. Crustal thickness of the Tibetan plateau in a 800 km west to east band centered on the Lhasa to Golmud transect has been summarized in recent reviews (Mechie et al., 2011; Mechie and Kind, 2013). The crust of the Tibetan plateau is thought to be about 70 to 75 km thick in the south of plateau, thinning to ca. 62 to 68 km beneath the Lhasa terrane and southern Qiangtang terrane, slightly deepening to ca. 66 to 72 km in the northern Qiangtang terrane and Songpan-Ganzi terranes to the south of the Kunlun fault before dramatically thinning to ca. 50 km beneath the Qaidam basin.

The INDEPTH I & II reflection profiles only recorded Moho reflections beneath a short segment of the Tethyan Himalaya, where prominent reflections at 70-75 km were interpreted to be from a piece of the Moho (Zhao et al., 1993; Nelson et al., 1996; Brown et al., 1996). The short INDEPTH III test section suggested a crustal thickness of about 65 km in central Tibet as interpreted from the cessation of strong lower crustal reflectivity at depth (Ross et al., 2004). However, the SINOPROBE profile exhibits a Moho reflection whose depth varies from 66 km beneath Lhasa terrane to ca. 60 km beneath southern Qiangtang terrane, then deepening to 63 km beneath northern Qiangtang terrane. The INDEPTH IV reflection profile shows that a thick crust of about 67 km beneath the Songpan-Ganzi terrane which abruptly thins to about 46 km beneath the Qaidam basin.

The crustal thickness shown by the SINOPROBE reflection profile is generally consistent with the compilations by Mechie et al. (2011) and Mechie and Kind (2013), which include both controlled-source (including INDEPTH III) and passive source (mainly receiver function) observations.

The morphology of the Moho, particulary the existence of large scale offsets, has been a major issue for virtually all geophysical surveys in Tibet since the Sino-French investigations of the 1980's (Hirn et al., 1984a, 1984b). Fan profile recording by Hirn et al. (1984a, 1984b) indicated two abrupt Moho offsets on a order of 20 km, one beneath the High Himalaya in the southern Tibet, the other beneath the Bangong-Nujiang suture. Since then, Moho offsets beneath the Himalaya and Tibetan plateau have been a topic of continued debate.

"Steps" in the Moho have also been reported along internal sutures and at the active margins of Tibetan plateau from various delay time, waveform and receiver function studies (Zhu and Helmberger, 1998; Vergne et al., 2002; Wittlinger et al., 2004; Shi et al., 2009; Zhang et al., 2010; Zhao et al., 2010; Karplus et al., 2011; Yue et al., 2012) (Figure 1-14).

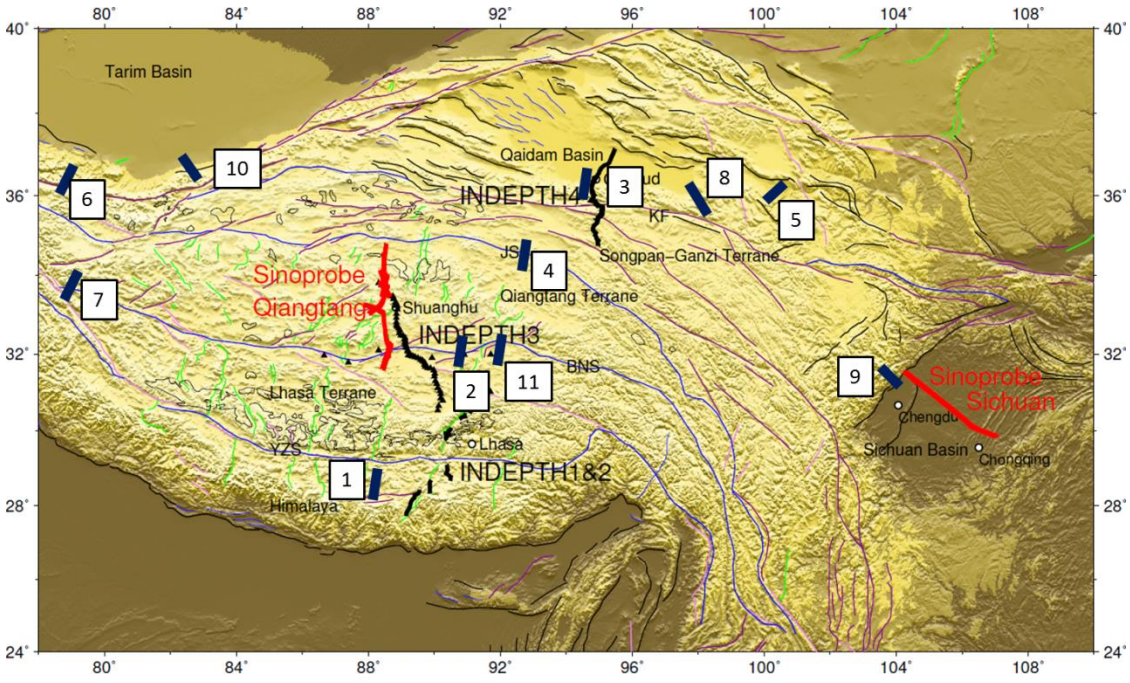

Figure 1-14 Regional topography map with active structures from Taylor and Yin (2009). Dark blue = proposed Moho offsets. Moho offset from previous studies: (1) Hirn et al 1984a, 1984b; (2) Hirn et al 1984b; (3) Zhu and Helmberger 1998, Vergne et al. 2002, Karplus et al. 2011, Yue et al.

2012; (4) Vergne et al. 2002; (5) Vergne et al. 2002; (6) Wittlinger et al. 2004; (7) Wittlinger et al. 2004; (8) Shi et al. 2009; (9) Zhang et al. 2010; (10) Zhao et al. 2010; (11) Yue et al. 2012.

One of the most promient Moho offsets, of about 20 km in size, was first reported beneath the northeastern margin by Zhu and Helmberger (1998) on the basis of multi-pathing of teleseismic arrivals near the boundary with the Qaidam Basin. It has been subsequently confirmed by a variety of seismic techniques such as receiver functions (Vergne et al. (2002) Yue et al. (2012) and refraction (Karplus et al., 2011) (No. 3 in Figure 1-14). In Vergne et al. (2002), Moho is observed to change its depth from about 55 km depth to about 65 km near the Gonghe basin, just south of the Kunlun fault (No. 5 in Figure 1-14). Shi et al. (2009) reported the Moho at ~58 km under the Kunlun mountains shallowing to ~45 km beneath the Qaidam basin (No. 8 in Figure 1-14).

Other Moho offsets at the edge of the Tibetan plateau have been reported. Wittlinger et al. (2004) and Zhao et al. (2010) reported a Moho offset of about 20 km beneath the Altyn-Tagh fault between the Tibetan plateau and Tarim basin (No. 6 and No. 10 in Figure 1-14). Zhang et al. (2010) reported a Moho step of about 20 km under the Longmenshan fault at the boundary between the eastern Tibetan plateau and the Sichuan basin (No. 9 in Figure 1-14).

Interpretations for these Moho offsets varies: deep roots of overlying strike-slip faults (Hirn et al., 1984b; Vergne et al., 2002), thrust faults in the lowermost crust (Vergne et al., 2002; Wittlinger et al., 2004), changes in mode of crustal shortening (Zhao et al., 2010) or just contrasts in deep deformational style in adjacent terranes (Zhu and Helmberger, 1998; Shi et al., 2009).

Besides the 20-km Moho step beneath Bangong-Nujiang suture discovered by

Hirn et al. (1984b) (No. 2 in Figure 1-14), there are also several Moho offsets observed beneath older suture zones (e.g. Bangong-Nujiang suture and Jinsha suture) within the plateau. Wittlinger et al. (2004) and Yue et al. (2012) reported a 10-km Moho step beneath the Bangong-Nujiang suture in the western and eastern part of the Tibetan plateau, respectivley (No. 7 and No. 11 in Figure 1-14). Vergne et al. (2002) showed a ca. 10 km Moho step beneath Jinsha suture (No. 4 in Figure 1-14).

Our INDEPTH III and SINOPROBE profiles are located a few hundreds kilometers to the west of the 20-km Moho step observed by Hirn et al. (1984b) (Figure 1-14 and Figure 1-15), a few hundred kilometers further west of the 10-km Moho offset claimed by Yue et al. (2012) and almost 1000 km to the east of the 10-km Moho offset reported by Wittlinger et al. (2004). However, neither the INDEPTH III nor SINOPROBE exhibit any abrupt Moho depth change beneath Bangong-Nujiang Suture.

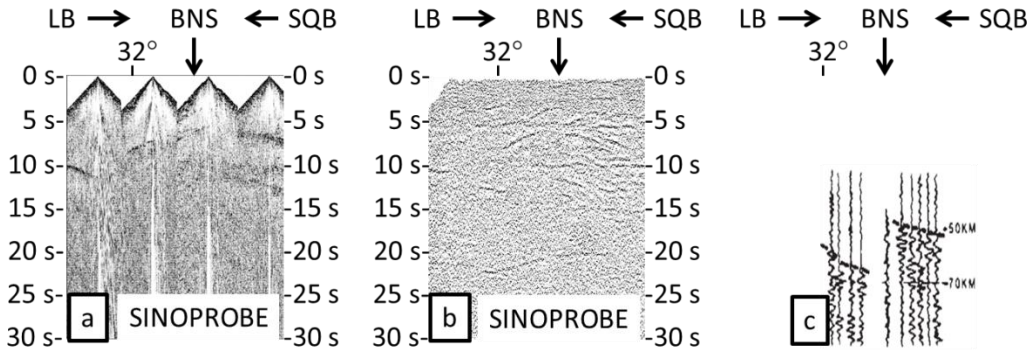

Figure 1-15 SINOPROBE southern part CMP section (a) single fold, maintain relative amplitude (b) stacked profile after migration, fold=72 and (c) Moho offset observed from wide-angle reflection from (Hirn et al., 1984b), plotted in the same scale (time to depth conversion: assuming Vp=6km/s). Notice the result from (Hirn et al., 1984b) was about 100 km east of our SINOPROBE profile and the claimed Moho step was beneath the BNS in situ.

Instead, the SINOPROBE profile shows a clear, coherent Moho reflection whose depth varies smoothly from about 66 km in the south to 60 km in the middle

and 63 km in the north. These reflection depths are consistent with the Moho depths indicated by the INDEPTH wide-angle seismic refraction/reflection results (Zhao et al., 2001) (Figure 1-16) and receiver function profile (Shi et al., 2004) (Figure 1-17) and (Saul, unpublished) (Figure 1-18). The absence of an abrupt Moho offset beneath the Bangong-Nujiang suture from our reflection observations could be due to lateral changes in the Moho character as the SINOPROBE transect lies west of the original SinoFrench reflection points by Hirn et al. (1984b). However, the SINOPROBE profile also confirms the existence of a number of intracrustal reflective interfaces which could have provided a wide angle arrival that might have appeared correlative with true Moho segments on the older fan profiles.

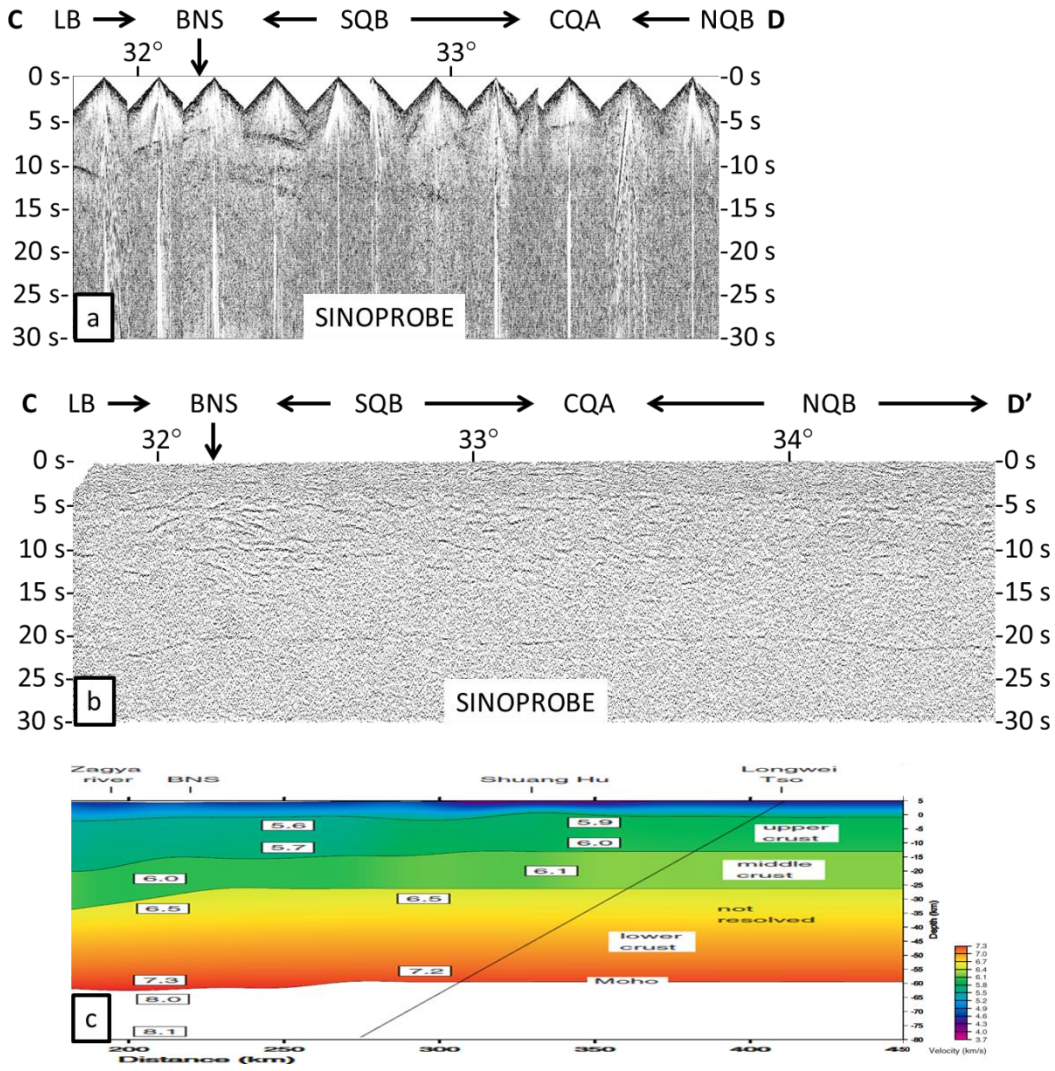

Figure 1-16 SINOPROBE CMP section (a) single fold preserving relative amplitudes (b) stacked profile after migration, fold=72 and (c) Vp model from (Zhao et al., 2001), plotted in the same scale (time to depth conversion: assuming Vp=6km/s).

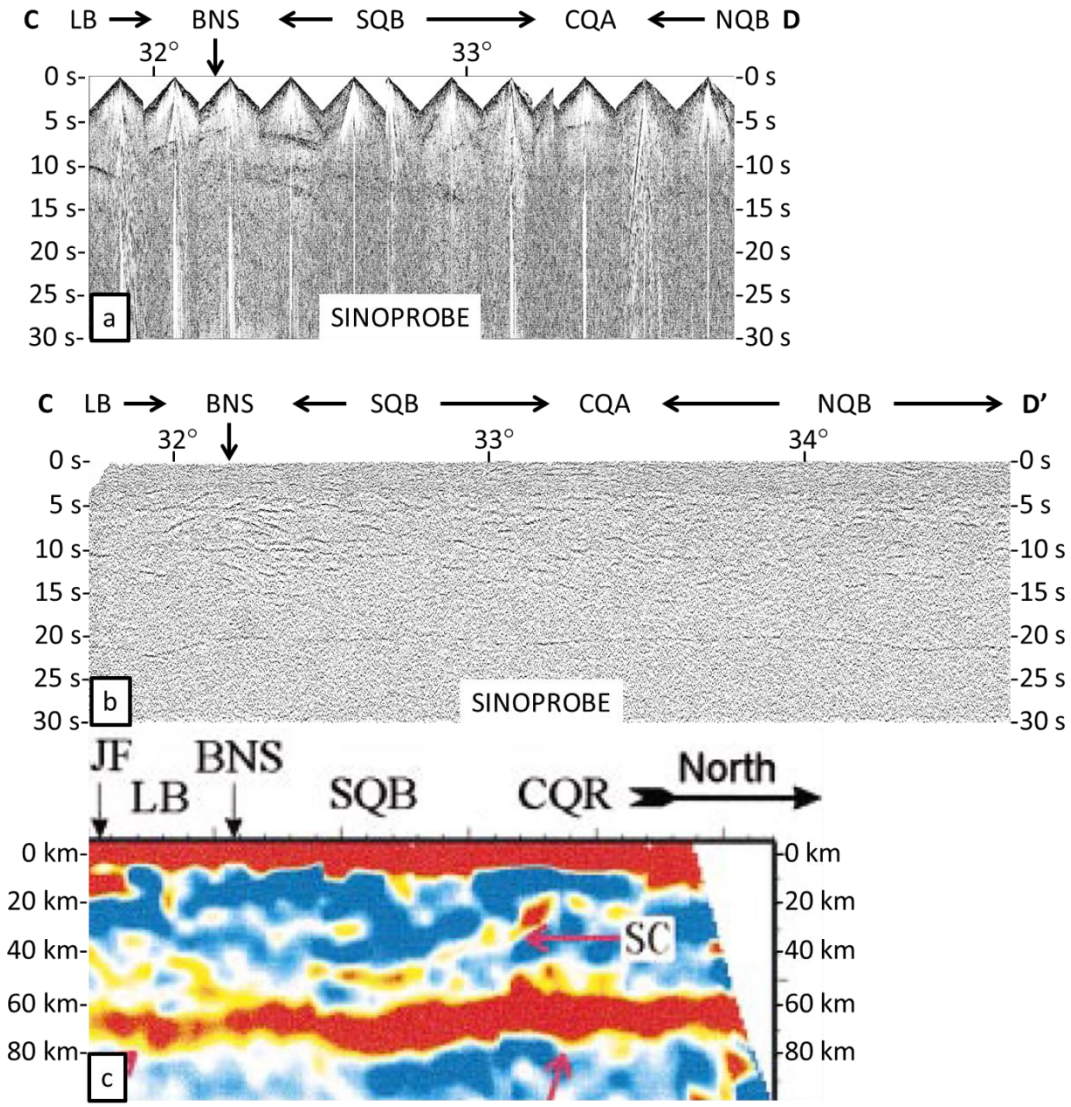

Figure 1-17 SINOPROBE CMP section (a) single fold, preserving relative amplitudes (b) stacked profile after migration, fold=72 and (c) P wave receiver function from INDEPTH III by (Shi et al., 2004), plotted in the same scale.

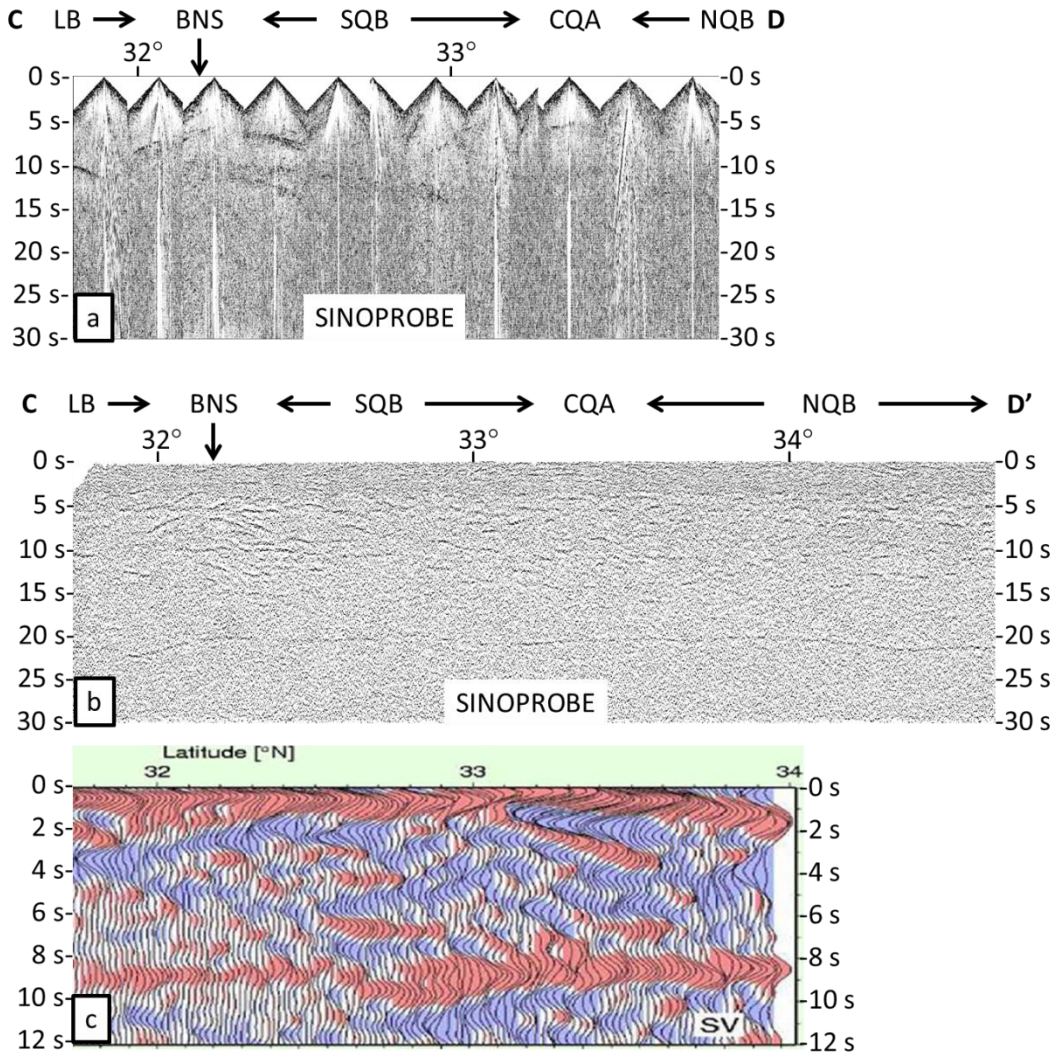

Figure 1-18 SINOPROBE CMP section (a) single fold, preserving relative amplitudes (b) stacked profile after migration, fold=72 and (c) S wave receiver function from INDEPTH III by Saul at GFZ, unpublished, plotted in the same scale.

In any case, the "smooth" Moho seems consistent with a weak lower crust and upper mantle as suggested by proponents of the "channel flow" model of Tibetan tectonics proposed by (Zhao and Morgan, 1987; Royden et al., 1997; Clark and Royden, 2000; Klemperer, 2006).

The Moho offset of most interest to our study is the Golmud "step" at the northeastern margin of the Tibetan plateau traversed by INDEPTH IV. Zhu and

Helmberger (1998) first proposed a step in the Moho under the Kunlun Mountains from anomalous double-pulse teleseismic P-wave arrivals. They argued for an abrupt thinning of the crust from 55 km under the plateau to about 35 to 40 km beneath the Qaidam basin. Furthermore, they proposed that this abrupt change of 15 to 20 km occurs over a distance of less than 5 km. More recently, Vergne et al. (2002) and Yue et al. (2012) reported a similar Moho offset near the same location using receiver functions. These results suggest that a Moho at 50-55 km under the Qaidam Basin increases in depth to ~ 70 km under the Kunlun mountains. Li et al. (2004) also detected a Moho offset, from 61 km at depth beneath south of Golmud to 52 km depth beneath the Qaidam Basin, from active source seismic refraction surveys in 1983 and 1992.

Wide-angle reflection recording of the northernmost big shot KS5 from our INDEPTH IV profile shows a distinct reflection (M1) beneath the Qaidam basin that is interpreted as the Moho at a 46 km depth below the surface (Karplus et al., 2011). This event can be traced at least as far south as position 20km in Figure 1-12 and Figure 1-13. We propose that a deeper reflection (M2) at a time equivalent to a depth of about 67 km (also below the surface) marks the Moho south of Golmud (e.g. beneath the Tibetan plateau). The depths are calculated using velocities from the wide angle data directly using the BSNMO method stated above. These values confirm a change in Moho depth of 21 km within 20 km lateral distance. While one can not rule out the possibility that one or the other of these two distinct deep reflectors are from lower crust interfaces rather than the crust-mantle boundary, the consistency with the other seismic observations makes such an interpretion unlikely. Since our survey is basically

a 1-D line, we have little constraint on possible cross dip of these presumed Moho reflections. If these reflectors do have a significant dip perpindicular to the seismic line, their computed depths may be correspondingly uncertain.

The abruptness of the Golmud step is of special interest. There is a weak reflection (M3) on our seismic section (Figure 1-13) which could suggest that the Moho extends further south. Also, weak coherent energy suggests that the deep Moho may extend from M2 to M4 in Figure 1-11and Figure 1-13. If this is the case, the Moho would appear to overlap at a position north of Golmud. The deep Moho can also be seen from wide-angle reflection from KS4 (Figure 1-19). A reflection (M5) at similar depth is evident, which is equivalent of M2 beneath the Tibetan plateau but to further south.

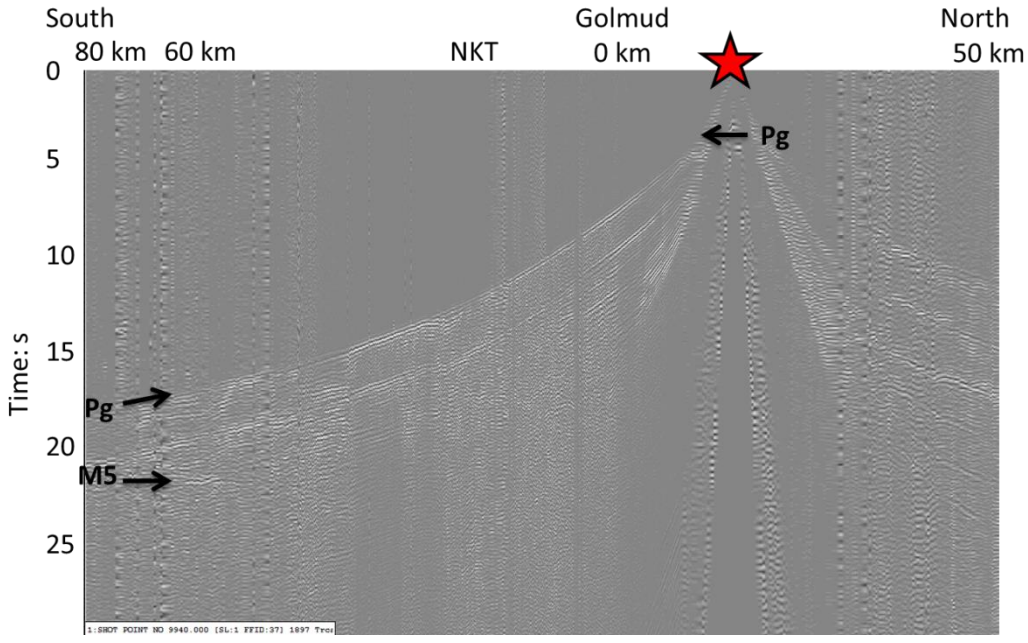

Figure 1-19 Shot gather as depth section for KS4. Red star = shot.

The upper bound on the lateral distance over which the Moho changes depth is 20 km if we consider M1 in Figure 1-11 and Figure 1-13 as the shallow Moho beneath

the Qaidam Basin and M2 as the deep Moho beneath the Eastern Kunlun Range. If we consider M3 as the same shallow Moho as M1 and M4 as M2, at north of Golmud in Figure 1-11 and Figure 1-13, the Mohos actually overlap with the shallower one at about 46 km depth, and the deeper one at about 67 km. This correlation is the one adopted in the wide-angle refraction interpretation of Karplus et al. (2011).

The Golmud Moho step as defined by the INDEPTH IV reflections lies about 50 to 70 km north of the south dipping North Kunlun fault, so it is unlikely to be related to this surface feature. Likewise, the focal mechanism of 2001 Ms 8.1 Central Kunlun Earthquake exhibits a nearly vertical fault plane for the west segment of the Kunlun left-slip fault (Lin et al., 2002). If we assume the Kunlun strike-slip fault does not change its dip significantly from the west to the east, then it too is unlikely to be related to the Golmud Moho step.

Moho reflections from KS4 underlie the North Kunlun left-slip fault, but they do not show any significant deformation of the Moho, which suggests that this major fault does not penetrate through the entire crust, at least as a vertical structure.
The frequency content of reflections M1 (also M3) and M2 (also M4) are different. M1 has its peak frequency at 5-8 Hz, while M2 peaks at 2-3 Hz. This may be due in part to the different instruments that were used in the experiment. M1 was recorded by 10Hz geophones while M2 was recorded by 4.5Hz geophones. However, the lower frequency character of the Moho reflection beneath the plateau is consistent with greater attenuation within the Tibetan crust. Partial melting in the crust just south of the Kunlun has been suggest by INDEPTH magnetotelluric surveys (Unsworth et al., 2004) as well as the lower crustal velocities for Tibetan crust estimate by Karplus et

al. (2011).

Topography analysis of Clark and Royden (2000) suggests that the Qaidam Basin is a region with intermediate strength, relatively weaker than Tarim Basin and Sichuan Basin, but much stronger than the Tibetan plateau. In contrast to the Sichuan basin and Tarim basin, which are both flat and lie at elevations less than 1 km, the Qaidam basin has an average elevation of 2.5 km. The Moho offset beneath the Kunlun Range at south of Golmud is consistent with the proposition that the Qaidam Basin has functioned as a strong mechanical barrier at the edge of the Tibetan plateau, which together with the Tarim and Sichuan Basins from a buttress to plateau growth. The receiver function studies of Wittlinger et al. (2004), Zhao et al. (2010), Zhang et al. (2010) suggest Moho offsets of about 20-25 km beneath Tarim Basin and Sichuan Basin in comparison with the INDEPTH IV estimate of a 25km Moho offset at the edge of the Qaidam Basin. If the magnitude of Moho offset is as an indicator of lithospheric strength, then the Qaidam Basin is likely to be as strong as or stronger than the Tarim and Sichuan lithospheres. The discrepancy of location between the elevation change and the Moho step (e.g. Figure 1-9) may reflect a relatively fast erosion rate at the surface or a relatively slow uplift rate due to lower crustal flow model (Yin et al., 2008).

Depending upon how much credence to place on the weaker "extensions" of the Moho reflections on the reflection section, the Golmud step could be interpreted as a steep (ca. 50°) Moho ramp or perhaps even a reverse Moho fault (Figure 1-20). A Moho ramp dipping to south could be consistent with subduction of Qaidam lithosphere subducting beneath the Tibetan plateau along a crustal detachment, as

suggested by Kind et al. (2002) from receiver functions. A south dipping Moho fault would also be consistent with the south-dipping crustal thrust model argued by Meyer et al. (1998). Perhaps the most intriguing possibility, suggested that the intepretation of overlapping Moho reflectors, is the existence of a steep, *north-dipping* reverse fault, either penetrating the entire crust as suggested by Meyer et al. (1998) or merely offsetting the lower crust (Yin et al., 2007, 2008). A line connecting the northmost point of the deep Moho reflection (M2) with southmost point of the shallow Moho reflection (M5?) intersects the surface more or less at North Kunlun Thrust, so a whole crust fault is at least plausible, althouth there is no evidence of this fault in the shallow crust (e.g. (Karplus et al., 2011)) .

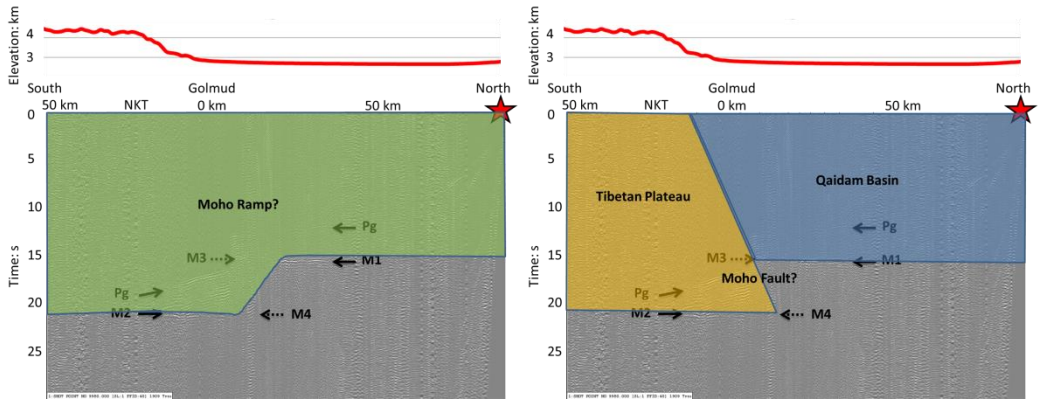

Figure 1-20 Possible models to interpret the Moho reflection: Moho ramp (on the left) or the Moho fault (on the right).

A reverse fault at the Moho step, whether restricted to the lower crust or penetrating to the surface, together with the large magnitude of the offset, begs the question of whether this fault predates the formation of the Tibetan Plateau. The formation of Moho offsets during pre-Himalayan collisions, e.g. the Triassic suturing of the Kulun itself, is certainly plausible and the preservation of such morophology could have played a role in localizing more recent plateau uplift at the edge of the

Qaidam basin. The existence of a significant change in Moho thickness at the edge of the Tibetan Plateau prior to Cenozoic collison would also imply that the plateau had pre-collisional elevation as well. If so, this has serious implications for models of modern plateau formation, e.g. the amount of modern uplift could be signficantly less that widely assummed.

1.4.3 Bright spots

A series of unusually strong, mid-crustal reflectors at 5-6s (15-18km) were observed by INDEPTH I & II at the southern edge of the Lhasa block. These events have been suggested to represent granitic magmas derived by partial melting of the tectonically thickened crust (Brown et al., 1996) or the presence of relatively large quantities of free aqueous fluids (Makovsky and Klemperer, 1999). The presence of these bright spots is cited by Nelson et al. (1996) in support of the hypothesis that much of the Tibetan crust is partial molten, and hence susceptible to ductive flow (e.g. (Royden et al., 1997; Clark and Royden, 2000)). The fluid interpretation of these bright spots is based on amplitude, polarity, and AVO (Amplitude Variation with Offset) (Brown et al., 1996; Makovsky and Klemperer, 1999) and correspondance to high conductivity (Unsworth et al., 2005).

Similar bright spots are also present on the SINOPROBE-2 Qiangtang profile. The single fold section (Figure 1-7a, c) was generated to highlight these bright spots in their original amplitudes, uncorrupted by more advanced processing.

Polarity of the bright spots have been used to discriminate the nature of the subsurface reflectors (e.g. Brown et al., 1996; Ross, PhD thesis). Negative polarity is indicative that fluids are involved. Bright spots with positive polarity have commonly

been interpreted as frozen sills (e.g. Siljan reflectors in Sweden (Eriksson and Malmqvist, 1979; Juhlin and Pedersen, 1987) and Wollastone bright spots in Canada (Drury, 1985; Mandler and Clowes, 1997)). Lacking other constraints on the nature of the bright spots on the SINOPROBE profile (e.g. AVO measurements like Makovsky and Klemperer, 1999), we have attempted to use polarity as a guide to there interpretation.

The bright spots in central Tibet beneath our SINOPROBE profile differ in their depth and polarity (Figure 1-21 and Figure 1-22). South of the Bangong-Nujiang Suture, a series of bright spots appear as single reflector with positive polarity. One bright spot at 10-12s TWT is steeply north dipping on the unmigrated seismic section (see single-fold section, Figure 1-7a, c) and migrates to a shallower position (10 sec) further south (see multi-fold section, Figure 1-7b, d). Another occurs at 6-8 secs as a south dipping event. Although the depth of the shallow bright spots (6-8 secs, or ca 20 km) is similar with those in southern Tibet that were interpreted as magma, the polarity of these SINOPROBE events appear to be the same polarity as the direct P wave (Figure 1-21). This positive polarity suggests that they are related to a contrast between high velocity/density rock underlying lower velocity/density rock. Thus these events more likely correspond to cold mafic bodies than recent melts.

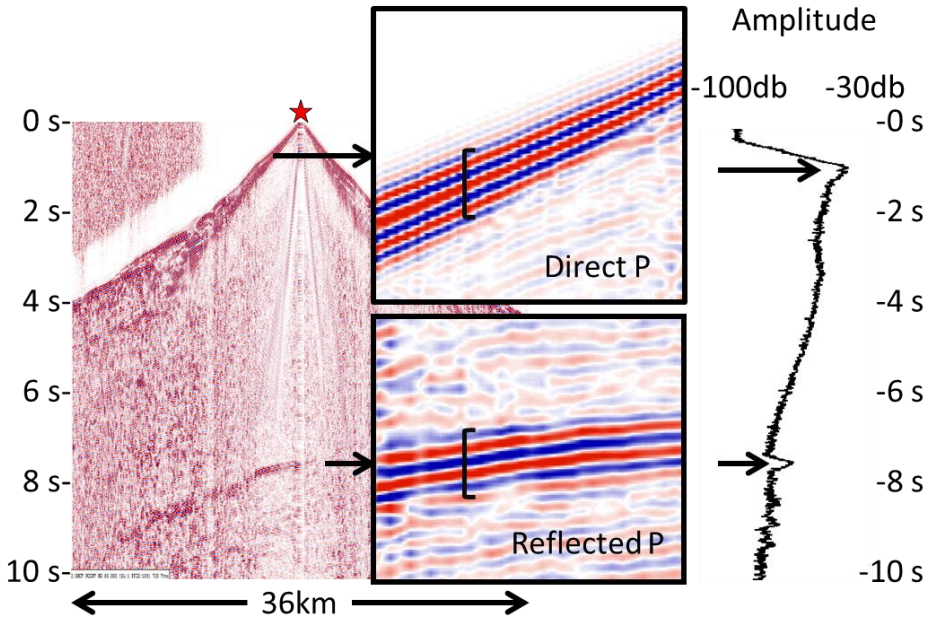

Figure 1-21 Shot gather from the southern part of SINOPROBE 2, between CMP 1000 and 2000 (profile A FFID 109) This corresponds to the second shot gather in the single fold section in Figures 2- 7 and 2-16 through 2- 19. The blow ups show the direct P and reflected P arrivals. The black brackets mark the arrival sequence (blue-red-blue-red-blue-red). Notice the direct P and reflected P arrivals appear to have the same polarity. Amplitude decay curve is displayed on the right to show the "brightness" of the bright spot.

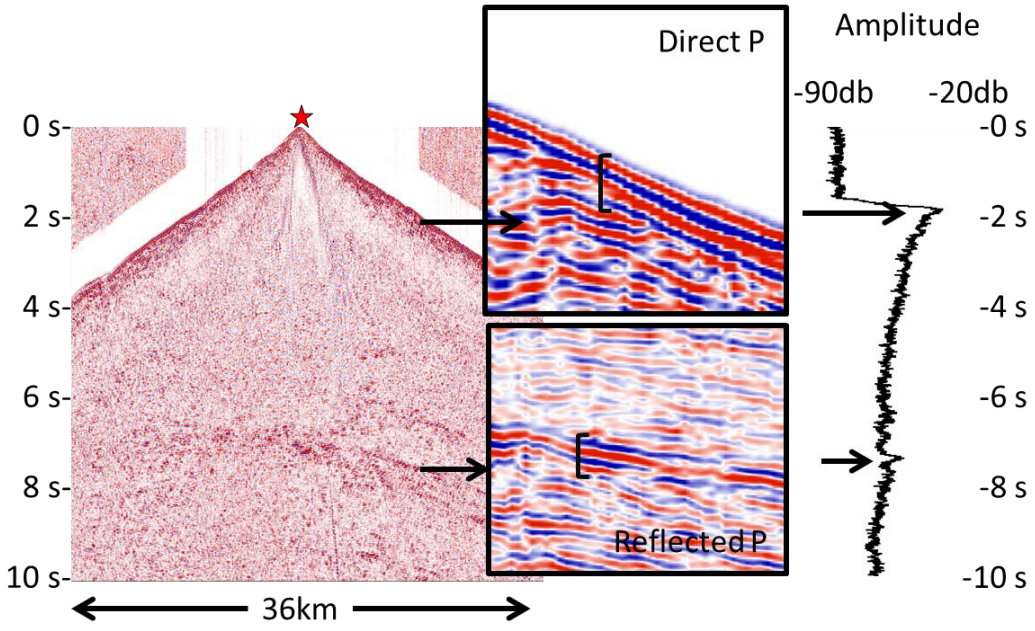

Figure 1-22 Shot gather from the southern part of SINOPROBE 2, between CMP 2000 to 3000 (profile BS FFID 312). (This corresponds to the fourth shot gather in the single fold sections). The blow ups show the direct P and reflected P arrivals. The black brackets mark the arrival

sequence "red-blue-red-blue" for direct P and "blue-red-blue-red" for reflected P arrival. Notice the reflected P arrivals appear to have a reversed polarity from direct P arrival. Amplitude decay curve is displayed on the right to show the "brightness" of the bright spot.

The bright spots to the north of the Bangong Nujiang Suture exhibit a different character (Figure 1-22). There are two bands, one at 6-8s TWT and the other at 12-14s (see single-fold section, Figure 1-7a, c). The shallow band seems to have a reversed polarity similar to the bright spots in the southern Tibet and thus is a candidate for magma or fluid, both possible indicators of partial melting. Partial melting would be consistent with the high conductivity of the lower crust of central Tibet found by INDEPTH III magnetotelluric measurements (Wei et al., 2001) and the nearby presence of a large extensional graben (e.g. the Shuang Hu graben), not to mention the presence of Neogene volcanism in the northern Qiantang (Turner et al., 1996). The bright spot at 12-14s is not well enough defined to determine polarity.

A number of the SINOPROBE bright spots near the Bangong suture are generally dipping northward (Figure 1-7c) in similar fashion to the surrounding weaker events (Figure 1-7d). This package of reflectors coincides with a broad reflective zone beneath the BNS at the surface. The overall reflective character could represent a shear fabrics in the crust associated with Jurassic thrusting along BNS. If so, it is plausible that the positive polarity bright spots could correspond to mafic material entrained in this shearing, either as sills (now solid) intruded contemporaneously or as mafic components of the collisional collage (ophiolitic fragments). Kapp et al. (2003) proposed a two-stage model for the early Mesozoic evolution of the central Qiangtang metamorphic belt of the blueschist-bearing melange. The model suggests the melange underthrust southward beneath the

Qiangtang Block and then was exhumed to the upper crust by Late Triassic-Early Jurassic normal faulting. Even though our SINOPROBE profile did not go as far north as the JS, where this proposed underthrusting reaches the surface, we would expect to have encountered south dipping structures in the upper to middle crust on our profile. However, we observe no south dipping reflectors north of CQA. It is possible that the melange underthrusting envisioned by Kapp et al. (2003) is not reflective and thus would not be detected by reflection techniques. It is also possible that later geolocial events erased any signature of early Mesozoic underthrusting. However, we suggest the reflection data is most consistent with northward underthrusting of the melange as proposed by Li et al (1995).

In Figure 1-23, the seismicity located by INDEPTH III [Langin et al., 2003] was projected onto a N-S profile subparallel to the SINOPROBE profile. 99% of the seismicity occurs at depths < 25km (Figure 1-23). Although there seems to be little correlation of the seismicity with the bright spots on the SINOPROBE section, their shallow depths of earthquakes (Chen and Molnar, 1983; Zhao and Helmberger, 1991; Langin et al., 2003) are consistent with high tempertures of the crust in central Tibet, and thus with a magmatic origin for the SINOPROBE bright spots within the Qiangtang.

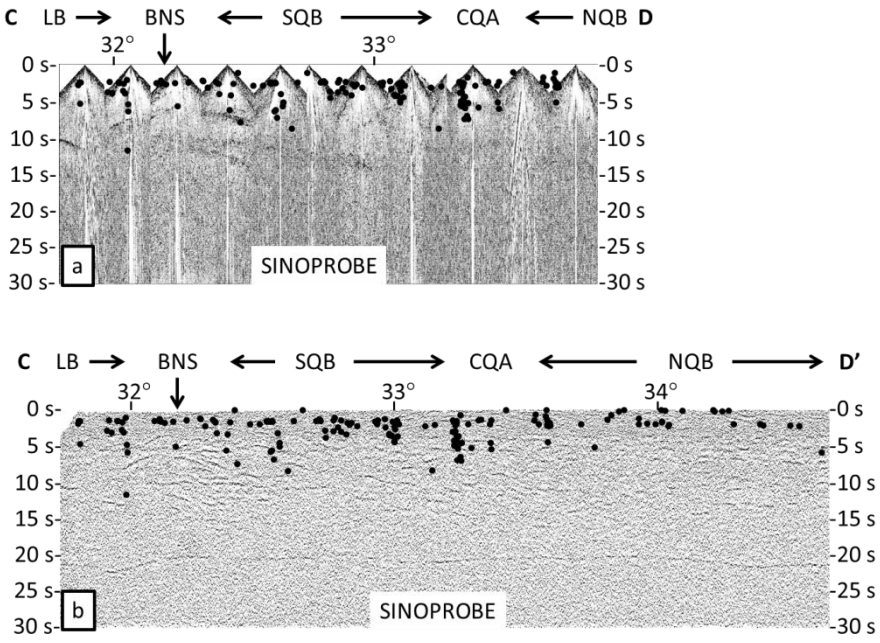

Figure 1-23 Seismicity in central Tibetan Plateau from (Langin et al., 2003) projected onto a N-S plane following the SINOPROBE profile.

Mechie et al. (2004) claimed that an abrupt increase in velocity in the mid-crust inferred from INDEPTH III refraction data corresponds to the α-β quartz transition (ABQT). Since the ABQT is temperature dependent, such a marker would be an important indicator of the contemporary thermal state of the Tibetan crust. The velocity contrast associated with this phase change should constitute a reflective interface. The SINOPROBE profile exhibits no unequivocally clear continuous reflections in the appropriate depth range on either the single fold or fully processed sections. However a zone of weak, discontinous subhorizontal events at travel times of 5-6 sec on the fully processed data could be interpreted as evidence of the ABQT at approximately 18 km depth.

1.4.4 Lower crustal flow

The role of lower crustal flow in the formation of the Tibetan Plateau has been

championed by many (e.g. Zhao and Morgan, 1987; Nelson et al., 1996; Royden et al., 1997; Clark and Royden, 2000; Klemperer, 2006) to explain the high and flat topography of the Tibetan plateau relatively to the surrounding Tarim Basin, Sichuan Basin and the lack of substantial upper crustal shortening of the plateau interior. Although the reflection bright spots have been used to support the model of crustal flow (e.g. (Nelson et al., 1996)), more direct expression of flow in the reflection data from the INDEPTH-SINOPROBE reflection surveys is ambiguous.

A zone of non-reflectivity in the lower crust between about 40 km and the Moho is observed on the SINOPROBE survey. This lack of reflectivity in our reflection profile is unlikely to result from lack of energy penetration or other imaging problems because the underlying Moho has been successfully imaged. This non-reflective lower crust could be intepreted as an expression of crustal flow essentially homogenizing any pre-existing reflectivity. Lack of seismicity below about 25 km [Langin et al., 2003] and high electrical conductivity below about 40 km [Wei et al., 2001; Rippe and Unsworth, 2010] are also consistent with lower crustal flow.

The association of deep transparency with flow is at odds with previous interpretations that deep crustal shear results in laminated reflection sequences (Warner, 1990a, 1990b). Layered reflections in the lower crust observed from the very short INDEPTH III reflection profiles were used to argue for lower-crustal flow by Ross et al. (2004). However the very small area sampled by the INDEPTH III test survey is not as likely to be representative of Tibetan crust as the much longer SINOPROBE profile.

Karplus et al. (2011) argued that the Moho offset seen from the INDEPTH IV

reflection profile is evidence that the lower crust of the Songpan-Ganzi terrane underthrustor flowed northward beneath the Moho of the Qaidam Basin. They argue that the low P wave velocity (6.8-7.1 km/s) beneath M1 represents crustal material. This low P wave velocity zone beneath M1 is inverted from the traveltime of KS5 and an earthquake to the north. However, this inversion rests upon relative few arrival times, and other models could be equally consistent with these observations (e.g. Figure 1-20).

Huang et al. (2000) showed significant SKS and SKKS shear wave splitting from south of the BNS to the northern end of INDEPTH III profile. This strong anisotropy region is basically coincident with the C-D part of the SINOPROBE transect. Huang et al. (2000) suggested that this anisotropy is located in the lower crust and/or upper mantle. Together with the previously described absence of strong reflectivity in the lower crust on the SINORPROBE transect, this inferred anisotropy could be construed as further evidence of lower crustal flow at depth.

1.5 SUMMARY

The new images of Tibetan crust represented by this compilation re-emphasizes key points of their original interpretations but in a larger context. Among the highlights are:

1. A prominent reflector beneath southern Tibet that marks the decollement beneath which Indian lithosphere underthrusts the Euroasian lithosphere. Similarly distinct reflections are noticably absent at both the northern Plateau boundary and the internal sutures of the plateau.

2. The lack of an abrupt Moho offset beneath the Bangong Nujiang Suture along the

SINOPROBE Qiangtang profile. Rather the Moho deepens "smoothly" beneath a non-reflective lower crust (below 40km) that may be construed as a weak lower crustal channel.

3. Although there is no clear megathrust associated with the Bangong-Nujiang Suture of central Tibet, a broad band of north dipping reflectors beneath southern Qiangtang suggests south vergent subducting/underthrusting of the Lhasa terrane beneath the Qiangtang terrane in late Jurassic to early Cretaceous.

3. An abrupt, 20-km Moho offset is observed between the northeastern Tibetan plateau and Qaidam basin near the north Kunlun fault, supporting the concept of the Qiadam basin as part of a strong lithospheric buttress.

4. The crustal thickness is about 60-66 km beneath central Tibet and 46 km beneath Qaidam basin as revealed by SINOPROBE and INDEPTH IV profiles. These seismic reflection results agree well with other geophysical studies e.g. refraction, receiver function.

5. Bright spots beneath central Tibet appear to have different causes. Positive polarity bright spots south of the BNS may be relict mafic material (ophiolitic fragments?) related to the collision between the Lhasa and Qiangtang blocks. Negative polarity bright spots north of the BNS are evidence of partial melting that is consistent with both the high conductive lower crust and Neogene volcanism of the Qiangtang block.

REFERENCES

Alsdorf, D., 1997. Noise reduction in seismic data using Fourier correlation coefficient filtering. Geophysics 62, 1617.

Alsdorf, D., Brown, L., Nelson, D., 1996. Possible upper mantle reflection fabric on seismic profiles from the Tethyan Himalaya: Identification and tectonic interpretation. J. Geophys. Res. 101, 25305–25.

Alsdorf, D., Brown, L., Nelson, K.D., Makovsky, Y., Klemperer, S., Zhao, W., 1998a. Crustal deformation of the Lhasa terrane, Tibet plateau from Project INDEPTH deep seismic reflection profiles. Tectonics 17, 501–519.

Alsdorf, D., Brown, L., Nelson, K.D., Makovsky, Y., Klemperer, S., Zhao, W., 1998b. Crustal deformation of the Lhasa terrane, Tibet plateau from Project INDEPTH deep seismic reflection profiles. Tectonics 17, 501–519.

Alsdorf, D., Makovsky, Y., Zhao, W., Brown, L.D., Nelson, K.D., Klemperer, S., Hauck, M., Ross, A., Cogan, M., Clark, M., others, 1998c. INDEPTH (International Deep Profiling of Tibet and the Himalaya) multichannel seismic reflection data: description and availability. J. Geophys. Res. 103, 26.

Argand, E., 1924. La tectonique de l'Asie. Int Geol Cong Rep Sess 13, 170–372.

Bally, A.W., China, A.S.B.D. to the P.R. of, (US), G.S., 1986. Notes on sedimentary basins in China: Report of the American Sedimentary Basins Delegation to the People's Republic of China. Department of the Interior, US Geological Survey.

Barazangi, M., Ni, J., 1982. Velocities and propagation characteristics of Pn and Sn beneath the Himalayan arc and Tibetan plateau: Possible evidence for underthrusting of Indian continental lithosphere beneath Tibet. Geology 10, 179.

Beghoul, N., Barazangi, M., Isacks, B.L., 1993. Lithospheric structure of Tibet and western North America: Mechanisms of uplift and a comparative study. J. Geophys. Res. 98, 1997–2016.

Brown, L.D., Zhao, W., Nelson, K.D., Hauck, M., Alsdorf, D., Ross, A., Cogan, M., Clark, M., Liu, X., Che, J., 1996. Bright spots, structure, and magmatism in southern Tibet from INDEPTH seismic reflection profiling. Science 274, 1688.

Burchfiel, B.C., Quidong, D., Molnar, P., Royden, L., Yipeng, W., Peizhen, Z., Weiqi, Z., 1989. Intracrustal detachment within zones of continental deformation. Geology 17, 748–752.

Chen, W.-P., Chen, C.-Y., L N âbelek, J., 1999. Present-day deformation of the Qaidam basin with implications for intra-continental tectonics. Tectonophysics 305, 165–181.

Chen, W.-P., Molnar, P., 1983. Focal depths of intracontinental and intraplate earthquakes and their implications for the thermal and mechanical properties of the lithosphere. J. Geophys. Res. Solid Earth 1978–2012 88, 4183–4214.

Clark, M.K., Royden, L.H., 2000. Topographic ooze: Building the eastern margin of Tibet by lower crustal flow. Geology 28, 703.

Drury, M.J., 1985. Heat flow and heat generation in the Churchill Province of the Canadian Shield, and their palaeotectonic significance. Tectonophysics 115, 25–44. doi:10.1016/0040-1951(85)90097-6

Eriksson, K.G., Malmqvist, D., 1979. A review of the past and the present investigations of heat flow in Sweden, in: Terrestrial Heat Flow in Europe. Springer, pp. 267–277.

Gao, R., Chen, C., Lu, Z., Brown, L.D., Xiong, X., Li, W., Deng, G., 2013. New constraints on crustal structure and Moho topography in Central Tibet revealed by SinoProbe deep seismic reflection profiling. Tectonophysics, Special Issue derived from "International Symposium on Deep Exploration into the Lithosphere", Beijing, November 2011 606, 160–170. doi:10.1016/j.tecto.2013.08.006

Gao, R., Lu, Z., Li, Q., Guan, Y., Zhang, J., He, R., Huang, L., 2005. Geophysical survey and geodynamic study of crust and upper mantle in the Qinghai-Tibet Plateau. Episodes 28, 263.

Hirn, A., Lepine, J.-C., Jobert, G., Sapin, M., Wittlinger, G., Zhong Xin, X., En Yuan, G., Xiang Jing, W., Ji Wen, T., Shao Bai, X., Pandey, M.R., Tater, J.M., 1984a. Crustal structure and variability of the Himalayan border of Tibet. Nature 307, 23–25. doi:10.1038/307023a0

Hirn, A., Nercessian, A., Sapin, M., Jobert, G., Xin, X.Z., Yuan, G.E., Yuan, L.D., Wen, T.J., 1984b. Lhasa block and bordering sutures[mdash] a continuation of a 500-km Moho traverse through Tibet. Nature 307, 25–27. doi:10.1038/307025a0

Huang, W.C., Ni, J.F., Tilmann, F., Nelson, D., Guo, J., Zhao, W., Mechie, J., Kind, R., Saul, J., Rapine, R., others, 2000. Seismic polarization anisotropy beneath the central Tibetan Plateau. J. Geophys. Res. 105, 27–979.

Jin, W., Liu, Z., Zhang, X., 2008. Study on linear interference-removing method in GRISYS processing system. Oil Geophys. Prospect.

Juhlin, C., Pedersen, L.B., 1987. Reflection seismic investigations of the Siljan impact structure, Sweden. J. Geophys. Res. Solid Earth 1978–2012 92, 14113–14122.

Kapp, P., DeCelles, P.G., Gehrels, G.E., Heizler, M., Ding, L., 2007. Geological records of the Lhasa-Qiangtang and Indo-Asian collisions in the Nima area of central Tibet. Geol. Soc. Am. Bull. 119, 917.

Kapp, P., Yin, A., Harrison, T.M., Ding, L., 2005. Cretaceous-Tertiary shortening, basin development, and volcanism in central Tibet. Bull. Geol. Soc. Am. 117, 865.

Karplus, M.S., Zhao, W., Klemperer, S.L., Wu, Z., Mechie, J., Shi, D., Brown, L.D., Chen, C., 2011. Injection of Tibetan crust beneath the south Qaidam Basin: Evidence from INDEPTH IV wide-angle seismic data. J Geophys Res 116, B07301. doi:10.1029/2010JB007911

Kind, R., Yuan, X., Saul, J., Nelson, D., Sobolev, S.V., Mechie, J., Zhao, W., Kosarev, G., Ni, J., Achauer, U., others, 2002. Seismic images of crust and upper mantle beneath Tibet: Evidence for Eurasian plate subduction. Science 298, 1219.

Klemperer, S.L., 2006. Crustal flow in Tibet: geophysical evidence for the physical state of Tibetan lithosphere, and inferred patterns of active flow. Geol. Soc. Lond. Spec. Publ. 268, 39.

Langin, W.R., Brown, L.D., Sandvol, E.A., 2003. Seismicity of central Tibet from Project INDEPTH III seismic recordings. Bull. Seismol. Soc. Am. 93, 2146.

Li, C., Cheng, L.R., Hu, K., Yang, Z.R., Hong, Y.R., 1995. Study on the paleo-Tethys suture zone of Lungmu Co-Shuanghu, Tibet. Geol Publ House Beijing.

Li, C., van der Hilst, R.D., Meltzer, A.S., Engdahl, E.R., 2008. Subduction of the Indian lithosphere beneath the Tibetan Plateau and Burma. Earth Planet. Sci. Lett. 274, 157–168.

Lin, A., Fu, B., Guo, J., Zeng, Q., Dang, G., He, W., Zhao, Y., 2002. Co-seismic strike-slip and rupture length produced by the 2001 Ms 8.1 Central Kunlun earthquake. Science 296, 2015–2017.

Li, Q., Peng, S., Gao, R., Guan, Y., Fan, J., 2004. Deep tectonic background of the 8.1 Ms earthquake in the East Kunlun. Acta Geosci. Sin. 25, 11–16.

Lu, Z., Gao, R., Li, Y., Xue, A., Li, Q., Wang, H., Kuang, C., Xiong, X., 2013. The upper crustal structure of the Qiangtang Basin revealed by seismic reflection data. Tectonophysics 606, 171–177.

Makovsky, Y., Klemperer, S.L., 1999. Measuring the seismic properties of Tibetan bright spots- Evidence for free aqueous fluids in the Tibetan middle crust. J. Geophys. Res. 104, 10–795.

Mandler, H.A.F., Clowes, R.M., 1997. Evidence for extensive tabular intrusions in the Precambrian shield of western Canada: A 160-km-long sequence of bright reflections. Geology 25, 271–274.

Mechie, J., Kind, R., 2013. A model of the crust and mantle structure down to 700 km depth beneath the Lhasa to Golmud transect across the Tibetan plateau as derived from seismological data. Tectonophysics. doi:10.1016/j.tecto.2013.04.030

Mechie, J., Kind, R., Saul, J., 2011. The seismological structure of the Tibetan Plateau crust and mantle down to 700 km depth. Geol. Soc. Lond. Spec. Publ. 353, 109–125. doi:10.1144/SP353.7

Mechie, J., Sobolev, S.V., Ratschbacher, L., Babeyko, A.Y., Bock, G., Jones, A.G., Nelson, K.D., Solon, K.D., Brown, L.D., Zhao, W., 2004. Precise temperature estimation in the Tibetan crust from seismic detection of the α-β quartz transition. Geology 32, 601.

Meyer, B., Tapponnier, P., Bourjot, L., Metivier, F., Gaudemer, Y., Peltzer, G., Shunmin, G., Zhitai, C., 1998. Crustal thickening in Gansu-Qinghai, lithospheric mantle subduction, and oblique, strike-slip controlled growth of the Tibet plateau. Geophys. J. Int. 135, 1–47.

Nábělek, J., Hetényi, G., Vergne, J., Sapkota, S., Kafle, B., Jiang, M., Su, H., Chen, J., Huang, B.S., 2009. Underplating in the Himalaya-Tibet collision zone revealed by the Hi-CLIMB experiment. Science 325, 1371.

Nelson, K.D., Zhao, W., Brown, L.D., Kuo, J., Che, J., Liu, X., Klemperer, S.L., Makovsky, Y., Meissner, R., Mechie, J., Kind, R., Wenzel, F., Ni, J., Nabelek, J., Leshou, C., Tan, H., Wei, W., Jones, A.G., Booker, J., Unsworth, M., Kidd, W.S.F., Hauck, M., Alsdorf, D., Ross, A., Cogan, M., Wu, C., Sandvol, E., Edwards, M., 1996. Partially Molten Middle Crust Beneath Southern Tibet: Synthesis of Project INDEPTH Results. Science 274, 1684 –1688. doi:10.1126/science.274.5293.1684

Ni, J., Barazangi, M., 1984. Seismotectonics of the Himalayan collision zone: Geometry of the underthrusting Indian plate beneath the Himalaya. J. Geophys. Res. 89, 1147–1163.

Ross, A.R., Brown, L.D., Pananont, P., Nelson, K.D., Klemperer, S., Haines, S., Wenjin, Z., Jingru, G., 2004. Deep reflection surveying in central Tibet: lower-crustal layering and crustal flow. Geophys. J. Int. 156, 115–128. doi:10.1111/j.1365-246X.2004.02119.x

Royden, L.H., Burchfiel, B.C., King, R.W., Wang, E., Chen, Z., Shen, F., Liu, Y., 1997. Surface deformation and lower crustal flow in eastern Tibet. Science 276, 788–790.

Rupert, G.B., Chun, J.H., 1975. The block move sum normal moveout correction. Geophysics 40, 17–24.

Schulte-Pelkum, V., Monsalve, G., Sheehan, A., Pandey, M.R., Sapkota, S., Bilham, R., Wu, F., 2005. Imaging the Indian subcontinent beneath the Himalaya. Nature 435, 1222–1225.

Shi, D., Shen, Y., Zhao, W., Li, A., 2009. Seismic evidence for a Moho offset and south-directed thrust at the easternmost Qaidam-Kunlun boundary in the Northeast Tibetan plateau. Earth Planet. Sci. Lett. 288, 329–334.

Shi, D., Zhao, W., Brown, L., Nelson, D., Zhao, X., Kind, R., Ni, J., Xiong, J., Mechie, J., Guo, J., others, 2004. Detection of southward intracontinental subduction of Tibetan lithosphere along the Bangong-Nujiang suture by P-to-S converted waves. Geology 32, 209.

Song, T., Wang, X., 1993. Structural styles and stratigraphic patterns of syndepositional faults in a contractional setting: examples from Quaidam basin, northwestern China. AAPG Bull. 77, 102–117.

Taylor, M., Yin, A., 2009. Active structures of the Himalayan-Tibetan orogen and their relationships to earthquake distribution, contemporary strain field, and Cenozoic volcanism. Geosphere 5, 199.

Tilmann, F., Ni, J., INDEPTH III Seismic Team, 2003. Seismic imaging of the downwelling Indian lithosphere beneath central Tibet. Science 300, 1424.

Turner, S., Arnaud, N., LIU, J., Rogers, N., Hawkesworth, C., Harris, N., Kelley, S., Van Calsteren, P., Deng, W., 1996. Post-collision, shoshonitic volcanism on the Tibetan Plateau: implications for convective thinning of the lithosphere and the source of ocean island basalts. J. Petrol. 37, 45–71.

Unsworth, M., Jones, A., Wei, W., Marquis, G., Gokarn, S., Spratt, J., Bedrosian, P., Booker, J., Leshou, C., Clarke, G., others, 2005. Crustal rheology of the Himalaya and Southern Tibet inferred from magnetotelluric data. Nature 438, 78–81.

Unsworth, M., Wenbo, W., Jones, A.G., Li, S., Bedrosian, P., Booker, J., Sheng, J., Ming, D., Handong, T., 2004. Crustal and upper mantle structure of northern Tibet imaged with magnetotelluric data. J. Geophys. Res. 109, B02403.

Vergne, J., Wittlinger, G., Hui, Q., Tapponnier, P., Poupinet, G., Mei, J., Herquel, G., Paul, A., 2002. Seismic evidence for stepwise thickening of the crust across the NE Tibetan plateau. Earth Planet. Sci. Lett. 203, 25–33. doi:16/S0012-821X(02)00853-1

Warner, M., 1990a. Absolute reflection coefficients from deep seismic reflections. Tectonophysics 173, 15–23.
Warner, M., 1990b. Basalts, water, or shear zones in the lower continental crust? Tectonophysics 173, 163–174.
Wei, W., Unsworth, M., Jones, A., Booker, J., Tan, H., Nelson, D., Chen, L., Li, S., Solon, K., Bedrosian, P., others, 2001. Detection of widespread fluids in the Tibetan crust by magnetotelluric studies. Science 292, 716.
Wittlinger, G., Farra, V., Vergne, J., 2004. Lithospheric and upper mantle stratifications beneath Tibet: new insights from Sp conversions. Geophys Res Lett 31, L19615.
Yilmaz, Ö., 2001. Seismic data analysis: processing, inversion, and interpretation of seismic data. SEG Books.
Yin, A., Dang, Y.Q., Zhang, M., Chen, X.H., McRivette, M.W., 2008. Cenozoic tectonic evolution of the Qaidam basin and its surrounding regions (Part 3): Structural geology, sedimentation, and regional tectonic reconstruction. Geol. Soc. Am. Bull. 120, 847.
Yin, A., Dang, Y., Zhang, M., McRivette, M.W., Burgess, W.P., Chen, X., 2007. Cenozoic tectonic evolution of Qaidam basin and its surrounding regions (part 2): Wedge tectonics in southern Qaidam basin and the Eastern Kunlun Range. Geol. Soc. Am. Spec. Pap. 433, 369.
Yue, H., Chen, Y.J., Sandvol, E., Ni, J., Hearn, T., Zhou, S., Feng, Y., Ge, Z., Trujillo, A., Wang, Y., 2012. Lithospheric and upper mantle structure of the northeastern Tibetan plateau. J. Geophys. Res. Solid Earth 1978–2012 117.
Zeng, R.S., Gan, R.J., 1961. Reflected waves from crustal interface in western Qaidam basin. Acta Geophys. Sin. 10, 120–125.
Zhang, Z., Yuan, X., Chen, Y., Tian, X., Kind, R., Li, X., Teng, J., 2010. Seismic signature of the collision between the east Tibetan escape flow and the Sichuan Basin. Earth Planet. Sci. Lett. 292, 254–264.
Zhao, J., Yuan, X., Liu, H., Kumar, P., Pei, S., Kind, R., Zhang, Z., Teng, J., Ding, L., Gao, X., others, 2010. The boundary between the Indian and Asian tectonic plates below Tibet. Proc. Natl. Acad. Sci. 107, 11229.
Zhao, L.-S., Helmberger, D.V., 1991. Geophysical implications from relocations of Tibetan earthquakes; hot lithosphere. Geophys. Res. Lett. 18, 2205–2208.
Zhao, W., Brown, L., Wu, Z., Klemperer, S.L., Shi, D., Mechie, J., Su, H., Tilmann, F., Karplus, M.S., Makovsky, Y., 2008. Seismology across the northeastern edge of the Tibetan Plateau. Eos Trans. Am. Geophys. Union 89, 487–487.
Zhao, W., Kumar, P., Mechie, J., Kind, R., Meissner, R., Wu, Z., Shi, D., Su, H., Xue, G., Karplus, M., 2011. Tibetan plate overriding the Asian plate in central and northern Tibet. Nat. Geosci. 4, 870–873.
Zhao, W.L., Morgan, W.J., 1987. Injection of Indian crust into Tibetan lower crust: A two-dimensional finite element model study. Tectonics 6, 489–504.
Zhao, W., Mechie, J., Brown, L.D., Guo, J., Haines, S., Hearn, T., Klemperer, S.L., Ma, Y.S., Meissner, R., Nelson, K.D., others, 2001. Crustal structure of central Tibet as derived from project INDEPTH wide-angle seismic data. Geophys. J. Int. 145, 486–498.

Zhao, W., Nelson, K.D., Che, J., Quo, J., Lu, D., Wu, C., Liu, X., 1993. Deep seismic reflection evidence for continental underthrusting beneath southern Tibet. Nature 366, 557–559.
Zhu, L., Helmberger, D.V., 1998. Moho Offset Across the Northern Margin of the Tibetan Plateau. Science 281, 1170 –1172. doi:10.1126/science.281.5380.1170

CHAPTER 2

SINOPROBE DEEP REFLECTION PROFILE REVEALS A NEO-PROTEROZOIC SUBDUCTION ZONE BENEATH THE SICHUAN BASIN

2.0 ABSTRACT

A new multichannel seismic reflection profile collected across the Sichuan Basin in southern China by the SINOPROBE Project images prominent reflectors that originate within the lower crust and penetrate well into the underlying mantle. The geometry of these mantle reflectors is very similar to those observed on other deep reflection profiles that have been interpreted as relicts of ancient subduction. Considering the geological history of the basement beneath and surrounding the Sichuan Basin, we propose that these newly revealed reflectors are the remnants of Neo-Proterozoic subduction that occurred along the NW margin of the Yangtze Craton, which gave rise to the magmatic arc rocks in the southeast Sichuan Basin. Moreover, preservation of these reflectors supports the interpretation of the Sichuan lithosphere as a well consolidated tectonic buttress against which the Tibetan Plateau has impinged to produce the Longmenshan orogenic belt.

2.1 INTRODUCTION

Deep seismic reflection profiling has been widely used to probe crustal structure since COCORP initiated large-scale systematic exploration of the continental crust with multichannel seismic surveys in the late 1970s. Subsequent programs such

as BIRPS, DEKORP, ECORS and LITHOPROBE in Europe and North America, among others, have compiled an extensive archive of lithospheric imagery across a variety of tectonic features. Inspired in part by the success of deep seismic profiling programs like COCORP, BIRPS and especially LITHOPROBE, as well as new array initiatives such as EarthScope, the SINOPROBE project was launched in 2007 to probe the crust and mantle beneath Asia. A key part of the SINOPROBE effort is the collection of regional multichannel deep reflection profiles across key tectonic features within China. This analysis is focused on a portion of one of those profiles, the South China profile, which currently extends about 1000 km from the southeastern Tibetan Plateau across the adjacent Sichuan Basin (Figure 2-1).

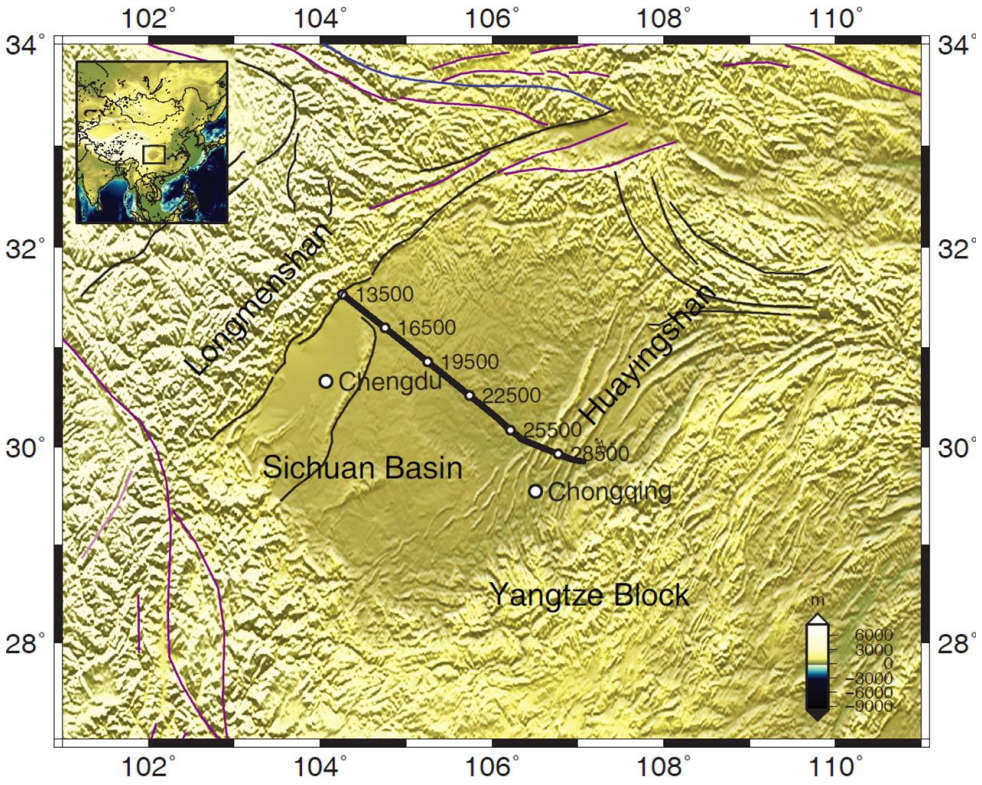

Figure 2-1 Location of Sinoprobe Sichuan profile (thick black line) between CDP (Common Depth Point) 13500 and 30000. Well Wei-28/117 (very close) is marked as square. Thin black lines=thrust faults, thin dark purple lines=left-lateral strike-slip faults, thin light purple lines=right-lateral strike-slip faults, thin blue lines=old suture zone (Taylor and Yin, 2009).

Of particular relevance to this study are those previous surveys which have recorded reflections from interfaces that lie well beneath the local Moho, i.e. mantle reflectors (Steer et al., 1998). One of the first and still one of the most dramatic examples of mantle reflectivity was acquired by BIRPS marine deep seismic surveys off the coast of northern England. The "Flannan Feature" (Figure 2-2a), first reported by Smythe et al. (1982) remains in many ways the archetype for dipping mantle reflectors, although subsequent BIRPS surveys found that it was not the only mantle structure delineated by reflection profiling in northern Britain. The competing interpretations of the "Flannan Feature" as either a fossil subduction zone (Morgan et al., 1994) or mantle extensional fault (Reston, 1990a) are also germane to this analysis.

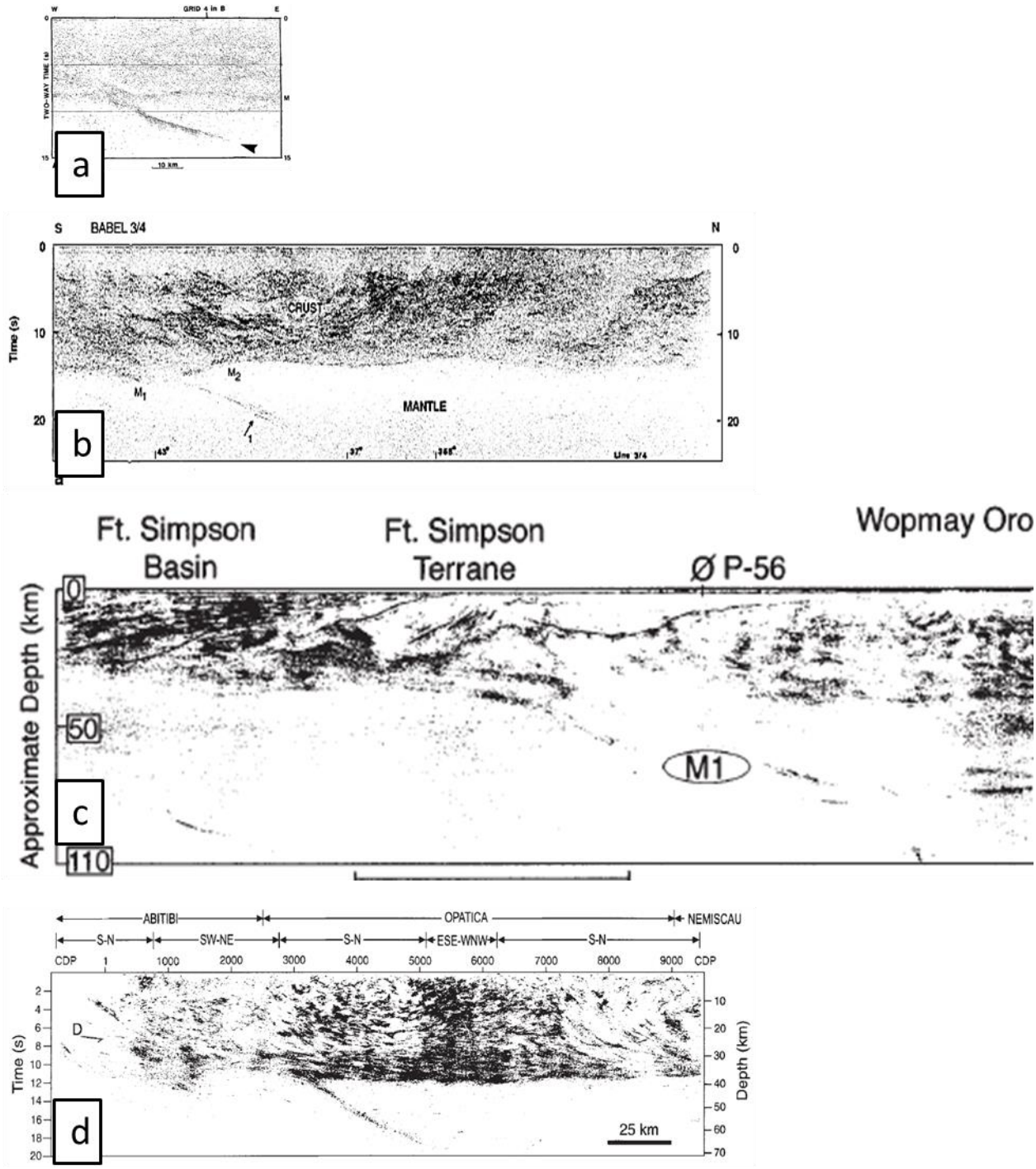

Figure 2-2 a) Migrated section GRID 11 profile from BIRPS program in north of Scotland (Flack et al., 1990); proposed fossil subduction age: Pre-Caledonian. b) Migrated profiles 3 and 4 of the BABEL project (Balling, 2000), proposed fossil subduction age: Early Proterozoic. c) Migrated LITHOPROBE profile across northwest Canada (Cook et al., 1999), only a part of which is shown here, proposed fossil subduction age: Early Proterozoic. d) Migrated LITHOPROBE profile 48 across eastern Canadian Precambrian terranes (Calvert et al., 1995), proposed fossil

subduction age: Archean. All seismic sections are shown at approximate 1:1 vertical-horizontal scale.

This Sichuan Basin segment of the SinoProbe transect is about 330 km long, consisting of over 16,500 CDPs (Common Depth Points) spaced 20-m apart (Figure 2-1). Explosive sources (20 to 100 kg) spaced 150 to 5000 m apart were used, resulting in nominal stacking folds of 50-60. This portion of the profile extends from the eastern foothills of the Longmenshan on the west to the middle of the Huayingshan fold and thrust belt on the east. The profile spans sedimentary rocks of the Sichuan Basin that range in age from Quaternary to Lower Jurassic and Triassic at the surface.

2.2 RESULTS AND DISCUSSION

2.2.1 The Sichuan Basin

The stacked (unmigrated and migrated) reflection section produced for this profile (Figure 2-3a,b) clearly delineates the sedimentary layers of the Sichuan Basin extending to depths in excess of 15 km beneath the western end of the profile. These sedimentary reflectors gradually thin from west to east, with their base becoming less distinct on the eastern end of the profile, where the layers above are tightly folded to form the Huayingshan thin-skin fold and thrust belt that characterizes the surface morphology (Figure 2-1).

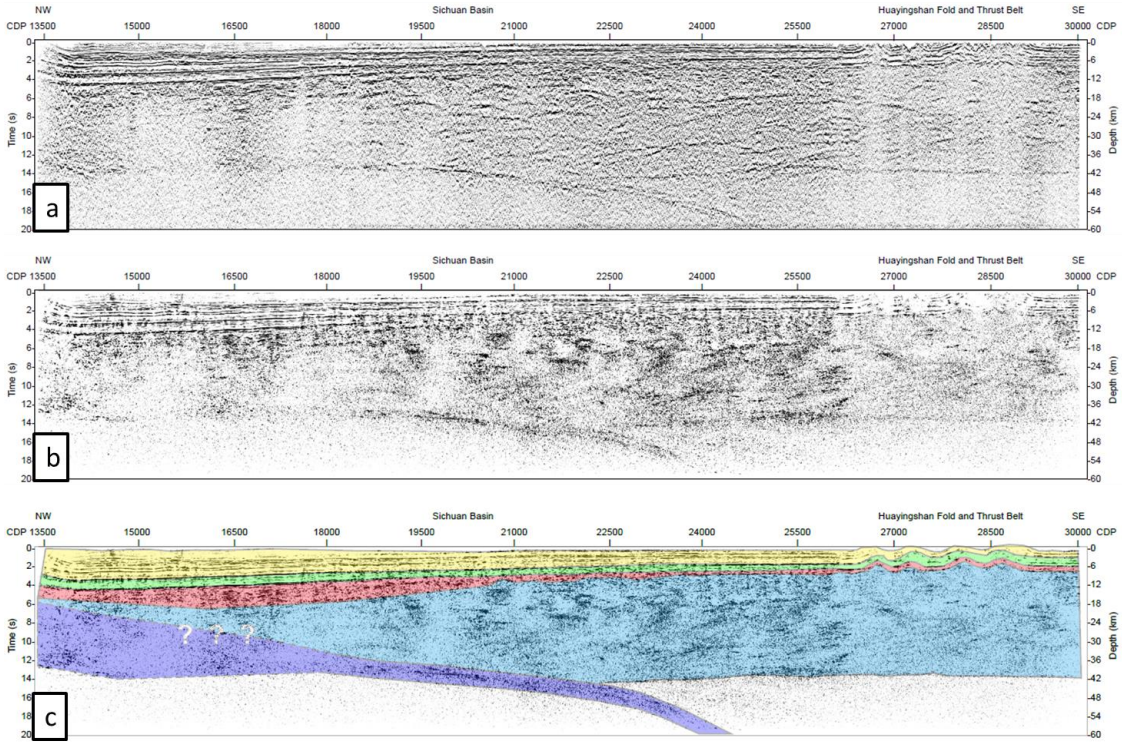

Figure 2-3 Sinoprobe Sichuan reflection profile. (a): Unmigrated seismic section, recorded to 20s two-way time, equivalent to about 60 km depth. Middle panel (b): Migrated seismic section using Vp=6.2 km/s for the subsedimentary crust. (c): Migrated section with interpretation. (Yellow: Mesozoic Strata; Green: Paleozoic Strata; Red: Precambrian Strata; Light Blue: crust beneath sedimentary layers; Dark Blue: subducting crust)

The dipping reflectors corresponding to the sedimentary rock layers on this profile can be easily correlated to those identified by previous seismic reflection and drilling data reported by Kang (1986) and Korsch et al. (1991). These stratigraphic correlations are shown in Figure 2-3c. Recent study by Zhang et al. (2012) interpret the oldest sedimentary rock recovered from drilling to belong to the Doushantuo group of ca. 555-635 Ma. (Doushantuo Formation: 555-635Ma (Condon et al., 2005; Zhang et al., 2005)). Kang (1986) and Zhang et al. (2012) both imply that there are perhaps several kilometers of even older sedimentary rocks beneath the known strata of Doushantuo Formation (Ediacaran age).

2.2.2 Moho and Basement

The most distinctive reflector beneath the sedimentary layering is a more or less continuous subhorizontal event that extends from about 15s (45 km) beneath CDP 22000 up to 14s (42 km) beneath CDP 30000. The seismic section above this marker is relatively and complexly reflective while few reflections lie below. This contrast is characteristic of the reflection Moho, or crust-mantle boundary, as seen on many other deep seismic profiles (e.g. (Cook et al., 2010; Mooney and Brocher, 1987)). Our interpretation of this event as the Moho beneath the central and southeastern Sichuan Basin is consistent with Moho depths estimated from receiver function studies (Robert et al., 2010; Zhang et al., 2010) and P wave tomography results (Xu and Song, 2010) beneath the western Sichuan basin. This Moho is variable in character, marked by strong amplitudes beneath the eastern basin but weak or non-existent, reflectivity beneath parts of the western basin. The westward weakening of Moho reflectivity may result in part from increased attenuation of seismic energy penetrating the thicker overlying sedimentary section, but the possibility that these amplitudes mark changes in the Moho itself cannot be ruled out.

Between the sedimentary units and the Moho, the seismic section corresponding to the middle to lower crust exhibits a laterally varying character across our profile. The central portion, between CDP 19500 and CDP 26500, shows stronger reflectivity in the middle to lower crust compared to segments to the northwest or southeast. The relative lack of reflectivity of the basement on the northwestern part (CDP 13500 to CDP 19500) may be due to a lateral change in crustal material but, like the weaker Moho, may also simply result from greater attenuation through the thicker

sedimentary section. The southeastern part (CDP 26500 to CDP 30000) has a reflective lower crust, but with generally lower amplitudes than the middle portion of the profile. However, here the presence of distinct Moho reflections suggests that shallow attenuation (insufficient penetration) is not responsible. We will argue below that at least some of these weakly crustal reflective areas may be associated with extensive plutonism during the neo-Proterozoic.

2.2.3 A Mantle Suture

The most striking feature of the Sichuan profile is a band of southeast dipping reflections that extend from about 13s (40 km) on the west to at least 20s (60 km) to the east, e.g. well into the mantle. We refer to this reflection sequence hereafter as the SESS (South-East Sichuan Subduction) sequence.

The geometry of these reflectors is very similar to the mantle reflections reported from other deep seismic profiles, especially those from Europe and Canada. Such events (e.g. Figure 2-2) have been reported from Scotland (Smythe et al., 1982; Morgan et al., 1994; Flack et al., 1990; Flack and Warner, 1990; Warner and McGeary, 1987; Warner et al., 1996), the Baltic Sea (BABEL Working Group, 1990; Balling, 2000), the North Sea (MONA LISA Working Group, 1997; Reston, 1990b), Canada (Calvert et al., 1995; Cook et al., 1999), and the Pyrenees (Choukroune, 1989; Suriñach et al., 1993) (not shown). Many of these studies attribute such reflections to fossil or relict subduction zones of different ages, spanning from the Cenozoic (Pyrenees), mid-Paleozoic (Caledonian), early Proterozoic (Balling, 2000; Cook et al., 1999) and Archean (BABEL Working Group, 1990; Calvert et al., 1995; Choukroune, 1989; Cook et al., 1999; Morgan et al., 1994; Suriñach et al., 1993; Warner et al.,

1996).

The subduction zone interpretation is attractive, not only because it provides a convenient explanation for the dipping geometry, but also because phase changes in the subducted materials (e.g. basaltic crust to eclogite) can explain the strong reflectivity of these events (Balling, 2000; Morgan et al., 1994). The top of the subduction zone presumably transformed to eclogite from oceanic basalt. It is argued that the density contrast between eclogite and peridotite together with the corresponding velocity contrast (together as impedance contrast) is likely to give a strong seismic reflection (Morgan et al., 1994).

However, other explanations have been proposed, including mantle shear zones associated with either extension, compression or both (BABEL Working Group, 1990; Flack et al., 1990; Klemperer and Hurich, 1990; MONA LISA Working Group, 1997; Reston, 1990b; Snyder et al., 1997). Geophysical studies using other approaches in this region may shed some light on the character of this feature beneath Sichuan Basin. Ambient noise surface wave tomography (Zheng et al., 2010) shows relatively high shear wave velocities (15% higher) beneath the southeastern Sichuan Basin at depth of 40-50 km, up to 15% higher than the northwest Sichuan lithosphere. This high S wave velocity could be interpreted as being due to eclogitized oceanic crust at depth (Worthington et al., 2013). Gravity (Lou and Wang, 2005) also suggests an anomaly from a deep, relatively high density source beneath southeastern Sichuan Block, again consistent with an eclogitized mass in the upper mantle. Other results suggest a crustal terrane boundary at depth, as might be expected across a suture zone. For example, two areas of high P wave velocity in the lower crust and high Pn velocity

beneath the Sichuan Basin are shown by Xu and Song (2010). The most recent magnetotelluric study (L. Zhang et al., 2013) from Sinoprobe along the same profile indicates a lower crust and upper mantle beneath the southeast part of Sichuan block with resistivities of about 1000 Ωm in contrast to the 100-300 Ωm resistivity values at the same depths beneath the northwestern Sichuan block.

2.2.4 Neo-Proterozoic orogeny in the Yangtze Craton

The subduction interpretation also provides an important new constraint on tectonic models of the evolution of the South China Block. The Sichuan Basin is geologically considered as the most stable and coherent part of the Yangtze craton. It contains a metamorphic basement and cover successions ranging from Neoproterozoic to Cenozoic, well established by petroleum exploration. Ages of the basement are poorly constrained, but the basement rocks can be traced to surrounding exposures.

Luo et al. (1986) first reports a 740.99 Ma age for granite pluton encountered by the Wei-28 well (Figure 2-1). In a more recent study, Gu et al. (2014) report the age of basal granite from Wei-117, which is very close to Wei-28 geographically, of 794+/-11 Ma. Zhou et al. (2002; 2002; Zhou et al., 2006) reports gneiss and granite of similar age (e.g., 750 to 860 Ma) at the surface along the western and northern margins of the Yangtze Block adjacent to the Sichuan basin.

Several tectonic models have been proposed to as explain the evolution of the Yangtze craton. One speculates that widespread bimodal magmatism represents the first episode of Neoproterozoic plume activity which commenced at ~825 Ma, which resulted in crustal melting and continental rifting as young as ~740 Ma (Cryogenian) (Wang and Li, 2003; X. Li et al., 2003; Li et al., 2008; Wang et al., 2007; Zhang et al.,

2008).

Other models, however, interpret the 825–740 Ma magmatism in South China as a result of arc magmatism (Cawood et al., 2013; M. F. Zhou et al., 2002), or post-orogenic slab break-off (Wang et al., 2006).

These dates have been used to argue for a subduction event along the western and northern edges of the Yangtze Block during the Neoproterozoic when the Yangtze Block was positioned next to India or western Australia (Cawood et al., 2013; S. Zhang et al., 2013).

We suggest that the SESS reflection sequence supports a plate tectonic origin, in particular Neoproterozoic subduction along the NW margin of Yangtze block (M. Zhou et al., 2002; M. F. Zhou et al., 2002; Zhou et al., 2006). If these reflectors originated before 750-860 Ma, it seems unlikely that they would have survived the overprint of a mantle superplume. In other words, we believe that the mantle superplume activity speculated by Li et al. (2003) to accompany an intensive continental uplift and rifting would most likely have obliterated any pre-existing sub-Moho structure.

Close inspection of the reflections marking the strata with the sedimentary Sichuan base reveal of number of relatively small fault offsets and minor folding, probably related to recent compression along the southeast margin of the Tibetan Plateau. However we argue that the relative lack of major disruption of the earliest sedimentary and igneous rock outcrops along the west margin of the Sichuan basin as well as those imaged as relatively continuous and undeformed reflections at the base of the Sichuan basin by this survey places a lower limit on the age of lithospheric

deformation to be at least ~830 Ma (M. F. Zhou et al., 2002; Z. X. Li et al., 2003), i.e. the last major thermotectonic event recognized in the area. Any earlier event of major extent should have seriously deformed or obliterated the SESS sequence.

The SESS sequence lies at a depth of 35 to 55 km (after migration) relative to the base of the Sichuan sedimentary sequence. After stripping the sedimentary wedge and applying migration using the seismic velocities estimated from the reflection survey, the key mantle reflections exhibit an apparent dip of 15 degrees (assuming Vp=8 km/s in the mantle). Linking these deep events to surface manifestations of presumably related subduction is far from straightforward. Clearly an east directed (in modern coordinates) subduction polarity is involved. However, the mantle reflections lie about 100 km to the east of Chengdu, while the subducting slab proposed by Zhou et al. (2002) must have had its trench and volcanic arc a few hundred kilometers to the west of Chengdu (Figure 2-4). The upward/westward extension of the interpreted lithospheric suture as represented by the SESS sequence is poorly constrained by the crustal reflectivity patterns. The greater reflectivity of the basement under the eastern Sichuan Basin, as compared to the westernmost portion of this profile might simply be an artifact of greater attenuation through the thicker sedimentary strata to the west. However it is also consistent with the juxtaposition of two different crustal terranes. Furthermore, any shallow crustal “suture” must be laterally displaced by several hundred kilometers from its mantle counterpart as represented by the SESS sequence. However, such far travelled, low angle underthrusting is not unreasonable; similar underthrust geometries have been proposed, for example, for the geometry of continent-continent collision of the Himalayas and the Tibetan Plateau (Hauck et al.,

1998; Nelson et al., 1996). Thus the interpretation in Figure 2-4 is one plausible but non-unique extrapolation of our interpretation.

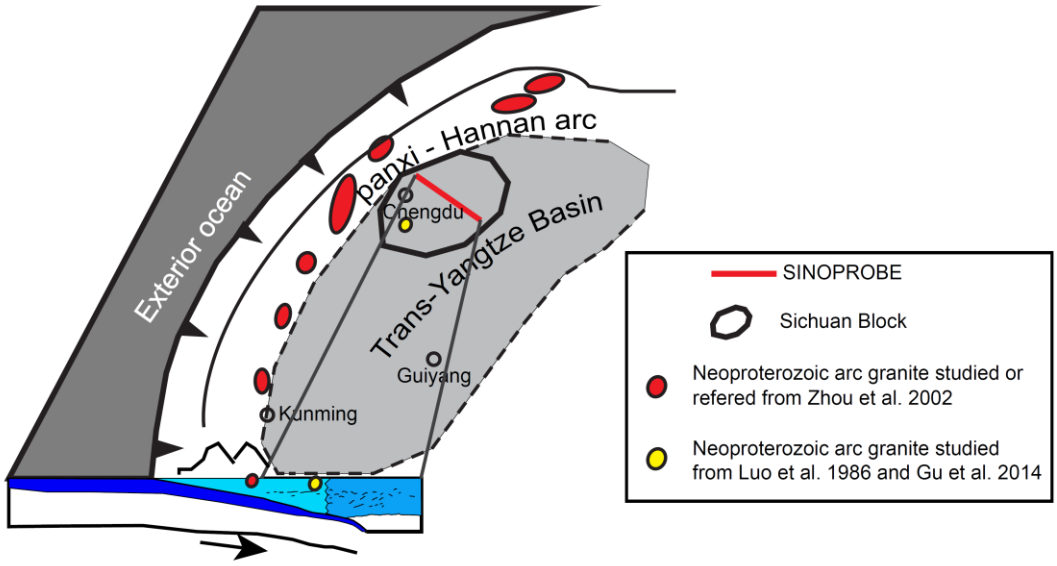

Figure 2-4 A recent (M. F. Zhou et al., 2002) plate tectonic model for Neoproterozoic amalgamation of the Yantze block, with key elements of the interpretation of the SINOPROBE deep seismic profile superimposed.

A low angle, far traveled correlation of the mantle reflectors into the upper crust to the west begs the question of whether the mantle reflections correspond to the mantle root of faulting related to the much younger formation of the Longmenshan or the Sichuan sedimentary basin. We find this interpretation less plausible because the thrust sense of offset is opposite to that one would expected from any downfaulting associated with basin subsidence or uplift of the Longmenshan(Guo et al., 2013). Moreover, it seems unlikely that far traveled faults of Cenozoic vintage would not leave a more impressive record in the older Sichuan Basin sedimentary rocks (Liu et al., 2012).

If this Neoproterozoic subduction zone beneath the Sichuan Basin has retained its rather complex yet coherent shape for some 800 million years, there cannot be any

major disturbance (e.g. delamination of the lower crust or upper mantle) at depth beneath the Sichuan Basin since the Neoproterozoic. This situation is very different from the North China Block, where there is abundant evidence of Mesozoic lithospheric thinning associated with delamination mainly in its eastern part (Zhai et al., 2007; Zhu et al., 2011).

2.3 IMPLICATIONS FOR CENOZOIC TECTONICS

The Sichuan Basin has long been viewed as a tectonic buttress resisting eastward expansion of the Tibetan Plateau (Royden et al., 2008; Zhao and Morgan, 1985). With due respect to faulting of the basin near the Longmenshan (Guo et al., 2013), the lack of major deformation within the basin contrast to the deformation of the Longmenshan region, is strong evidence of contrasting lithospheric rheology. The presence and preservation of this Neo-Proterozoic feature suggests that the lowermost crust and upper mantle are major contributors to the contemporary lithospheric strength of the Sichuan block (Clark and Royden, 2000).

REFERENCES

BABEL Working Group, 1990. Evidence for early Proterozoic plate tectonics from seismic reflection profiles in the Baltic shield. Nature 348, 34–38.

Balling, N., 2000. Deep seismic reflection evidence for ancient subduction and collision zones within the continental lithosphere of northwestern Europe. Tectonophysics 329, 269–300.

Calvert, A.J., Sawyer, E.W., Davis, W.J., Ludden, J.N., 1995. Archaean subduction inferred from seismic images of a mantle suture in the Superior Province.

Cawood, P.A., Wang, Y., Xu, Y., Zhao, G., 2013. Locating South China in Rodinia and Gondwana: A fragment of greater India lithosphere? Geology 41, 903–906. doi:10.1130/G34395.1

Choukroune, P., 1989. The ECORS Pyrenean deep seismic profile reflection data and the overall structure of an orogenic belt. Tectonics 8, 23–39.

Clark, M.K., Royden, L.H., 2000. Topographic ooze: Building the eastern margin of Tibet by lower crustal flow. Geology 28, 703.

Condon, D., Zhu, M., Bowring, S., Wang, W., Yang, A., Jin, Y., 2005. U-Pb ages from the neoproterozoic Doushantuo Formation, China. Science 308, 95–98.

Cook, F.A., van der Velden, A.J., Hall, K.W., Roberts, B.J., 1999. Frozen subduction in Canada's Northwest Territories: Lithoprobe deep lithospheric reflection profiling of the western Canadian Shield. Tectonics 18, 1–24.

Cook, F.A., White, D.J., Jones, A.G., Eaton, D.W., Hall, J., Clowes, R.M., 2010. How the crust meets the mantle: Lithoprobe perspectives on the Mohorovicic discontinuity and crustmantle transition. Can. J. Earth Sci. 47, 315–351.

Flack, C.A., Klemperer, S.L., McGeary, S.E., Snyder, D.B., Warner, M.R., 1990. Reflections from mantle fault zones around the British Isles. Geology 18, 528–532.

Flack, C., Warner, M., 1990. Three-dimensional mapping of seismic reflections from the crust and upper mantle, northwest of Scotland. Tectonophysics 173, 469–481.

Guo, X., Gao, R., Randy Keller, G., Xu, X., Wang, H., Li, W., 2013. Imaging the crustal structure beneath the eastern Tibetan Plateau and implications for the uplift of the Longmen Shan range. Earth Planet. Sci. Lett. 379, 72–80.

Gu, Z., Zhang, W., Yuan, M., 2014. Zircon SHRIMP U-Pb dating of basal granite and its geological significance in Weiyuan area of Sichuan Basin. Chin. J. Geol.

Hauck, M.L., Nelson, K.D., Brown, L.D., Zhao, W., Ross, A.R., 1998. Crustal structure of the Himalayan orogen at 90 east longitude from Project INDEPTH deep reflection profiles. Tectonics 17, 481–500.

Kang, Y., 1986. The basement structure Of Sichuan Basin and its relationship to the overlying sequences. Exp Pet. Geol 8, 235–242.

Klemperer, S.L., Hurich, C.A., 1990. Lithospheric structure of the North Sea from deep seismic reflection profiling. Tecton. Evol. North Sea Rifts 37–63.

Korsch, R.J., Huazhao, M., Zhaocai, S., Gorter, J.D., 1991. The Sichuan basin, southwest China: a late proterozoic (Sinian) petroleum province. Precambrian Res. 54, 45–63.

Liu, S., Deng, B., Li, Z., Sun, W., 2012. Architecture of basin-mountain systems and their influences on gas distribution: A case study from the Sichuan basin, South China. J. Asian Earth Sci. 47, 204–215.

Li, X., Li, Z., Zhou, H., Liu, Y., Liang, X., Li, W., 2003. SHRIMP U-Pb zircon age, geochemistry and Nd isotope of the Guandaoshan pluton in SW Sichuan: Petrogenesis and tectonic significance. Sci. China Ser. Earth Sci. 46, 73–83.

Li, Z.X., Bogdanova, S.V., Collins, A.S., Davidson, A., De Waele, B., Ernst, R.E., Fitzsimons, I.C.W., Fuck, R.A., Gladkochub, D.P., Jacobs, J., Karlstrom, K.E., Lu, S., Natapov, L.M., Pease, V., Pisarevsky, S.A., Thrane, K., Vernikovsky, V., 2008. Assembly, configuration, and break-up history of Rodinia: A synthesis. Precambrian Res. 160, 179–210. doi:10.1016/j.precamres.2007.04.021

Li, Z.X., Li, X.H., Kinny, P.D., Wang, J., Zhang, S., Zhou, H., 2003. Geochronology of Neoproterozoic syn-rift magmatism in the Yangtze Craton, South China and correlations with other continents: evidence for a mantle superplume that broke up Rodinia. Precambrian Res. 122, 85–109.

Lou, H., Wang, C., 2005. Wavelet analysis and interpretation of gravity data in Sichuan-Yunnan region, China. Acta Seismol. Sin. 18, 552–561.

Luo, Z., 1986. IS THERE A PALEOCONTINENTAL NEUCLEUS IN CENTRAL SICHUAN [J]. J. Chengdu Univ. Technol. Sci. Technol. Ed. 3, 007.

MONA LISA Working Group, 1997. MONA LISA-Deep seismic investigations of the lithosphere in the southeastern North Sea. Tectonophysics 269, 1–19.

Mooney, W.D., Brocher, T.M., 1987. Coincident seismic reflection/refraction studies of the continental lithosphere: a global review. Geophys. J. R. Astron. Soc. 89, 1–6.

Morgan, J.V., Hadwin, M., Warner, M.R., Barton, P.J., Morgan, R.P., 1994. The polarity of deep seismic reflections from the lithospheric mantle: evidence for a relict subduction zone. Tectonophysics 232, 319–328.

Nelson, K.D., Zhao, W., Brown, L.D., Kuo, J., Che, J., Liu, X., Klemperer, S.L., Makovsky, Y., Meissner, R., Mechie, J., Kind, R., Wenzel, F., Ni, J., Nabelek, J., Leshou, C., Tan, H., Wei, W., Jones, A.G., Booker, J., Unsworth, M., Kidd, W.S.F., Hauck, M., Alsdorf, D., Ross, A., Cogan, M., Wu, C., Sandvol, E., Edwards, M., 1996. Partially Molten Middle Crust Beneath Southern Tibet: Synthesis of Project INDEPTH Results. Science 274, 1684 –1688. doi:10.1126/science.274.5293.1684

Reston, T.J., 1990a. The lower crust and the extension of the continental lithosphere: kinematic analysis of BIRPS deep seismic data. Tectonics 9, 1235–1248.

Reston, T.J., 1990b. Mantle shear zones and the evolution of the northern North Sea basin. Geology 18, 272–275.

Robert, A., Zhu, J., Vergne, J., Cattin, R., Chan, L.S., Wittlinger, G., Herquel, G., de Sigoyer, J., Pubellier, M., Zhu, L.D., 2010. Crustal structures in the area of the 2008 Sichuan earthquake from seismologic and gravimetric data. Tectonophysics 491, 205–210. doi:10.1016/j.tecto.2009.11.010

Royden, L.H., Burchfiel, B.C., van der Hilst, R.D., 2008. The geological evolution of the Tibetan Plateau. Science 321, 1054.

Smythe, D.K., Dobinson, A., McQuillin, R., Brewer, J.A., Matthews, D.H., Blundell, D.J., Kelk, B., 1982. Deep structure of the Scottish Caledonides revealed by the MOIST reflection profile. Nature 299, 338–340. doi:10.1038/299338a0

Snyder, D.B., England, R.W., McBride, J.H., 1997. Linkage between mantle and crustal structures and its bearing on inherited structures in northwestern Scotland. J. Geol. Soc. 154, 79–83.

Steer, D.N., Knapp, J.H., Brown, L.D., 1998. Super-deep reflection profiling: exploring the continental mantle lid. Tectonophysics 286, 111–121.

Suriñach, E., Marthelot, J.M., Gallart, J., Daignières, M., Hirn, A., 1993. Seismic images and evolution of the Iberian crust in the Pyrenees. Tectonophysics 221, 67–80.

Taylor, M., Yin, A., 2009. Active structures of the Himalayan-Tibetan orogen and their relationships to earthquake distribution, contemporary strain field, and Cenozoic volcanism. Geosphere 5, 199.

Wang, J., Li, Z.-X., 2003. History of Neoproterozoic rift basins in South China: implications for Rodinia break-up. Precambrian Res. 122, 141–158.

Wang, X.-C., Li, X.-H., Li, W.-X., Li, Z.-X., 2007. Ca. 825 Ma komatiitic basalts in South China: First evidence for> 1500 C mantle melts by a Rodinian mantle plume. Geology 35, 1103–1106.

Wang, X.-L., Zhou, J.-C., Qiu, J.-S., Zhang, W.-L., Liu, X.-M., Zhang, G.-L., 2006. LA-ICP-MS U-Pb zircon geochronology of the Neoproterozoic igneous rocks from Northern Guangxi, South China: Implications for tectonic evolution. Precambrian Res. 145, 111–130.

Warner, M., McGeary, S., 1987. Seismic reflection coefficients from mantle fault zones. Geophys. J. R. Astron. Soc. 89, 223–230.

Warner, M., Morgan, J., Barton, P., Morgan, P., Price, C., Jones, K., 1996. Seismic reflections from the mantle represent relict subduction zones within the continental lithosphere. Geology 24, 39–42.

Worthington, J.R., Hacker, B.R., Zandt, G., 2013. Distinguishing eclogite from peridotite: EBSD-based calculations of seismic velocities. Geophys. J. Int. 193, 489–505. doi:10.1093/gji/ggt004

Xu, Z.J., Song, X., 2010. Joint inversion for crustal and Pn velocities and Moho depth in Eastern Margin of the Tibetan Plateau. Tectonophysics 491, 185–193. doi:10.1016/j.tecto.2009.11.022

Zhai, M., Fan, Q., Zhang, H., Sui, J., Shao, J., 2007. Lower crustal processes leading to Mesozoic lithospheric thinning beneath eastern North China: Underplating, replacement and delamination. Lithos 96, 36–54. doi:10.1016/j.lithos.2006.09.016

Zhang, J., Shen, P., Yang, W., Yang, Y., Zeng, F., 2012. New understandings of Pre-Sinian sedimentary rocks in the Sichuan Basin and the significance of oil and gas exploration there. Nat. Gas Ind. 32, 1–5.

Zhang, L., Wei, W., Jin, S., Ye, G., Jing, J., Dong, H., Xie, C., Wang, H., Li, B., 2013. Lithospheric Structure of the Eastern Margin of the Tibetan Plateau Revealed by Magnetotelluric Data. AGU Fall Meet. Abstr.

Zhang, S., Gao, R., Li, H., Hou, H., Wu, H., Li, Q., Yang, K., Li, C., Li, W., Zhang, J., Yang, T., Keller, G.R., Liu, M., 2013. Crustal structures revealed from a deep seismic reflection profile across the Solonker suture zone of Central Asian Orogenic Belt, north China. An integrated interpretation. Tectonophysics in press.

Zhang, S., Jiang, G., Dong, J., Han, Y., Wu, H., 2008. New SHRIMP U-Pb age from the Wuqiangxi Formation of Banxi Group: Implications for rifting and stratigraphic erosion associated with the early Cryogenian (Sturtian) glaciation in South China. Sci. China Ser. Earth Sci. 51, 1537–1544.

Zhang, S., Jiang, G., Zhang, J., Song, B., Kennedy, M.J., Christie-Blick, N., 2005. U-Pb sensitive high-resolution ion microprobe ages from the Doushantuo Formation in south China: Constraints on late Neoproterozoic glaciations. Geology 33, 473–476.

Zhang, Z., Yuan, X., Chen, Y., Tian, X., Kind, R., Li, X., Teng, J., 2010. Seismic signature of the collision between the east Tibetan escape flow and the Sichuan Basin. Earth Planet. Sci. Lett. 292, 254–264.

Zhao, W.L., Morgan, W.J., 1985. Uplift of Tibetan plateau. Tectonics 4, 359–369.

Zheng, Y., Yang, Y., Ritzwoller, M.H., Zheng, X., Xiong, X., Li, Z., 2010. Crustal structure of the northeastern Tibetan plateau, the Ordos block and the Sichuan basin from ambient noise tomography. Earthq. Sci. 23, 465–476.

Zhou, M.F., Ma, Y., Yan, D.P., Xia, X., Zhao, J.H., Sun, M., 2006. The Yanbian terrane (Southern Sichuan Province, SW China): a Neoproterozoic arc assemblage in the western margin of the Yangtze block. Precambrian Res. 144, 19–38.

Zhou, M.F., Yan, D.P., Kennedy, A.K., Li, Y., Ding, J., 2002. SHRIMP U–Pb zircon geochronological and geochemical evidence for Neoproterozoic arc-magmatism along the western margin of the Yangtze Block, South China. Earth Planet. Sci. Lett. 196, 51–67.

Zhou, M., K. Kennedy, A., Sun, M., Malpas, J., Michael Lesher, C., 2002. Neoproterozoic Arc-Related Mafic Intrusions along the Northern Margin of South China: Implications for the Accretion of Rodinia. J. Geol. 110, 611–618. doi:10.1086/341762

Zhu, R., Chen, L., Wu, F., Liu, J., 2011. Timing, scale and mechanism of the destruction of the North China Craton. Sci. China Earth Sci. 54, 789–797.

CHAPTER 3

MAPPING LITHOSPHERIC STRUCTURE BY MULTICHANNEL PROCESSING OF EARTHSCOPE RECORDINGS OF DEPTH PHASE PRECURSORS ACROSS THE ANDEAN OROGENIC BELT

3.0 ABSTRACT

New large scale, high density seismic arrays provide a powerful means of detailing lithospheric features (including crustal and upper mantle) by exploiting rarely used seismic arrivals such as the precursors to the depth phase pP. From the EarthScope USArray dataset we have extracted recordings between 2003 and 2012 of 124 earthquakes from depths greater than 100km that lie within the subduction zone beneath the Andes. With proper signal enhancement, precursors to the pP phase from slab earthquakes as small as M=5.5 beneath South America were successfully identified as underside reflections from key lithospheric discontinuities. In this study we have detected and mapped a) intracrustal reflectors (pcP), including possible magma bodies, phase changes and decollements; b) the crust-mantle boundary, or Moho (pmP); and c) possible upper mantle discontinuities (puP). The redundancy provided by EarthScope's USArray allows us to increase signal-to-noise ratios by stacking within reflection point bins and by the application of multichannel coherency filters. Synthetic seismograms and traveltime calculations are used to confirm that the observed arrivals are appropriate for reflections from source side structure. Our results compare favorably with results from independent studies of these discontinuities where available, including controlled-source seismic reflection surveys, receiver

function studies, and previous teleseismic precursor studies in the Andes. In particular our results offer numerous new estimates of crustal thickness in areas where such information has been lacking, as well as evidence of previously unrecognized intracrustal discontinuities, thus providing important new constraints on models of Andean orogenic evolution.

3.1 INTRODUCTION

The Andes is a mountain range about 8000 km long, the most dramatic geomorphologic feature of the South America. Unlike the Himalaya, which formed by continent-continent collision, the Andes result from subduction of oceanic lithosphere beneath a continental margin. The most prominent feature of the central part of Andes, the Altiplano-Puna plateau, is the second highest and largest continental plateau after the Tibetan plateau in the world.

The Andes have variously been associated with crustal thickening caused by crustal shortening (Isacks, 1988), magmatic additions (Babeyko et al., 2006; Oncken et al., 2006), delamination of the lower crust and upper mantle (Kay and Kay, 1993), and lower crustal flow (Gerbault et al., 2005). There have been a number of reviews of the evolution of central Andes, including that of Allmendinger et al. (1997) and the more recent summary by Kay and Coira (2009).

There have been a number of conventional geophysical surveys in Andes, which are summarized in (Figure 3-1).

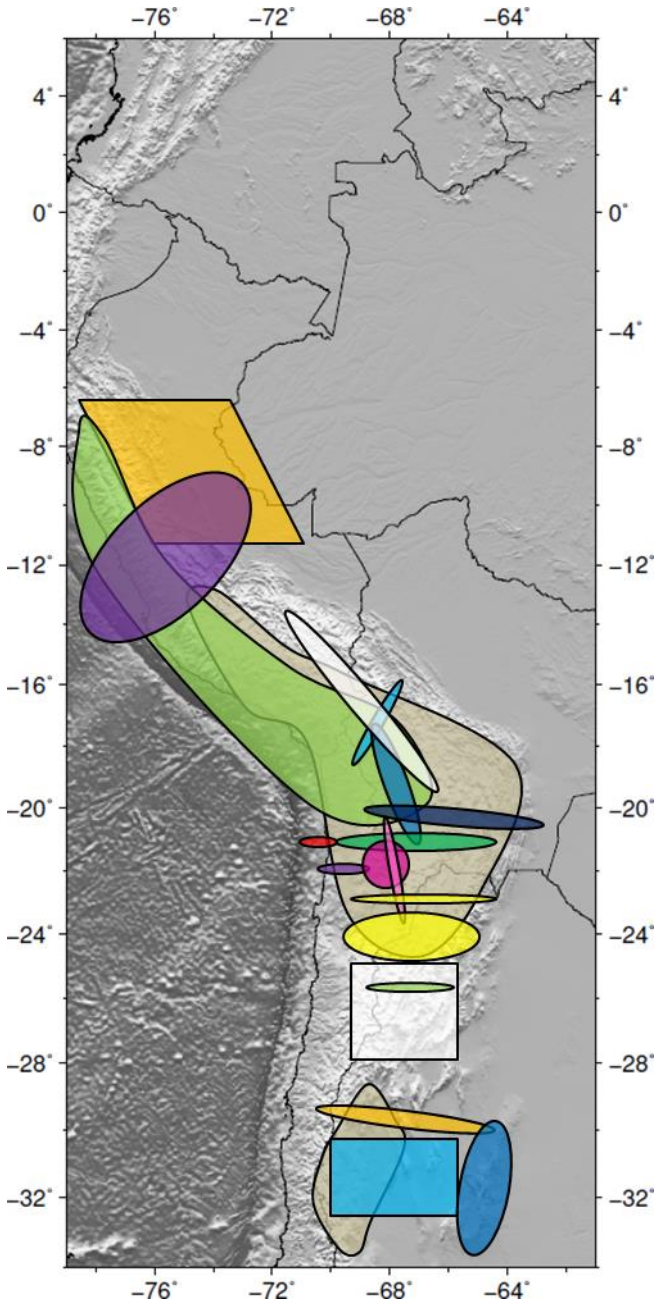

Figure 3-1 Previous seismic studies in the Andes (5°N to 33°S): a central Peru seismic array used to determine crustal discontinuities (James and Snoke, 1994) (Orange, north); a seismic velocity study using local earthquakes near central Peru (Dorbath, 1996) (purple, north); a study of seismicity and focal mechanisms study in Peru, Ecuador and southern Colombia (Suárez et al., 1983) (light green, north); an explosion seismic experiment in the Peru-Bolivia Altiplano (Ocola and Meyer, 1972) (white, north); a teleseismic survey in the northern Altiplano used to study lithospheric model (Dorbath et al., 1993) (turquoise, north); the SEDA and BANJO passive seismic experiments (Zandt et al., 1996; Swenson et al., 2000; Beck and Zandt, 2002) (light blue, north and dark blue); the PISCO seismic array (Graeber and Asch, 1999; Schmitz et al., 1999) (light purple) and the CALAMA passive seismic experiment in Chile for a seismic velocity study (Graeber and Asch, 1999) (purple); the ANCORP deep seismic reflection survey across Chile and

Bolivia (ANCORP Working Group, 1999, 2003; Wölbern et al., 2009) (green); the PAMB passive array in Altiplano-Puna volcanic complex (APVC) (Chmielowski et al., 1999; Zandt et al., 2003) (pink); the PUNA passive arrays in northwestern Argentina (Yuan et al., 2000, 2002) (yellow); the REFUCA passive experiment in Argentina (Heit et al., 2007; Wölbern et al., 2009) (light green, south); the Southern PUNA passive seismic array in northern Argentina and Chile (Bianchi et al., 2013; Calixto et al., 2014, 2013; Heit et al., 2014; Kay et al., 2014; Liang et al., 2014; Mulcahy et al., 2014) (white, south); the passive seismic CHARGE study in the central Argentina (Fromm et al., 2004; Gilbert et al., 2006; Gans et al., 2011) (orange, south); the passive SIEMBRA (Gans et al., 2011) (turquoise, south); and ESP arrays (Gans et al., 2011) in central Argentina (light blue, south); broad pP precursor study (McGlashan et al., 2008) (tan). However, large portions of the Andes, northern Peru for example, are still largely unprobed by any modern geophysical studies and many significant gaps remain in the central to southern Andes as well.

Precursors to the common teleseismic depth phases pP and sS (Figure 3-2) were first used to map the Moho in the Andes by Zandt et al. (1994). McGlashan et al. (2008) expanded on this work, reporting reflections from intracrustal and sub-crustal interfaces as well as the Moho. Precursors have been used to map various discontinuities within the mantle in other parts of the world (Zhang and Lay, 1993; Flanagan and Shearer, 1998, 1999; Schmerr and Garnero, 2006; Zheng et al., 2007). However, most of these studies were based on analysis of a single earthquake recorded by a few tens of stations (Zhang and Lay, 1993; Flanagan and Shearer, 1998) or by stacking relatively few seismograms from earthquakes at different locations or from different seismic networks (Flanagan and Shearer, 1999; Schmerr and Garnero, 2006; Zheng et al., 2007).

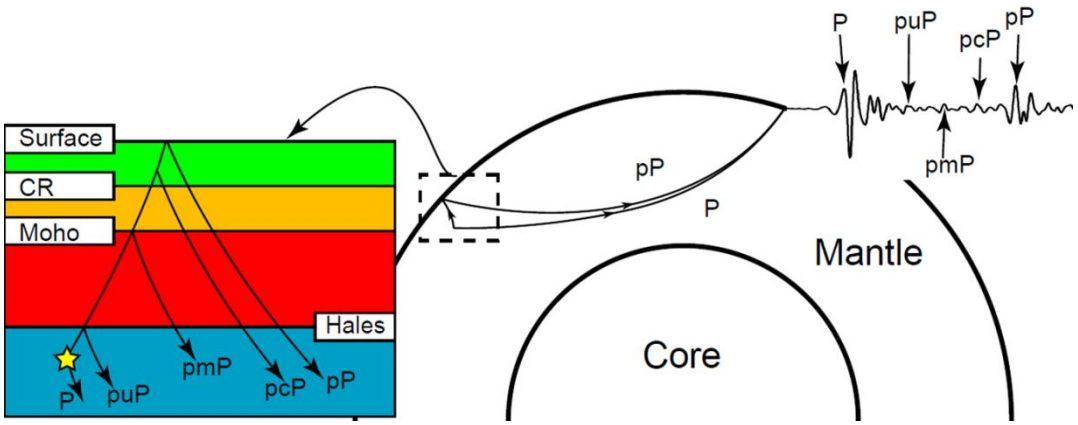

Figure 3-2 Illustration of raypaths for P, pP and precursor phases (pmP, pcP, puP etc.) expected for underside reflections from the Moho, crustal reflectors (CR) and upper mantle reflectors (MR) such as Hales discontinuity as recorded at teleseismic stations. From McGlashan et al. (2008)

EarthScope's USArray, which began deployment in 2004, has provided an unprecedented opportunity to improve on these prior results by facilitating the use of multichannel signal enhancement techniques. Here we collected seismograms for 124 earthquakes (Figure 3-2 and Figure 3-3) from South America with magnitudes greater than 5.5 and depths greater than 100km during the period 2003-2012, as recorded mainly by EarthScope USArray as well as other permanent and temporary stations in the U.S. operating during that period (Figure 3-4). We have been able to identify clear P and pP (the P wave reflected from the surface near the source) arrivals from 84 of those 124 events. We have used these data to derive new estimates of crustal thickness and structure in a region arranging from Colombia in the north to Central Chile and Argentina to the south. These results not only compare favorably with previous independent studies, where available, they provide the first estimates of crustal structure in several parts of the Andes and adjacent cratons.

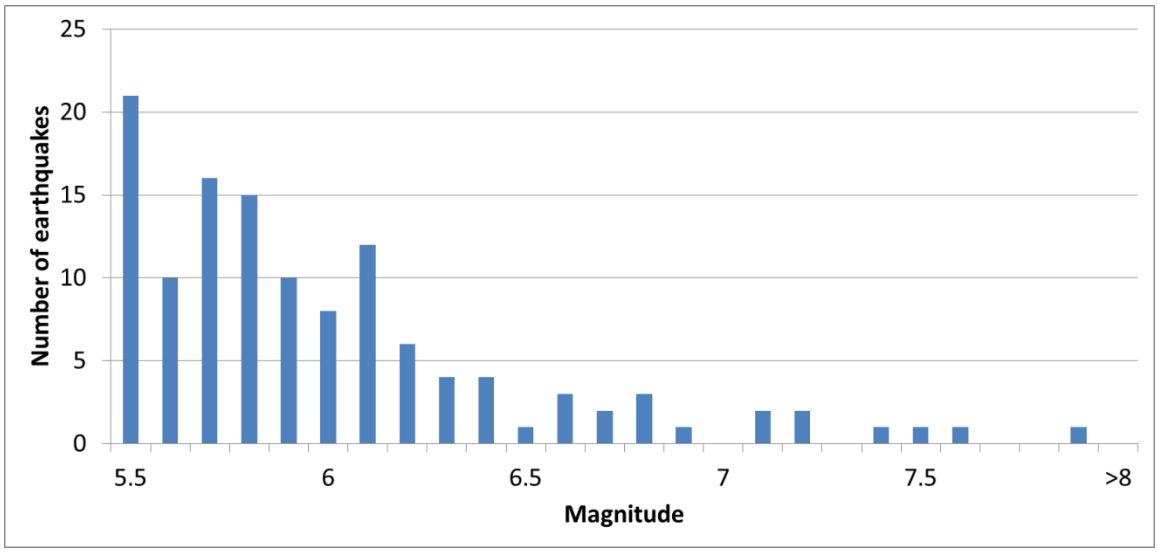

Figure 3-3 Magnitude distribution of events examined in our study. Array processing allowed the effective utilization of events as small as M=5.5.

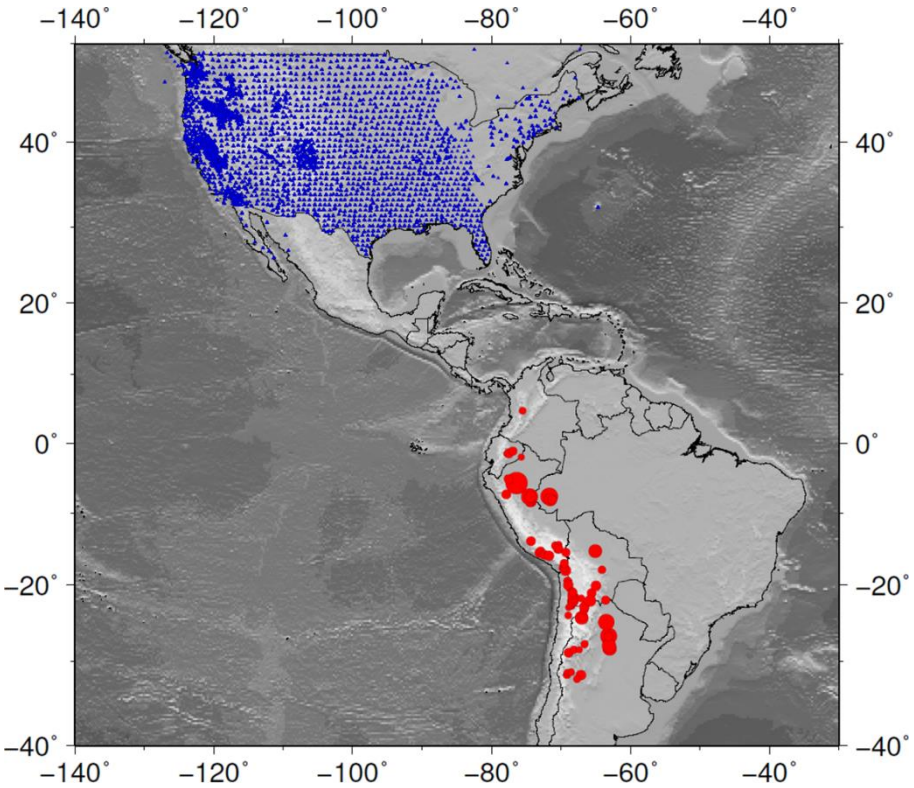

Figure 3-4 The 84 earthquakes with clear pP and P arrivals (red circles) and seismic stations (blue triangles) used for event detection in this study.

3.2 METHODS

3.2.1 Signal processing

The earthquake that occurred on 2007/07/12 (Figure 3-5) illustrates the processing used for signal enhancement in this study (Figure 3-6 and Figure 3-7). VISTA (™GEDCO, Schlumberger) exploration seismic processing software is the primary processing tool, augmented with MATLAB codes to facilitate its application to earthquake data (e.g. format conversions, header value populations). First the expected pP arrival time was calculated using the τ-p code (Crotwell et al., 1999) to initialize an automatic phase picking routine in the VISTA package to pick the pP arrival times. These automatic picks were visually reviewed and manually modified if necessary.

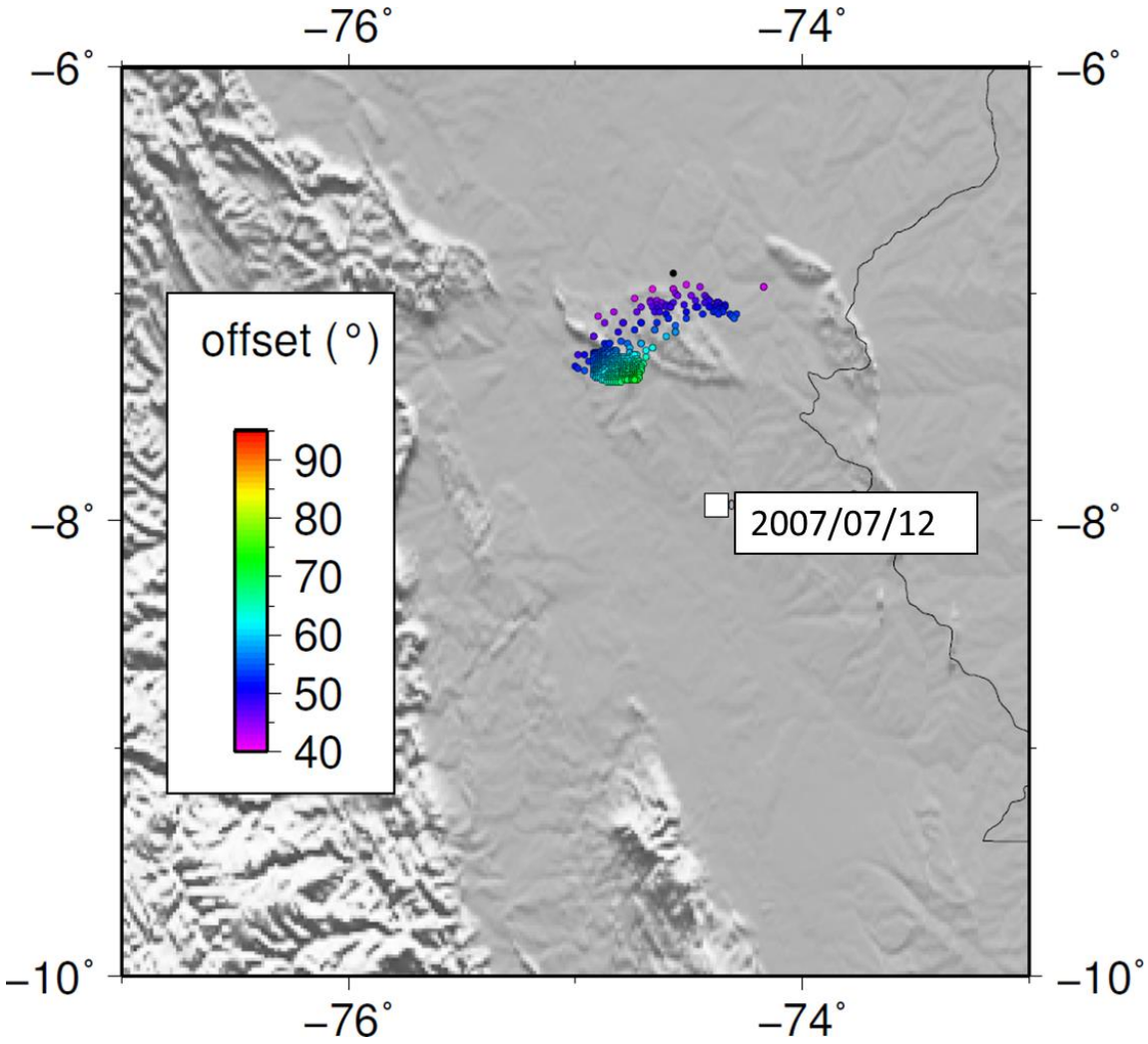

Figure 3-5 Map of pP phase surface bounce point (colored dots) for the earthquake (white square= epicenter) occurring on 2007/07/12 with M=6.1 at a depth of 152 km. Color scale represents epicentral distance from earthquake to recording station in the U.S.

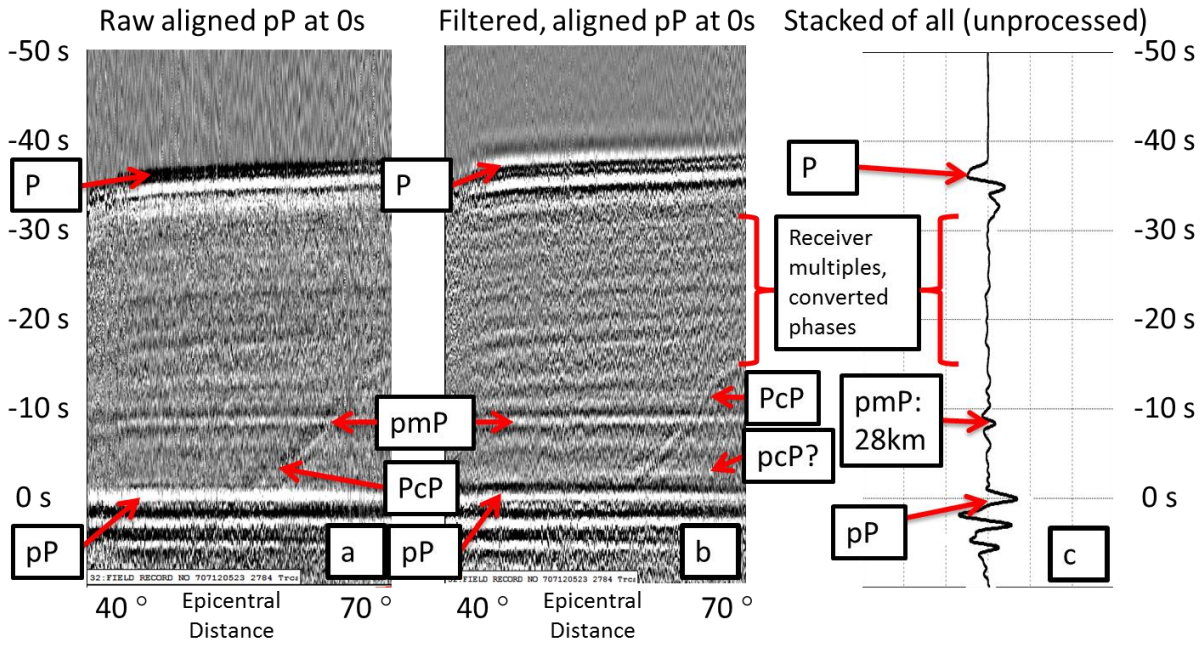

Figure 3-6 Event on 2007/07/12, M=6.1, depth=152 km. Data aligned with pP phase at 0s. Main phases and receiver side multiples and converted phases are interpreted as marked. (a) raw data without any frequency filter or signal enhancement processing (gray scale display). (b) data after a bandpass filter of 0.2-0.4-2-4 Hz. (c) data after stacking all traces (wiggle display). The strongest phase after P but before pP is identified as "pmP", an underside reflection off the Moho. Notice the subtle signal marked as "pcP?" which could correspond to a reflector within the crust. PcP is the steeply dipping event that corresponds to a reflection from the core-mangle boundary. Compare this with the signal improved by coherency enhancement in Figure 3-7.

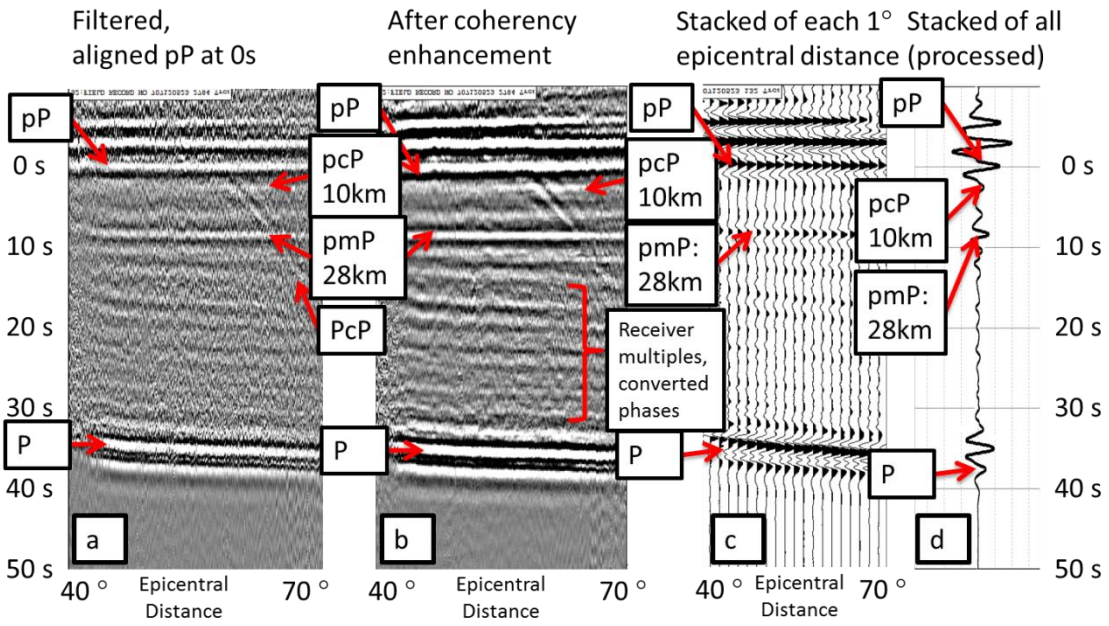

Figure 3-7 The same event as Figure 3-6. Data are here shown on a reverse time scale to simulate a depth section (e.g. depth increasing downward). All data are bandpass filtered with a window of 0.2-0.4-2-4 Hz. (a) data aligned at pP phase at 0s (gray scale display). (b) data after a series of coherency enhancement filters (including F-X deconvolution and trace averaging). (c) stacking of traces every 1° of epicentral distance (wiggle display). (d) stacking of all traces after processing (wiggle display). Notice receiver side multiples and converted phases show distinct moveout (a-c) and partially cancel in the full stack. (d). pmP phase has very little moveout (a-c) and stacks constructively into the single trace (d) The pcP phase is also more clearly expressed in the stack (compare with Figure 3-6).

The pP phase is normally used to ascertain the depth of the hypocenter when it can be identified. We align the pP phase for each station and set it at zero time, then plot the traces versus epicentral distance in degrees. All variations of the processed data from this earthquake show a clear positive phase that arrives about 8.5 s earlier than the pP phase (Figure 3-6 and Figure 3-7). This arrival shows a strong peak which has the same polarity as the pP phase. This polarity indicates that this precursor arrival is a reflection of upgoing P wave energy at an interface between a high velocity and/or density layer and an overlying low velocity and/or density layer (e.g. the surface in the case of pP). The matching polarity for the precursor is consistent with its interpretation as the upgoing P wave reflected from the underside of the crust-mantle boundary, i.e. the - Moho. We here adopt the notation of McGlashan et al (2008) so that pmP designates an upward propagating wave reflected from the Moho. Similarly pcP denotes an intracrustal reflection and puP corresponds to an upper mantle reflection.

We use equation (1) below from Zandt et al. (1994) to calculate the crustal thickness from identified pmP or pcP, puP arrivals, where t_{pP} is pP phase travel time, t_{pmP} is pP precursor from some interface or reflector (such as pmP phase) travel time, h is the depth of such interface or reflector, v_{pc} is average crustal P wave velocity, and p_1 is the ray parameter for the pP phase.

$$t_{pP} - t_{pmP} \cong 2h\sqrt{{v_{pc}}^{-2} - {p_1}^{-2}}$$

For all of our computations we use an average crustal velocity (Vp) of 6.2 km/s so that our results can be easily comparable with results from other studies in the area, e.g. by McGlashan et al. (2008) and by Yuan et al. (2002). McGlashan et al. (2008) used Vp=6 km/s in their northern zone and Vp=6.5km/s in their southern zone. Yuan et al. (2002) used Vp=6.1 km/s for modeling their receiver functions, even though depth from receiver functions are more sensitive to Vs than Vp. Therefore, our depth estimates for intracrustal and Moho reflectors may be inaccurate for regions where the bulk crustal velocity differs from this value, i.e. too shallow if the actual Vp<6.2km/s or too deep for Vp>6.2km/s.

The magnitude of this uncertainty can be estimated by considering the possible range of crustal velocities attributed to this region. For example the USGS South America Regional Crustal Models (http://earthquake.usgs.gov/research/structure/crust/sam.php) indicates that average P wave velocities in our study region range from 6.0 km/s to 6.6 km/s. This corresponds to an uncertainly in Moho (intracrustal) depth of less than an absolute value of 3 km (compared to the value calculated using Vp=6.2km/s). For calculation of the depths for sub-crustal events we have assumed mantle velocities consistent with ak135f model (Kennett et al., 1995).

One key advantage of using USArray data is that the stations are sufficiently dense to allow effective application of multichannel techniques on the scale of interest here. Even though the station spacing of USArray is nominally 70 km, the corresponding underside reflection (bounce) points at the velocity discontinuities

above the earthquakes are much denser, only a few kilometers or less apart from each other (e.g. Figure 3-5). The shallower the earthquakes, the closer their bounce points locate to their epicenters. Moreover the pP precursors from a 30 km deep discontinuity would have a total moveout across the recording array of less than 1s for an epicentral distance spanning from 40 to 70 degrees (Figure 3-6 and Figure 3-7) after alignment on the pP phase. In other words, aligning the signals on the pP phase effectively removes the expected travel time differences for the lithospheric (crustal and upper mantle) pP precursors across the recording array. A depth variation of about 3-4 km would correspond to 1s moveout for the precursor phases in the crust or the mantle. Thus the uncertainty caused by aligning with pP phase is on the order of, or less than, that resulting from uncertainty in the velocity model.

Processing of the data after pP alignment focused on a few relatively simple procedures, including band-pass frequency filtering, F-X deconvolution, common reflection point stacking and, in some cases, the application of trim statics.

We tested different frequency bandpass filters to enhance the target arrivals and best define their reflection character (e.g. sharp or gradational velocity changes). For events deeper than 500km, we examined 6 different filters: (1) 0.001-0.002-0.05-0.1Hz; (2) 0.001-0.002-0.1-0.2Hz; (3) 0.01-0.02-0.1-0.2Hz; (4) 0.01-0.02-0.2-0.4Hz; (5) 0.1-0.2-0.4-0.8Hz; (6) 0.1-0.2-1-2Hz (Figure 3-8). For events shallower than 500 km, we evaluated 3 different filters: (1) 0.1-0.2-0.4-0.8Hz; (2) 0.1-0.2-1-2Hz; (3) 0.2-0.4-2-4Hz. Only the higher frequency filters were used for events at depths less than 500km (most of them <250km) depth because the time separation between pP and P phases, generally less than 60s, is too short to allow distinct representation of phases

in between pP and P phases after low pass filtering. Vertical seismic vertical resolution is commonly adopted to be ¼ of the wavelength (Vermeer, 1999)

Trial and error methods were used to determine the best filter for identifying precursor phases for each particular earthquake. As an example, the pmP phase from event 2007/07/21 shows up more clearly as the frequency increases (Figure 3-8). This character may indicate a relatively sharp crust-mantle boundary. A broad range of filters was used in our study to avoid oversight of low frequency reflections, e.g. those that may be result from gradational boundaries. The LAB in particular is believed to be a gradational boundary for purely thermal reasons (Fischer et al., 2010)

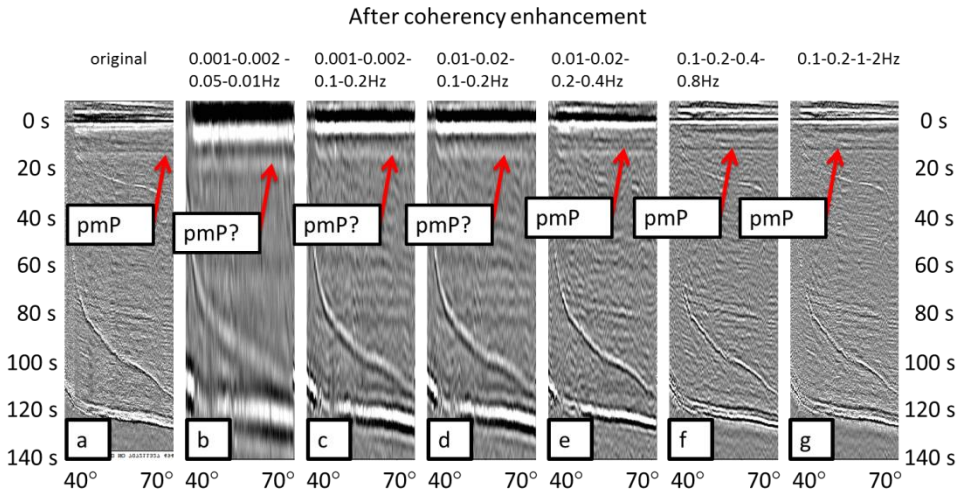

Figure 3-8 Examples of different frequency filters applied on a precursor phase such as the pmP. This event occurred on 2007/07/21 with M=6.1 at a depth=644 km. All sections were processed using F-X deconvolution and averaged over 2 neighboring traces. (a) no filter, (b) 0.001-0.002-0.05-0.1Hz; (c) 0.001-0.002-0.1-0.2Hz; (d) 0.01-0.02-0.1-0.2Hz; (e) 0.01-0.02-0.2-0.4Hz; (f) 0.1-0.2-0.4-0.8Hz; (g) 0.1-0.2-1-2Hz. pmP phase shows up more clearly as frequency increases.

F-X deconvolution (Canales, 1984; Gulunay, 1986) is a procedure that is commonly used in exploration seismology to enhance linear arrivals and reduce random noise (Yilmaz, 2001). F-X deconvolution includes 3 basic steps: (1) each trace of one event gather (time (t) and distance (x)) is Fourier transformed to frequency (f)

and distance (x). (2) Then a complex, Wiener, unit prediction filter in distance is applied for each frequency range so that random noise is reduced and signal is enhanced. (3) An inverse transform is then used to revert the data back to the t-x domain.

Another common signal enhancement procedure is data stacking. Stacking is implemented in two forms. First, we replace each trace by a running average with its nearest neighboring traces in order to further enhance near horizontal events while reducing the amplitudes of steeply dipping events (e.g. Figure 3-7). Furthermore, in a variation of the common-mid-point stacking procedure (Yilmaz, 2001) widely used to enhance conventional multichannel surface reflection profiles, we bin the reflection data whose bounce points are close to each other into common bounce points gathers (CBPs) at corresponding epicentral distances then stack the gathers (e.g. Figure 3-5). The average stacking fold corresponding to the 1°common-bounce-point bin is about 15-20, with some bins resulting in even higher redundancy. In the example case (figure 4-7) , moveout in each of our stacking bins is less than 0.03s, small enough relative to the periods involved (0.5~2.5 seconds) to ignore for our purposes here (0.03 sec corresponds to a depth error of about 0.2 km). Aligning on the pP phase could introduce a time shift related to the topography of the surface where the pP wave reflects. However, this shift would correspond to no more than 1s, given a maximum relief of 2 km within each stacking bin and assuming an extremely low average P wave velocity of 4km/s for the topmost part of crust.

Application of F-X deconvolution, trace averaging and stacking, together with selective bandpass filtering, significantly enhanced the amplitude and coherence of

arrivals in the interval between the P and pP waves, especially for the smaller magnitude events (e.g. compare Figure 3-9a, b and Figure 3-9b, c), thus greatly expanding the number of useful recordings available for phase identification.

3.2.2 Phase Identification

Once processing has enhanced a coherent event arriving between P and pP, the next step is to identify true underside reflections on the source side from other coherent arrivals following alternative raypaths (e.g. multiples, converted waves etc.).

To aid our identification of any coherent event, we computed synthetic seismograms and theoretical travel times for seismic phases expected for an appropriate earth velocity model. The velocity model we use to calculate expected seismic travel time and synthetic seismograms is modified from the original ak135f model (Kennett et al., 1995). Our basic model consists of a crust of average Vp=6.2 km/s, and Vs=3.6 km/s. Right below the Moho, Vp=8.04km/s and Vs=4.47km/s are used. We simplified the velocity model between the Moho and 410-km discontinuity to reduce the possible reflected phase at 210-km, presumably the LAB (Lithosphere-Asthenosphere Boundary), by just setting two velocity points at 77.5 km and 160 km. All velocities between the Moho to 77.5 km, 77.5 km to 160 km, 160 km to 410 km are linearly interpolated. Beneath the 410-km discontinuity, the original ak135f model is used.

We used the modeling program “qseis” (Wang, 1999) to create synthetic seismograms. The same velocity model mentioned above was used for both receiver and source side structures. The synthetic data were filtered with the same parameters as the real data. (Figure 3-9b)

Theoretical travel times were then calculated by the TauP program of Crotwell et al. (1999) (Figure 3-9c). P, P30s, PPv30P, pmP, S410P, pcP, pP, s^30P and receiver-side multiples and converted phase such as PPv30P, PPv30S,PSv30S, P30sSv30S (in an order of close to far from P phase), are distinguishable on the basis of their time of arrival after pP and, more significantly, on the basis of their moveout times across the recording arrays. For example, the arrival at 16-19s after pP in Figure 3-9a could be interpreted as an underside reflection from a sub-Moho event, but the modeling makes clear that its moveout is more appropriate for a PSv30S converted phase, which is direct P wave converted to S wave at the free surface on the receiver side and then reflected at the receiver side Moho (assuming 30km depth) before arriving at the recording station as an S wave. Better fits of the synthetic seismograms to observed travel times would be expected from more accurate velocity models at the receiver side. However, this exercise is sufficient to illustrate the importance of synthetic seismograms and moveout across the large array recording for identifying key seismic phases from extraneous arrivals.

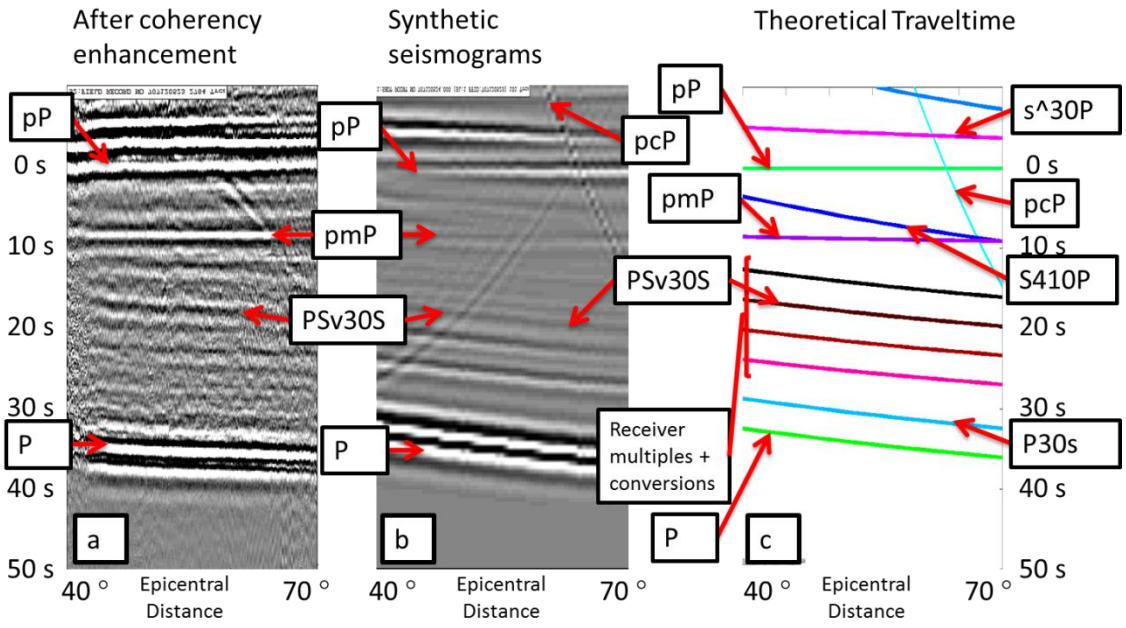

Figure 3-9 Compare (a) real data with (b) synthetic seismograms from "qseis" (*Wang*, 1999) and (c) theoretical traveltime from TauP (*Crotwell et al.*, 1999). Receiver side multiples and conversions include: PPv30P, PPv30S, PSv30S, P30sSv30S (close to far from P). Notice receiver side multiples and conversions are distinguishable from underside reflections by their greater moveout.

After identifying precursor phases, we classify them according to their visual recognizability. We subjectively rate the quality of these arrivals by 1(worst) to 5(best) (Figure 3-10 to Figure 3-12). Figure 3-13 shows a histogram of the number of earthquake in each quality category for the pmP arrivals with corresponding earthquake magnitude represented by color. The pmP phase is observed for about 2/3 of the events with clear pP and P arrivals. The 40 earthquakes with unclear P or pP phase represent approximately 1/3 part of the total of 124 events, with most of these in the range of M=5.5-5.9. The lack of an obvious pP in these cases is presumably because of the relative lack of seismic energy emitted by these smaller earthquakes. However, some larger events (M>7) also do not show clear P or pP, perhaps because of complicated source functions. Figure 4-13 demonstrates the value of being able to

use small events (M5.5-5.9) in our analysis because of their greater abundance compared to larger events.

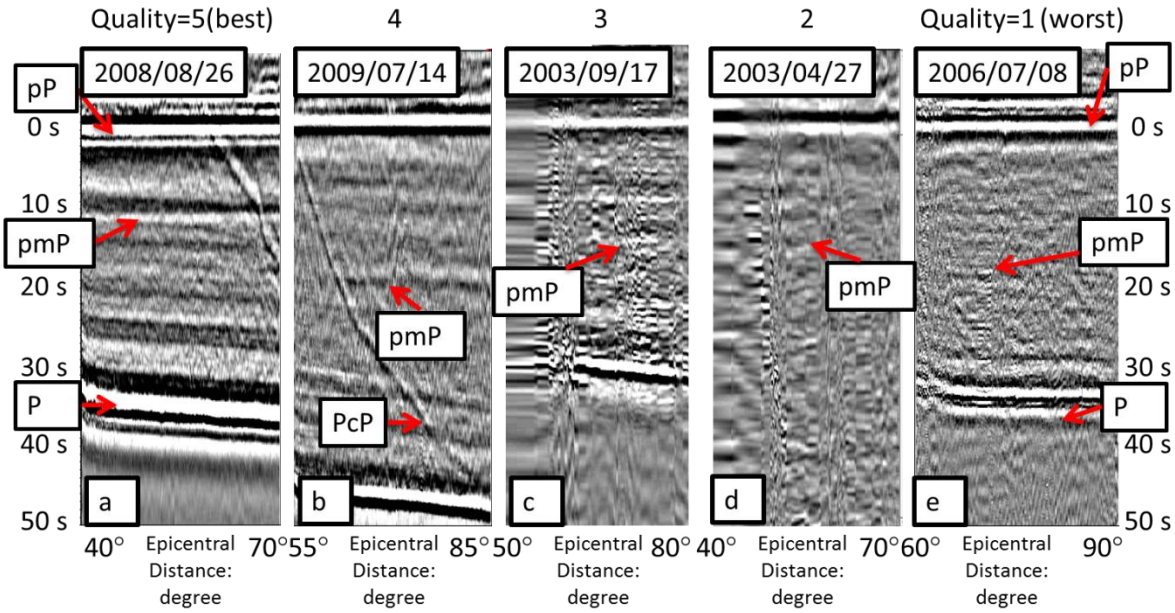

Figure 3-10 Examples of different quality rankings of pmP phases. Scale 5 to 1 (5 for the best quality, 1 for the worst quality). All examples are aligned with pP phase at 0s. The bottom arrivals are direct P phase. pmP phases are marked by the red arrows between pP and P. (a) Earthquake on 2008/08/26 (b) Earthquake on 2009/07/14 (c) Earthquake on 2003/09/17 (d) Earthquake on 2003/04/27 (e) Earthquake on 2008/06/07 (a),(b),(c),(d) are filtered with bandpass: 0.1-0.2-1-2 Hz. (e) are filtered with bandpass: 0.2-0.4-2-4 Hz. (What are the magnitudes of each of the events?}

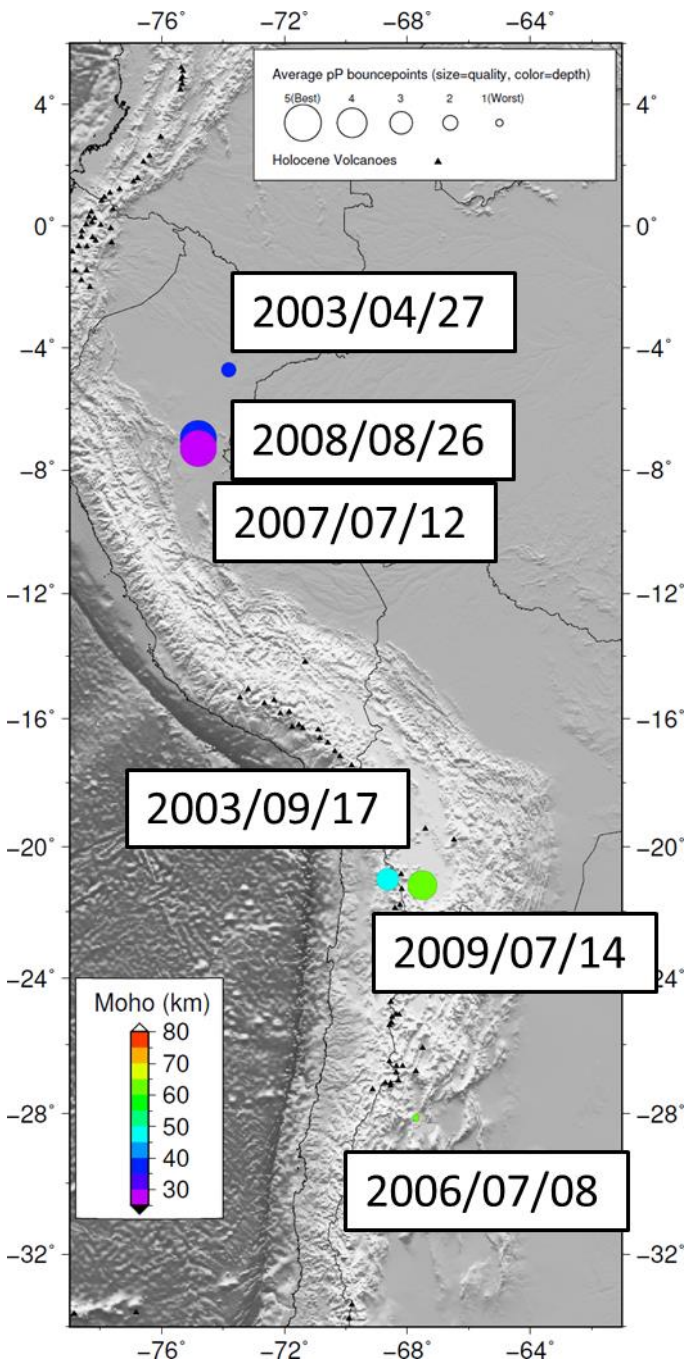

Figure 3-11 Moho depths for earthquakes in Figure 3-7 and Figure 3-10. Average pP surface bounce points are shown as circles. Color indicates Moho depths derived from pmP-pP time.

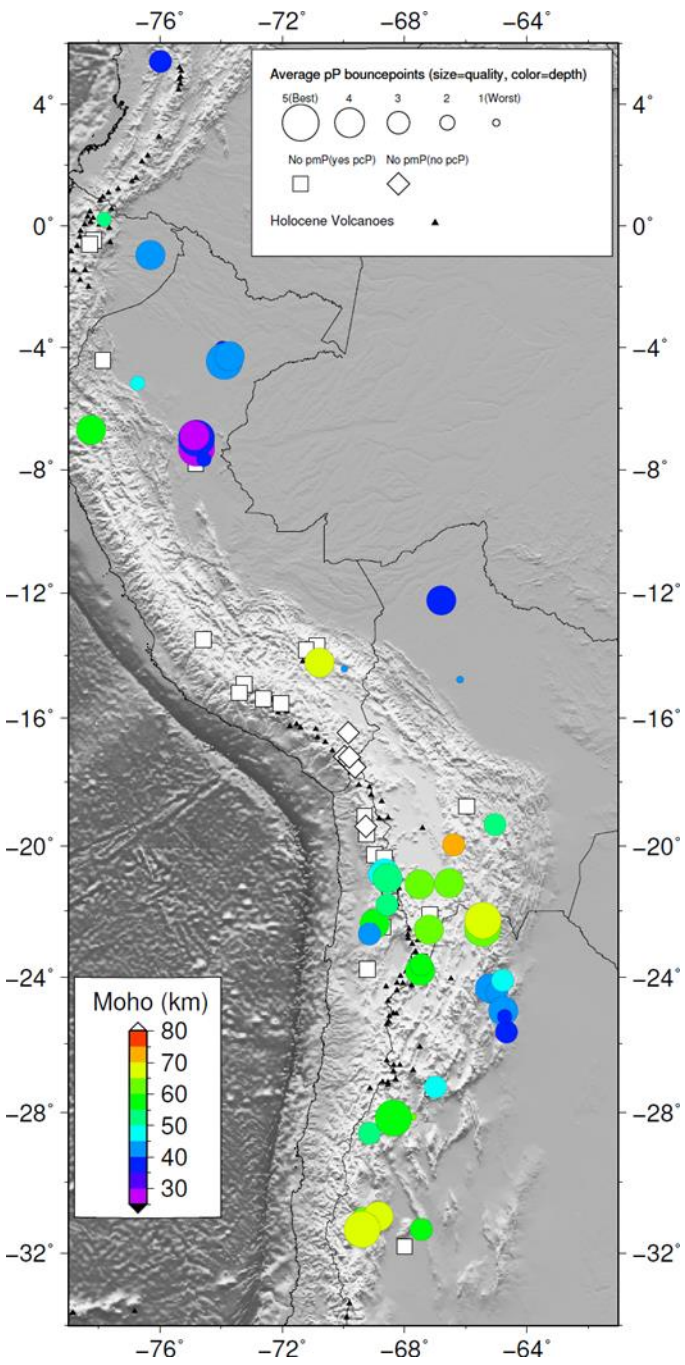

Figure 3-12 Moho depths: circles=average pP surface bounce points, white diamonds=no pmP or pcP arrival, white square=no pmP but pcP is observed. Color indicates Moho depth derived from pmP-Pp time, using average Vp=6.2km/s.

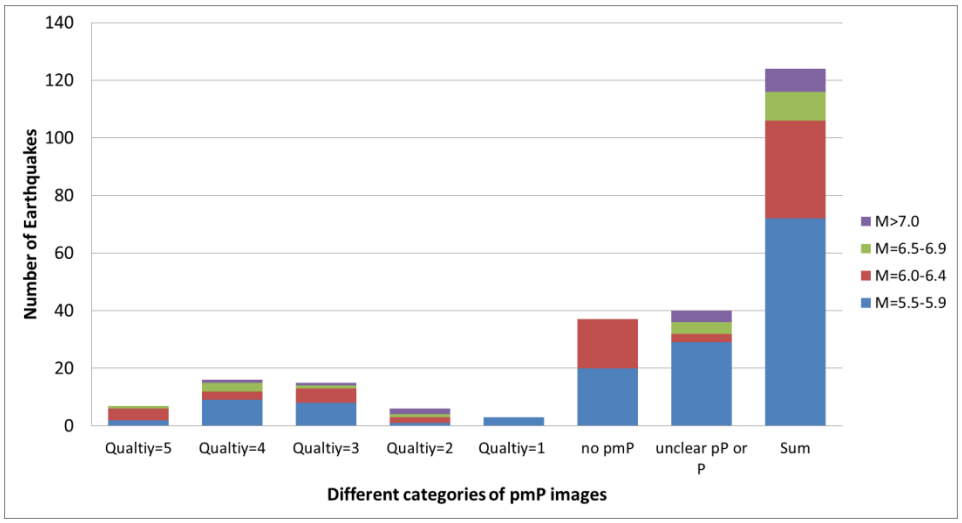

Figure 3-13 Earthquakes magnitude distribution for different categories of pmP images. Best pmP (quality=5) to worst pmP (quality=1), some earthquakes show no pmP arrivals, some earthquakes do not even show clear pP or P wave, most of which are caused by lack of energy (M5.5-6), or complicated source functions for too large magnitude (M>7).

3.3 RESULTS AND DISCUSSION

3.3.1 Moho

The most commonly observed interface of interest to this study is the Moho. The Moho is generally taken to mark a compositional boundary which separates the crust and mantle (Jarchow and Thompson, 1989; Christensen and Mooney, 1995), though some would argue it could also represent a tectonic boundary (Klemperer et al., 1986; Allmendinger et al., 1987; Cook, 1995) or phase change boundary (Lovering, 1958; Kennedy, 1959; Hess, 1959, 1962; O'Connell and Wasserburg, 1967; Moores and Jackson, 1974; Clague and Straley, 1977).

Strictly speaking the seismic Moho is defined as the rapid change in velocity inferred from recording of critically refracted seismic waves (Mohorovičić, 1909). It is usually interpreted to be a first-order (zero-thickness) discontinuity, across which the felsic/mafic rocks overly on the ultramafic rocks (Christensen and Mooney, 1995) but

others have argued it may be more gradational (e.g. Bamford and Prodehl, 1977; Owens et al., 1987)).

According to Christensen and Mooney (1995), a typical P wave velocity for the base of the average continental crust is about 7-7.2 km/s and for the uppermost mantle it is about 7.9-8.1 km/s. This corresponds to a ca. 10% velocity jump with a corresponding similar (9%) density increase, using equation (1) from (Brocher, 2005):

$$\rho(g/cm^3) = 1.6612V_p - 0.4721{V_p}^2 + 0.0671{V_p}^3 - 0.0043{V_p}^4 + 0.000106{V_p}^5$$

The resulting impedance contrast is about 10%, which corresponds to a reflection coefficient of 0.09, with should result in a relatively strong amplitude reflection (Zoeppritz, 1919). If the velocity/density change is rapid (within short distance), the reflection should contain relatively high frequencies as well. We have found that in general the reflections we interpret as Moho appear to be best imaged at the higher end of our testing filters (e.g. 0.1-0.2-1-2Hz or 0.2-0.4-2-4Hz) suggesting a relatively sharp transition (e.g. Christensen and Mooney (1995). For convenience of the discussion, these results were grouped according to their geographic locations, as shown in Figure 3-14.

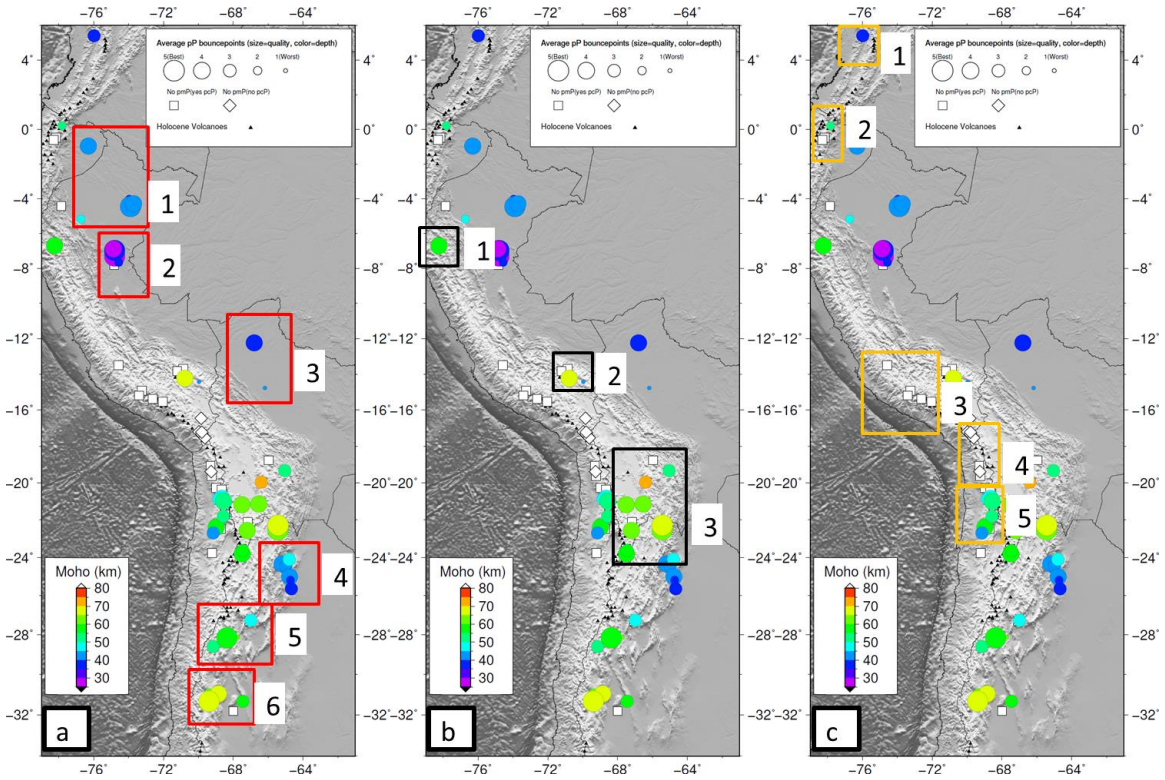

Figure 3-14 Moho depths enumerated in groups for different regions: (a) Andean Foreland: (a.1) Northern Peru and eastern Ecuador (box 1)(a.2) Central Peru (box 2)(a.3) Northern Bolivia (box 3)(a.4) Santa Barbara system (box 4)(a.5) Southern edge of Puna plateau at 28°S (box 5) (a.6) Southern Andes at 32°S (box 6) (b) Altiplano-Puna plateau: (b.1) Northern Altiplano at 7°S (box 1) (b.2) Northern Altiplano at 14°S (box 2) (b.3) Central Andes, Altiplano-Puna plateau 19°S-24°S (box 3) (c) Active volcanic arc: (c.1) Northern Colombia 5°N (box 1)(c.2) Northern Ecuador 0°N (box 2)(c.3) Southern Peru (box 3)(c.4) Northern Chile at 18°S-20°S (box 4)(c.5) Northern Chile at 20°S-24°S (box 5)

As the most ubiquitously observed, or interpreted, precursor arrival in our analyses, the Moho reflection also provides a basis for evaluating the validity of our technique against independent geophysical observations of crustal thickness in the Andes (Figure 3-19). This is particularly true for our measurements in the central Andes of Chile and Argentina. (Figure 3-14 a.4, b.3, c.4, c.5, Figure 3-25).

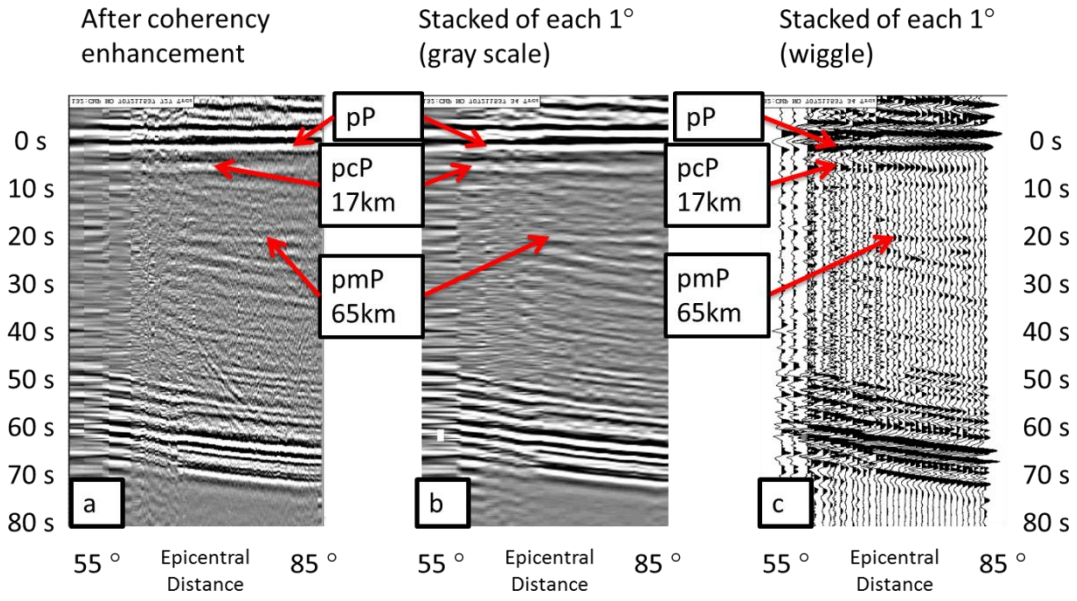

Figure 3-15 Event on 2007/07/21, M=6.4, Depth=289km (b.3, #4 in Figure 3-18). Data are filtered with window: 0.2-0.4-2-4 Hz. (a) data aligned at pP phase at 0s with a coherency enhancement (gray scale display). (b) stacking of traces every 1° of epicentral distance (gray scale display). (c) stacking of traces every 1° of epicentral distance (wiggle display).

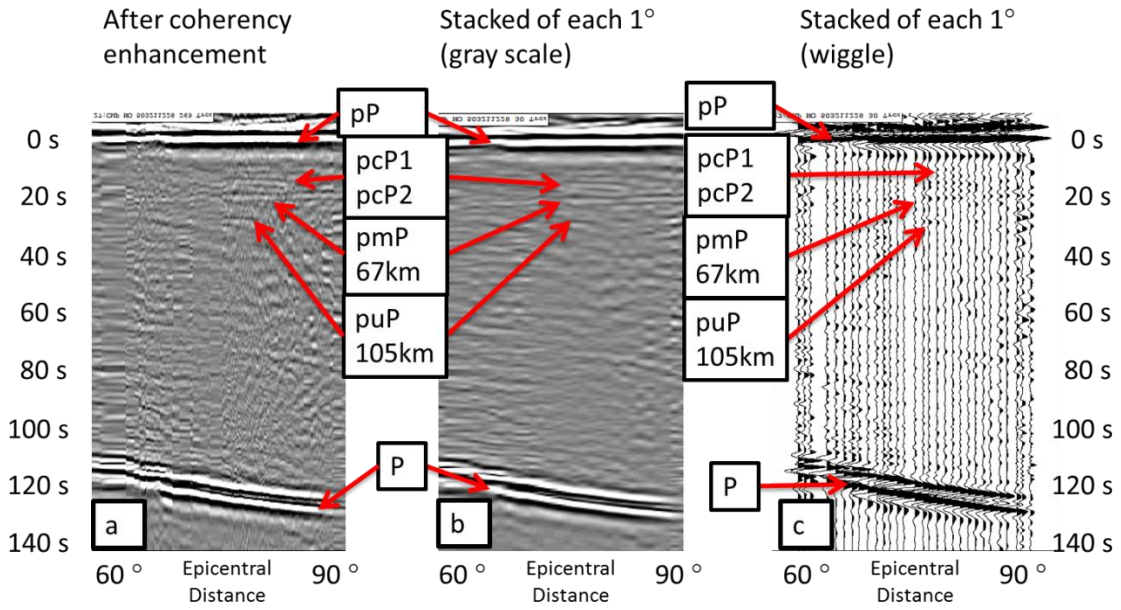

Figure 3-16 Event on 2005/03/21, M=6.9, Depth=579 km, (b.3, #7 in Figure 3-18). Data are filtered with window: 0.1-0.2-1-2 Hz. (a) data aligned at pP phase at 0s with a series of coherency enhancement (gray scale display). (b) stacking of traces every 1° of epicentral distance. (c) stacking of traces every 1° of epicentral distance (wiggle display). pcP1=underside reflection from crustal reflector 1. pcP2=underside reflection from crustal reflector 2. puP=underside reflection from upper mantle.

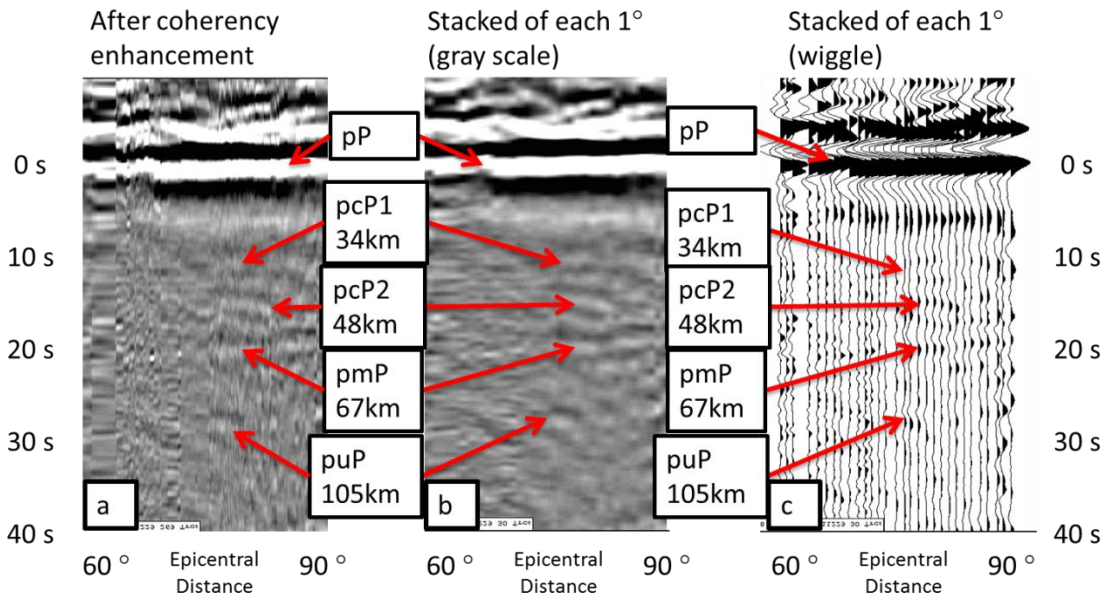

Figure 3-17 A detailed version of Figure 3-16.

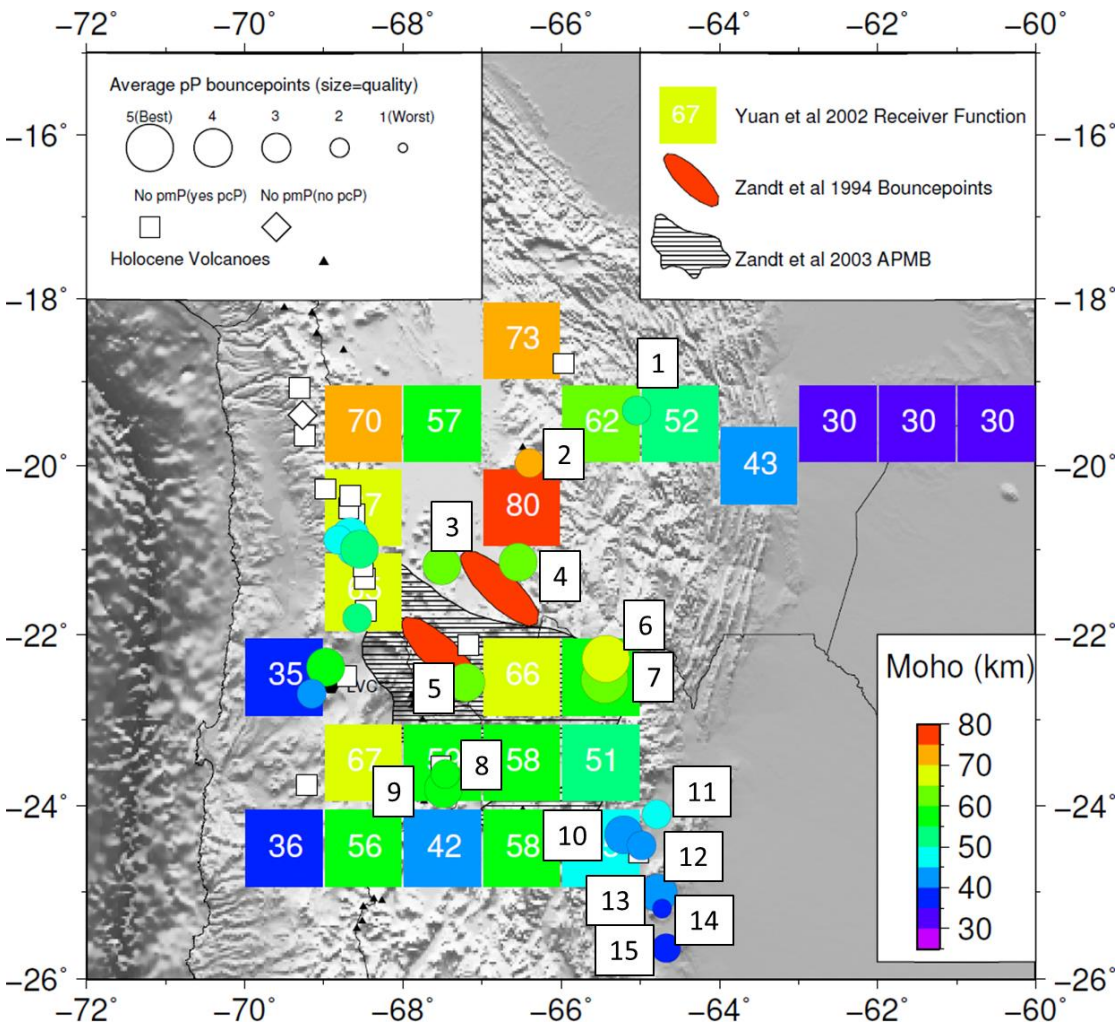

Figure 3-18 Moho depth map of Central Andes, earthquake locations and their average pP surface bounce points are shown as squares and circles. Colors of circles indicate Moho depths derived from pmP time. Sizes of circles indicate image quality. Colored squares = Moho depths from P wave receiver functions (Yuan et al., 2002). Red ellipses = crustal sampling zones from pP, sS precursors study (Zandt et al., 1994), indicating 75-80 km thick crust. Black dashed zone = Altiplano-Puna magma body (APMB) discovered from receiver functions study (Zandt et al., 2003), at 20km depth. Event list: Event list: (1) 2012/06/02, M=5.9, Depth=527km (2) 2004/03/17, M=6.1, Depth=289km (3) 2009/07/14, M=5.7, Depth=175km (4) 2007/07/21, M=6.4, Depth=289km (5) 2010/01/28, M=5.9, Depth=208km (6) 2005/03/21, M=6.4, Depth=570km (7)M=6.9, Depth=579km (8) 2007/05/25, M=5.9, Depth=180km (9) 2006/08/25, M=6.6, Depth=184km (10) 2004/11/12, M=6.1 Depth=568km (11) 2011/01/01, M=7.0, Depth=576km (12) 2008/09/03 M=6.3, Depth=569km (13) 2011/04/17, M=5.7, Depth=556km (14) 2012/05/28, M=6.7, Depth=586km (15) 2011/09/02, M=6.7, Depth=578km

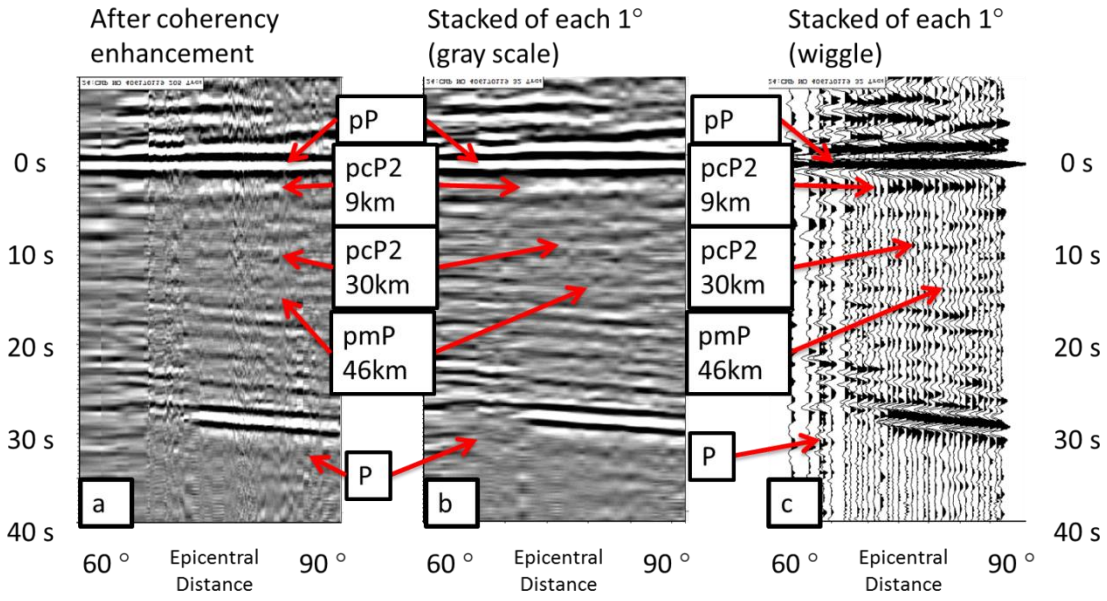

Figure 3-19 Event on 2004/06/17, M=5.7, Depth=115 km (c.5). Data are filtered with window: 0.2-0.4-2-4 Hz. (a) data aligned at pP phase at 0s with coherency enhancement (gray scale display). (b) stacking of traces every 1° of epicentral distance. (c) stacking of traces every 1° of epicentral distance (wiggle display).

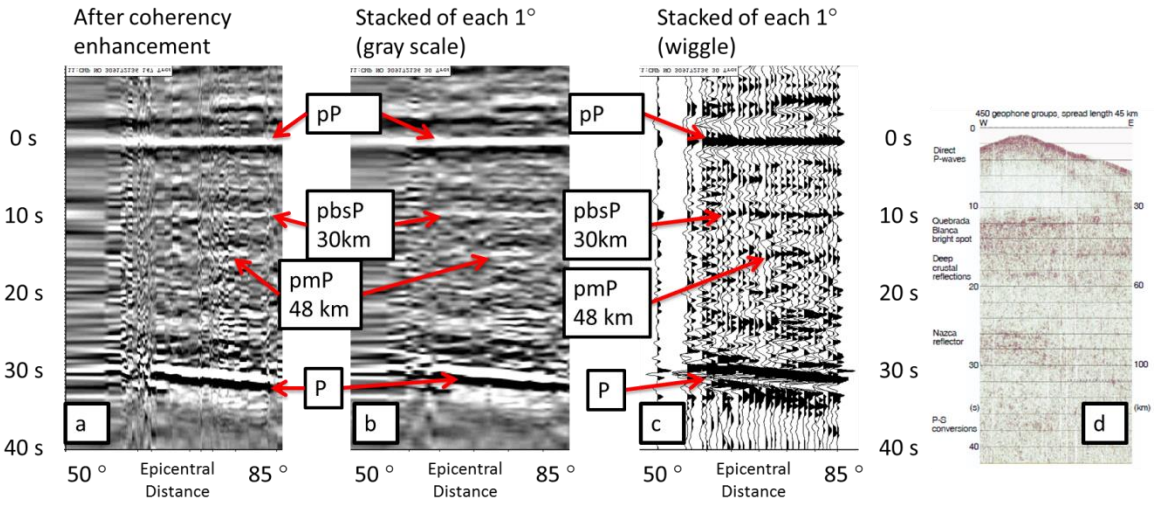

Figure 3-20 Event on 2003/09/17, M=5.8, Depth=127 km (c.5). Data are filtered with window: 0.1-0.2-1-2 Hz. (a) data aligned at pP phase at 0s with coherency enhancement (gray scale display). (b) stacking of traces every 1° of epicentral distance. (c) stacking of traces every 1° of epicentral distance (wiggle display). pP=underside reflection from Quebrada Blanca bright spot. (d) Quebrada Blanca bright spot from a shot gather of the seismic reflection experiment ANCORP (ANCORP Working Group, 1999) on the same time scale. Notice the similarity of the bright spot character between underside reflection from our study (a-c) and reflection from traditional seismic reflection survey (d).

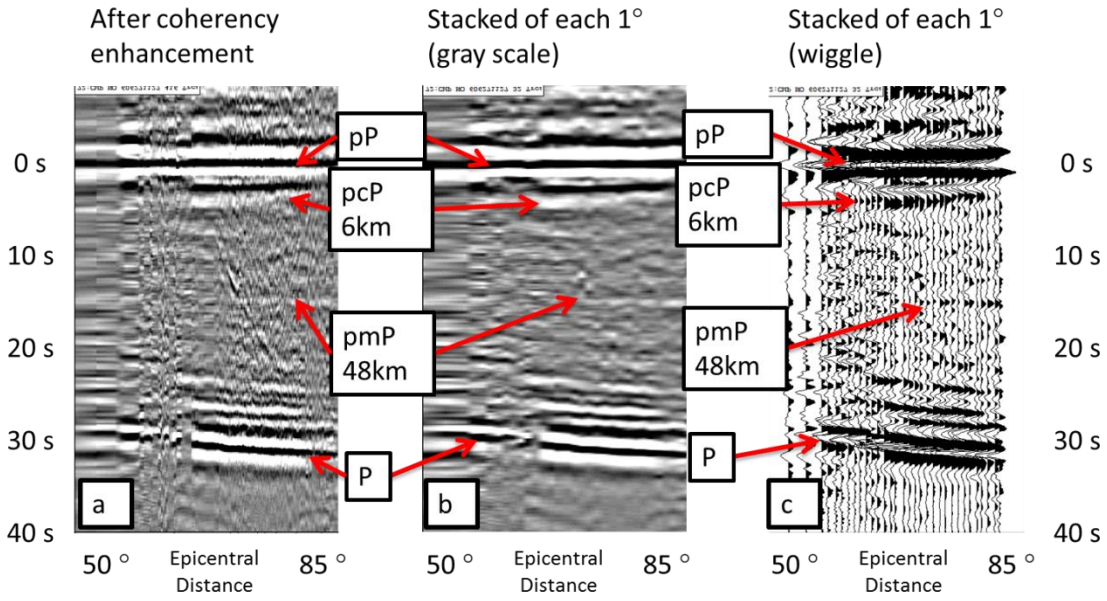

Figure 3-21 Event on 2006/06/27, M=5.5, Depth=122 km (c.5). Data are filtered with window: 0.2-0.4-2-4 Hz. (a) data aligned at pP phase at 0s with coherency enhancement (gray scale display). (b) stacking of traces every 1° of epicentral distance. (c) stacking of traces every 1° of epicentral distance (wiggle display).

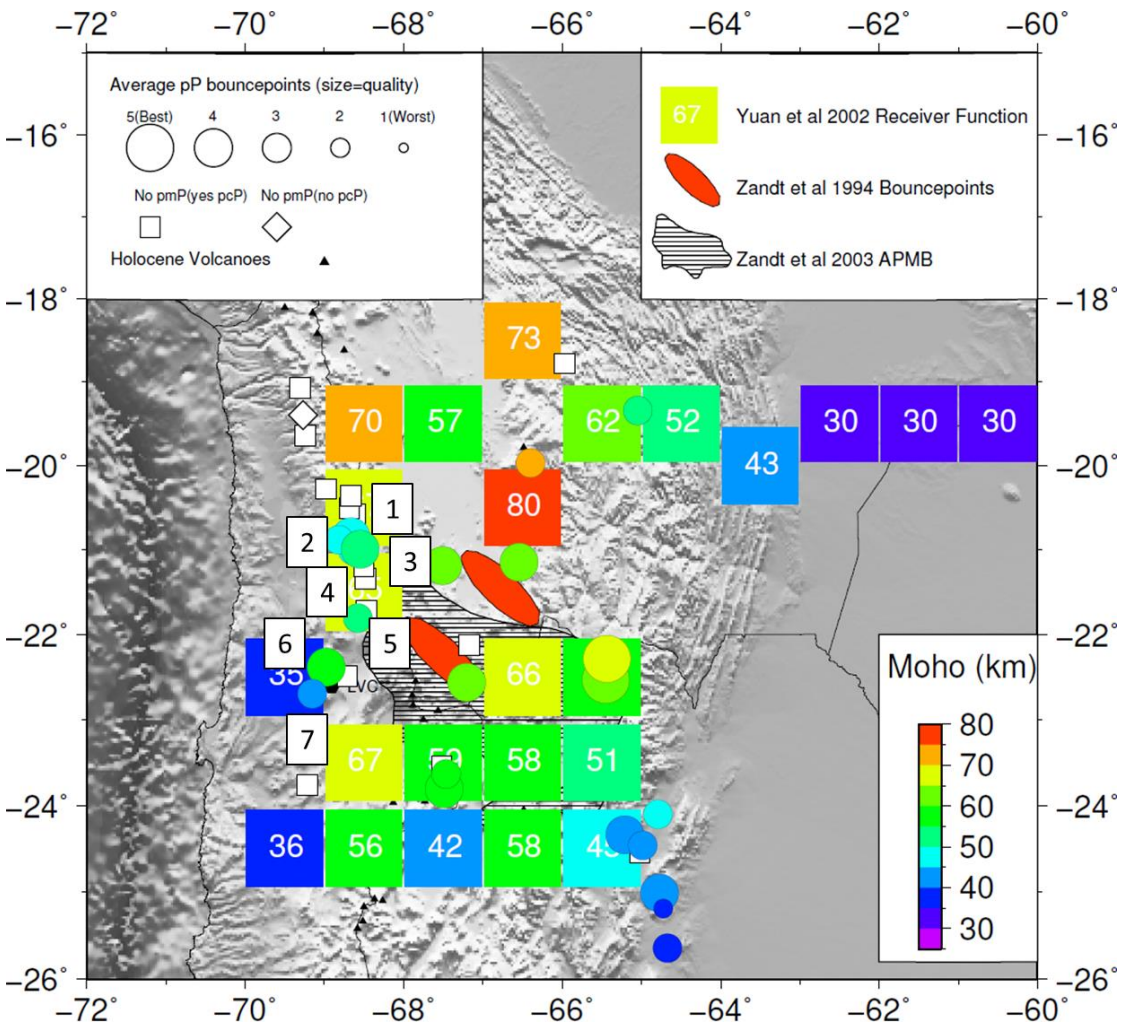

Figure 3-22 Moho depths map of Central Andes, earthquake locations and their average pP surface bounce points are shown as squares and circles. Colors of circles indicate Moho depths derived from pmP time. Sizes of circles indicate image quality. Colored squares = Moho depths from P wave receiver functions (Yuan et al., 2002). Red ellipses = crustal sampling zones from pP, sS precursors study (Zandt et al., 1994), indicating 75-80 km thick crust. Black dashed zone = Altiplano-Puna magma body (APMB) discovered from receiver functions study (Zandt et al., 2003), at 20km depth. Event list: (1) 2004/06/17, M=5.7, Depth=115km (2) 2006/06/27, M=5.5, Depth=122km (3) 2008/12/04, M=5.5, Depth=115km (4) 2003/09/17, M=5.8, Depth=127km (5) 2010/03/04, M=6.3, Depth=114km (6) 2006/06/27, M=5.5, Depth=115km (7) 2007/06/14, M=5.5, Depth=105km.

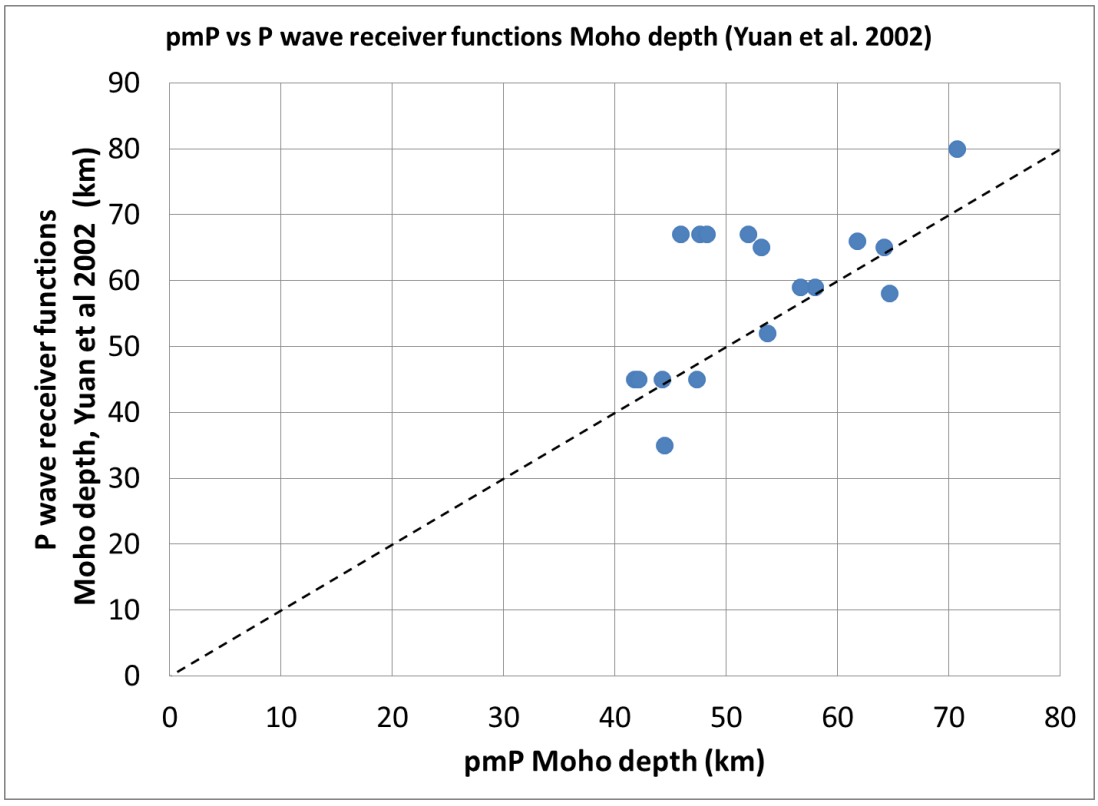

Figure 3-23 Comparison of pmP Moho depth of this study with previous P wave receiver functions study (Yuan et al., 2002), including central Andes, Altiplano-Puna plateau 19°S-24°S (Figure 3-14b box 3) and active volcanic arc in northern Chile at 20°S-24°S (Figure 3-14c box 5). Black dashed line: 1: 1 reference line on which pmP Moho depth equals P wave receiver function Moho depth.

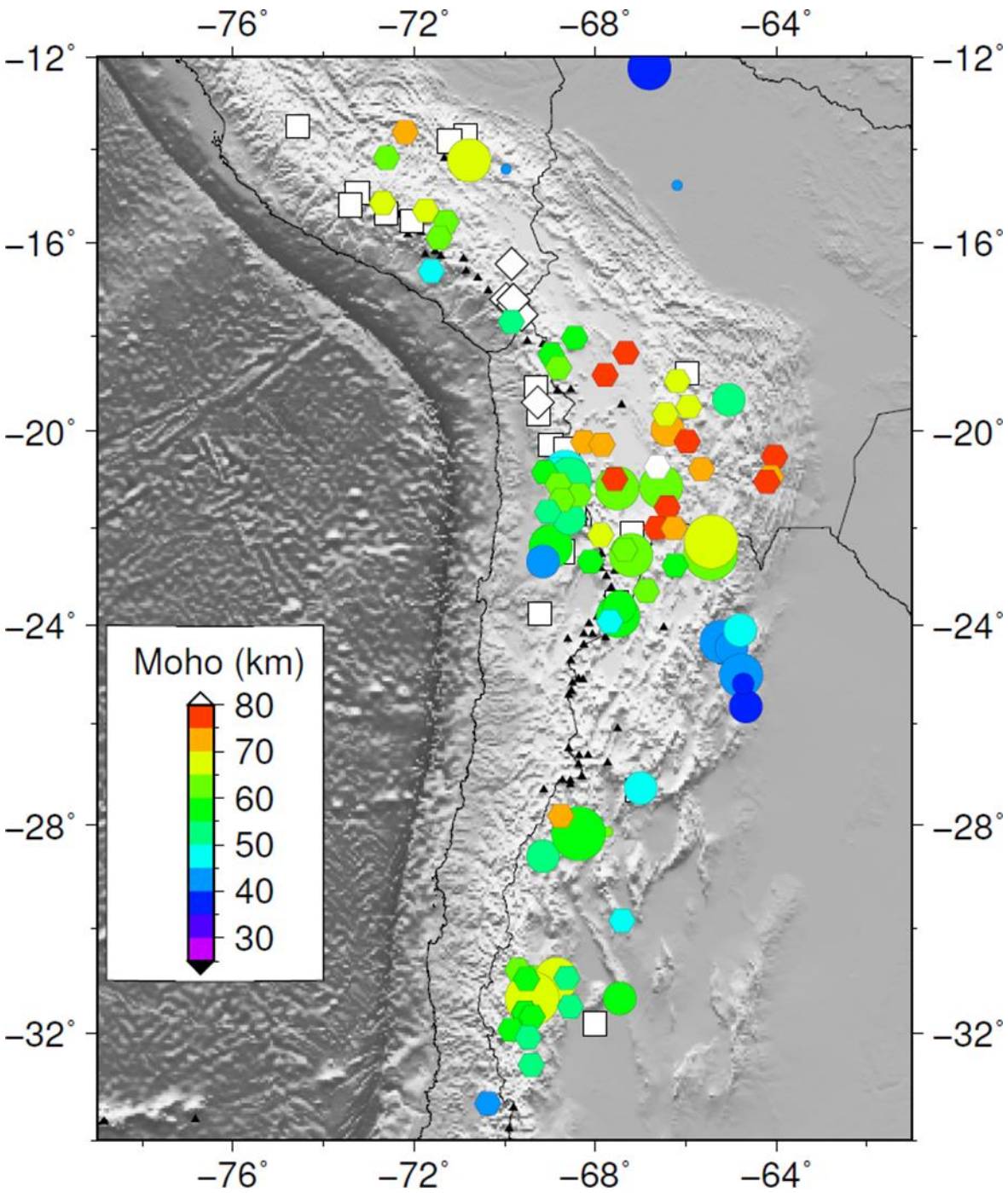

Figure 3-24 Moho depth: circles: this study; hexagons: previous pP precursor study (McGlashan et al., 2008). White squares indicated areas where no Moho reflector is observed.

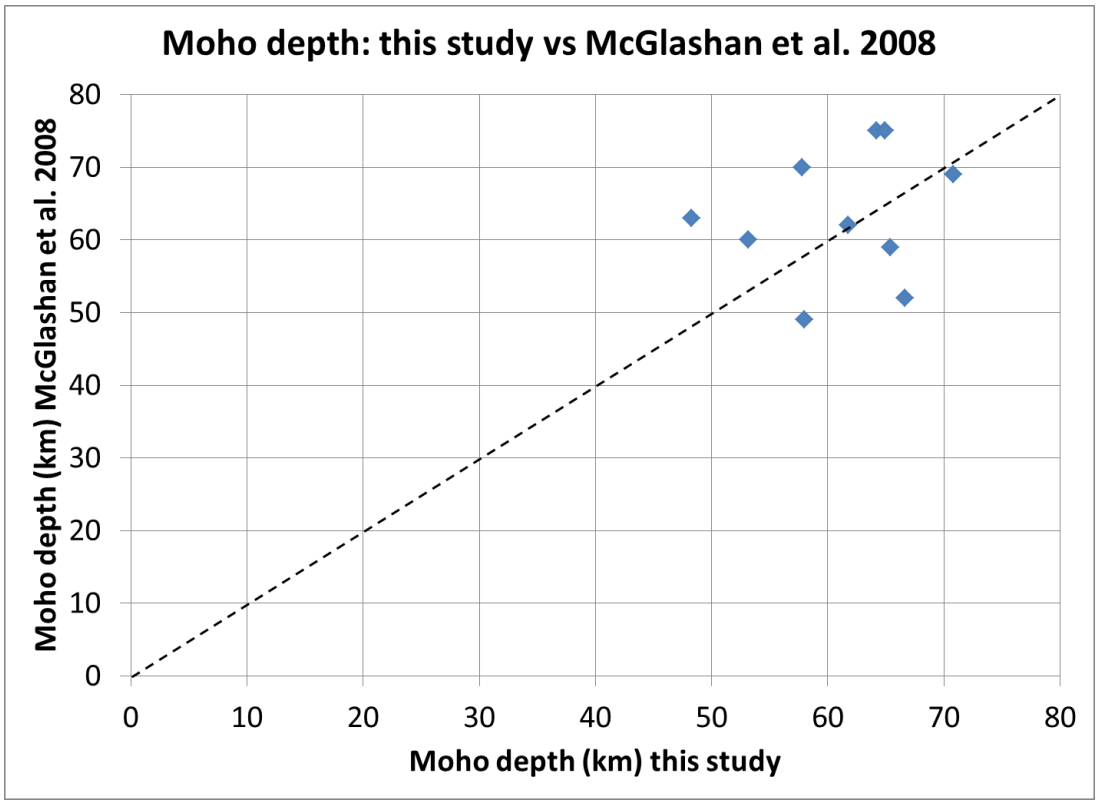

Figure 3-25 Comparison of pmP Moho depth of this study with previous precursor study (McGlashan et al., 2008), including central Andes, Altiplano-Puna plateau 19°S-24°S (Figure 3-14b box 3) and active volcanic arc in northern Chile at 20°S-24°S (Figure 3-14c box 5). Black dashed line: 1: 1 reference line on which pmP Moho depth in this study equals pmP Moho depth in McGlashan et al. (2008).

This region is the best geophysically studied part of the Andes. There have been receiver function studies (Yuan et al., 2002; Zandt et al., 2003), a teleseismic precursor study similar to ours (Zandt et al., 1994; McGlashan et al., 2008),and active source seismic reflection experiment ANCORP (ANCORP Working Group, 2003, 1999) (Figure 3-1, Figure 3-18, Figure 3-22, Figure 3-24).

Our data indicate that the central part of Altiplano-Puna plateau has a crustal thickness of 54-75 km (Figure 3-18). The event on 2007/07/21, for example, shows a pmP phase corresponding to a Moho at 65 km depth (Figure 3-15, #4 in Figure 3-18). Another event on 2005/03/21 shows the Moho at 67 km depth (Figure 3-16, Figure

3-17 and #7 in Figure 3-18). Both also show intracrustal reflectors, which will be discussed in the later section.

Most of our measurements beneath the Altiplano-Puna plateau in central Andes (b.3) match the receiver function results from Yuan et al. (2002) (Figure 3-18 to Figure 3-23). In the Altiplano-Puna region, the crust is about 54 km thick at 19°S (#1 in Figure 3-18), 70 km at 20°S (#2), 65 km at 21°S(#3, 4), 60-67 km at 22°S(#5, 6, 7), 57-58 km at 24°S (#8, 9), 48-39km at 24°S to 26°S at the southeastern edge of the plateau (#10-15). The crust is thinning from north (20°S) to south (24°S) about 22 km (70 to 48 km) beneath the plateau (#2 to #11), and thinning from northwest to southeast beneath the southeastern edge of the plateau, the Santa Barbara system (48 to 39 km) (#10-15).

The Moho depth beneath the volcanic arc in the central Andes (c.5) varies from 45 km to 52 km in our study (Figure 3-19 to Figure 3-21). The receiver function result (Yuan et al., 2002) showed crustal thicknesses about 65-67km (near event 1-5) and 35 km (near event 6,7) (Figure 3-22). However, their results (grids D3 and E3 in their study) show a positive arrival before the arrival that they interpreted as the Moho. Those "early" arrivals on the receiver functions suggest a discontinuity at about 40-50km, which coincides with the depths we report here for the Moho. Note also that constraints on the Moho depths for area D3 and E3 from the receiver functions are less robust because no converted multiples were used in those depth calculations (Yuan et al, 2002). It is possible that two discontinuities may exist in this area. If our precursor marks a reflection from the Moho at 48-53 km depth, then the discontinuity at 65-67 km as shown by Yuan et al. (2002) might be in the upper mantle. Conversely, our

precursor could be interpreted as from a lower crustal reflector at 45-52 km. This possibility will be discussed later.

Our measurements are inconsistent with two measurements from a similar study carried out by Zandt et al. (1994) and the discrepancy is about 15 km. Their results show the crust (red ellipse in Figure 3-18) to be about 80 km thick, whereas our nearby measurements (event 3, 4, 5 in Figure 3-18) indicate 62-65 km in thickness. However, their data was filtered with a bandpass of 5-10s to 50s, whereas ours used a much higher frequency range (0.5s to 2.5s). If this difference is not simply an artifact of the filters used, perhaps Zandt et al. (1994) detected a much longer wavelength boundary. For example, there might be a relatively sharp impedance contrast starting at the depth of 62-65 km but decaying gently in magnitude down to about 80km.

Comparing our results with the precursor study by McGlashan et al. (2008) that inspired this work indicates more disagreement than agreement (Figure 3-24 and Figure 3-25), Our results suggest a relatively uniform crustal thickness beneath the Altiplano-Puna plateau from 20°S to 24°S of about 60-67 km, whereas their results show more dramatic Moho topography, with depths ranging from 49 to 82 km. At 20°S, ours cluster near 70 km and theirs range slightly 67 to 77 km. Beneath the active volcanic arc, their results vary from 54 to 70 km, whereas ours yield shallower estimates of 48-53km. In general the difference between our measurements and theirs are on the order of 10 km (Figure 3-25). Both studies use similar average crustal velocity (theirs: 6km/s, ours: 6.2km/s), which at most would yield about a 1km difference in depth conversion. It is certainly possible that some of these differences could be due to large changes Moho depth over short distances (e.g. Hirn et al., 1984),

or other possible explanations exist.

For example, there are four Moho depth measurements (69,68,62,61km) given by McGlashan et al. (2008) in the region of southern Peru (c.3). Reflectors from such depths would appear around 20s after pP in our data (Figure 3-26 to Figure 3-30). We also see distinct arrivals around 20s from all four events. However, they exhibit moveout very similar to the direct P and match the expected travel times for receiver side multiples or receiver side conversion of P-to-S conversion at the Moho. Without the benefit of array data, it would be difficult to distinguish pmP from such complexities on the single trace stacks of McGlashan et al. (2008). However, more sophisticated modeling of site specific receiver structure is needed to confirm whether or not this is the case.

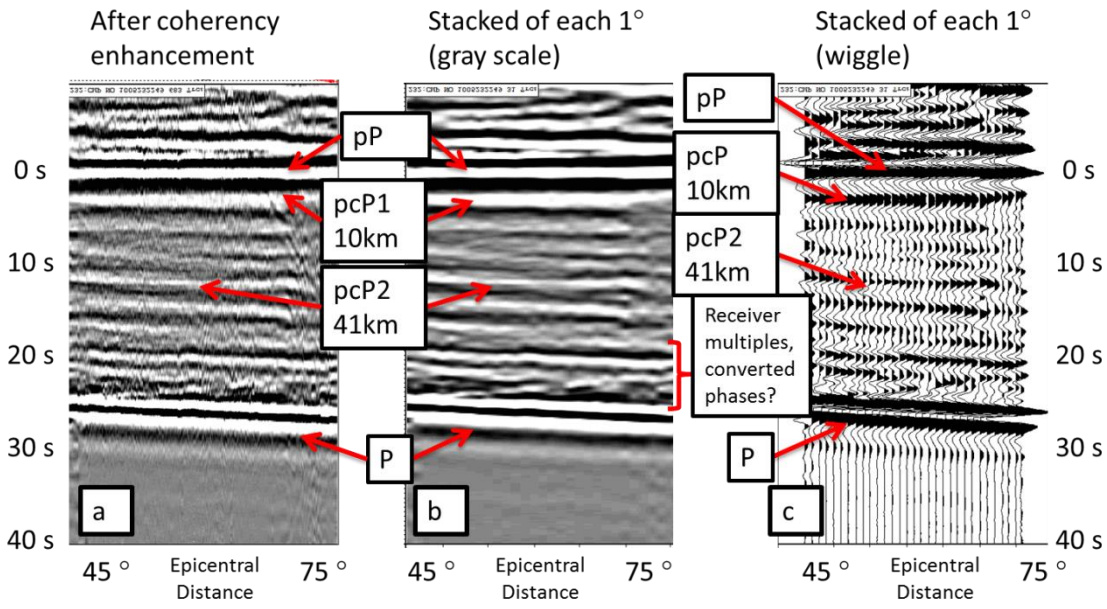

Figure 3-26 Event on 2010/05/23, M=6.1, Depth=101km (c.3). Data are filtered with window: 0.2-0.4-2-4 Hz. (a) data aligned at pP phase at 0s with a series of coherency enhancement (gray scale display). (b) stacking of traces every 1° of epicentral distance. (c) stacking of traces every 1° of epicentral distance (wiggle display).

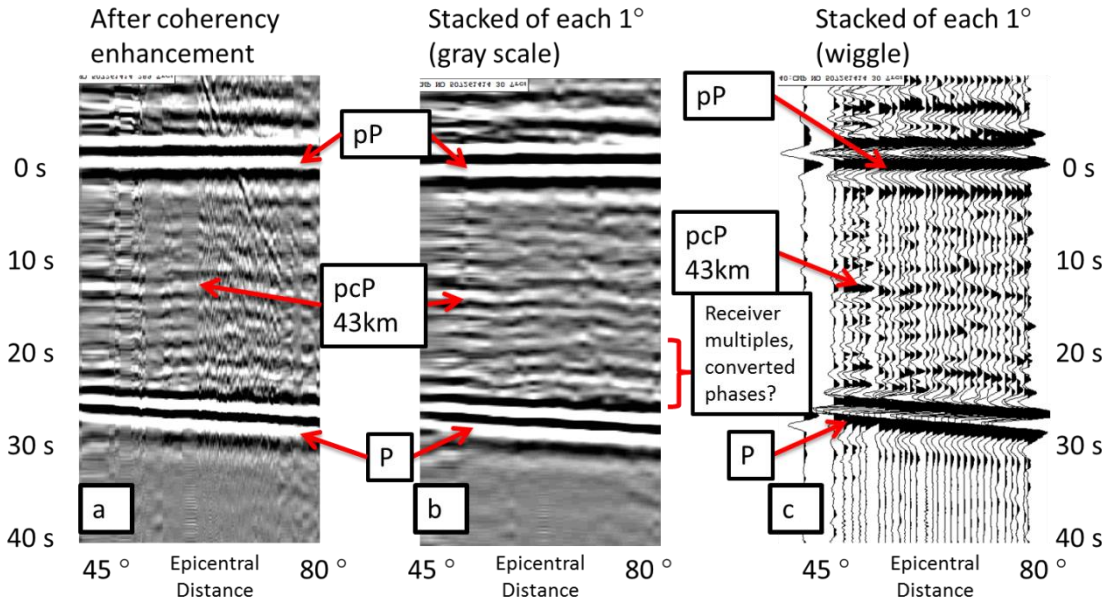

Figure 3-27 Event on 2005/07/26, M=5.9, Depth=110km (c.3). Data are filtered with window: 0.2-0.4-2-4 Hz. (a) data aligned at pP phase at 0s with a series of coherency enhancement (gray scale display). (b) stacking of traces every 1° of epicentral distance. (c) stacking of traces every 1° of epicentral distance (wiggle display).

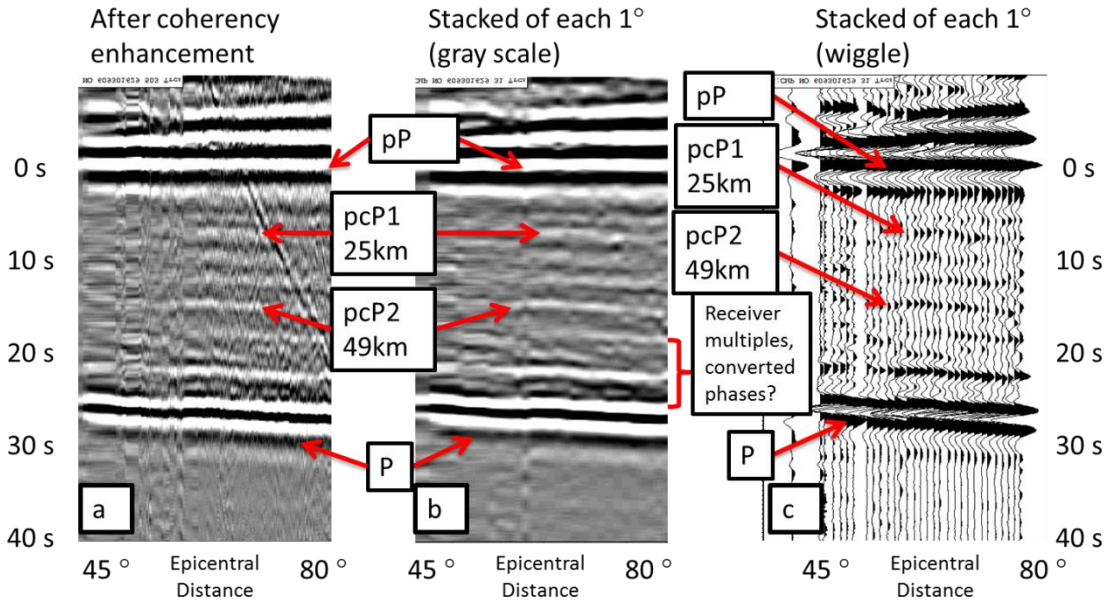

Figure 3-28 Event on 2006/09/30, M=6.0, Depth=107km (c.3). Data are filtered with window: 0.2-0.4-2-4 Hz. (a) data aligned at pP phase at 0s with coherency enhancement (gray scale display). (b) stacking of traces every 1° of epicentral distance. (c) stacking of traces every 1° of epicentral distance (wiggle display).

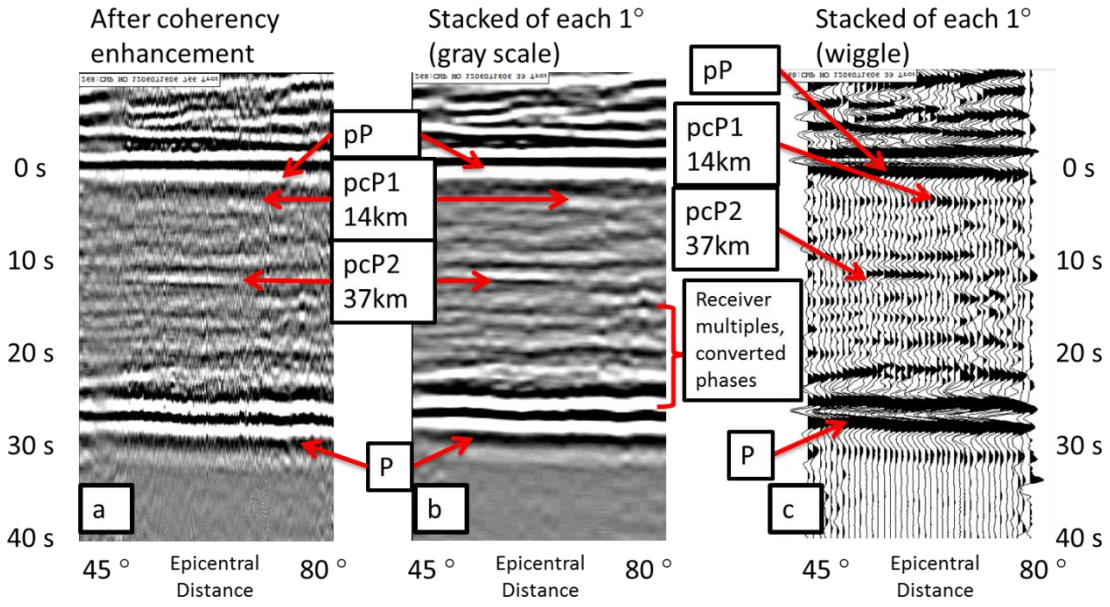

Figure 3-29 Event on 2012/06/07, M=6.1, Depth=110km (c.3). Data are filtered with window: 0.2-0.4-2-4 Hz. (a) data aligned at pP phase at 0s with a series of coherency enhancement (gray scale display). (b) stacking of traces every 1° of epicentral distance. (c) stacking of traces every 1° of epicentral distance (wiggle display).

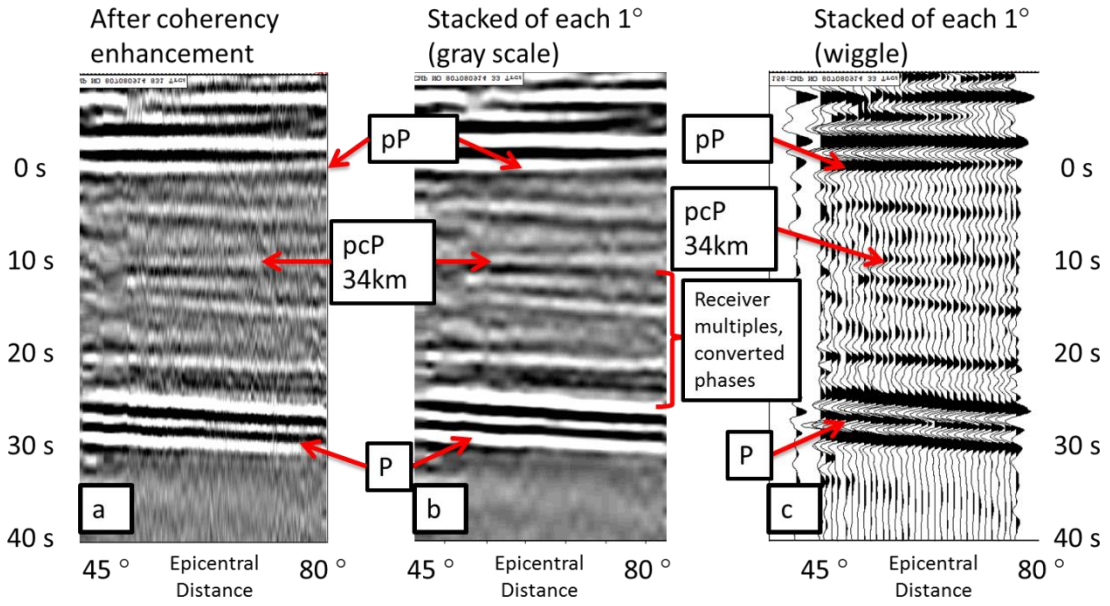

Figure 3-30 Event on 2008/07/08, M=6.2, Depth=123km (c.3). Data are filtered with window: 0.1-0.2-0.4-0.8 Hz. (a) data aligned at pP phase at 0s with a series of coherency enhancement (gray scale display). (b) stacking of traces every 1° of epicentral distance. (c) stacking of traces every 1° of epicentral distance (wiggle display).

Gravity provides another means of assessing the reasonableness of our

estimates. SRTM (Shuttle Radar Topography Mission) DEM (digital elevation model) averaged over a 0.5*0.5 degree area centered of our average pP bounce points are used as the elevations to calculate Airy isostatic crustal thickness. A mantle density of 3300 kg/m^3 and crustal density of 2750 kg/m^3 with a thickness of 40 km (global continental crust average from (Christensen and Mooney, 1995)) are assumed. Such assumption gives us:

$\Delta d=5*h$

(Δd: thickness of crust root, the part beneath normal 40-km-thick crust, h: elevation).

Figure 3-31suggests that isostatic equilibrium is reached in many parts of the Andean orogenic belt, including southern part of central Andes (25°S-30°S), northern Altiplano (10°S-15°S), northern Peru (0°S -5°S). However, there are several regions in the Andes seemingly not under isostatic equilibrium, such as southern part of central Andes (30°S-33°S), central part of central Andes (20°S-24°S), central Peru (7°S-8°S). Here below, we will discuss each of these areas.

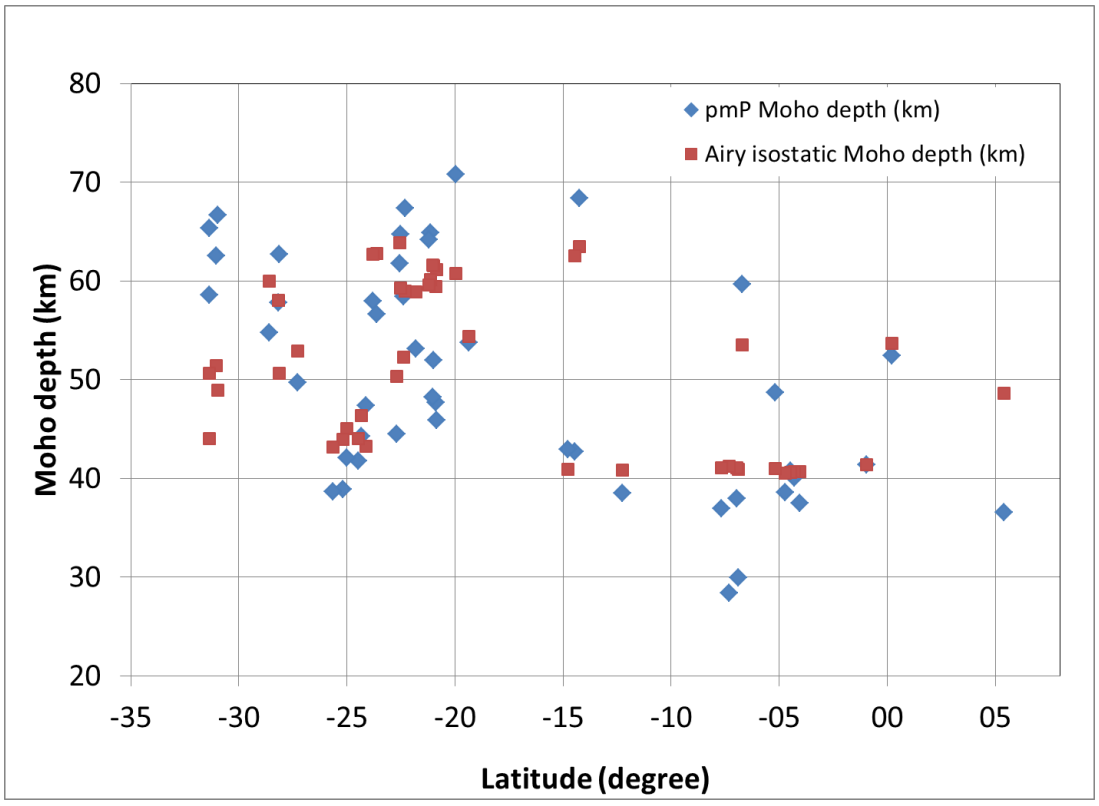

Figure 3-31 Comparison of our Moho depth measurements with Moho depth calculated from average elevation at the bounce points using the Airy isostatic model.

For the southern edge of Puna plateau at 28°S (a.5), isostatic equilibrium is apparently in effect (data between 30°S-28°S in Figure 3-31). Our crustal thickness estimates range from 50 to 62 km, (e.g. even shown in Figure 3-32). In 2008-2009, a passive seismic experiment was carried out in the southern Puna at 25°S-28°S by Cornell University, the University of Missouri and GFZ (Figure 3-1). The receiver function results from that experiment reported by Heit et al. (2014) indicate a crustal thickness of 50-60 km, which is consistent with our observations. There was only one measurement in this region by McGlashan et al. (2008), which indicated a Moho at 70 km depth. The difference might be attributed to their bounce point being located is closer to the plateau and sensing thicker crust there.

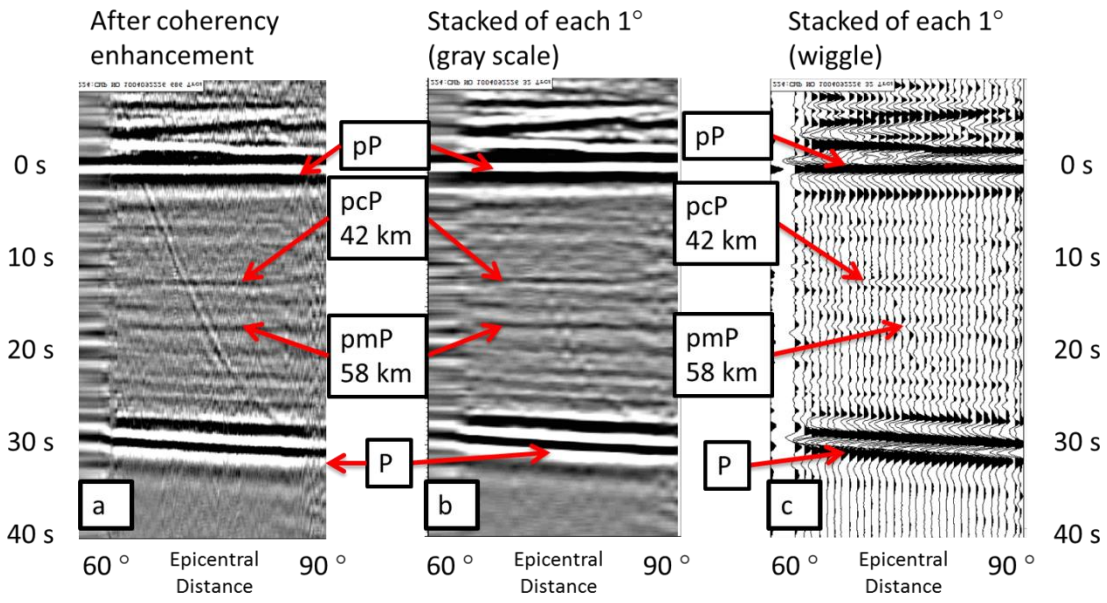

Figure 3-32 Event on 2010/04/09, M=5.8, Depth=117 km (a.5). Data are filtered with window: 0.2-0.4-2-4 Hz. (a) data aligned at pP phase at 0s with coherency enhancement (gray scale display). (b) stacking of traces every 1° of epicentral distance. (c) stacking of traces every 1° of epicentral distance(wiggle display).

For the northern Altiplano at 14°S (b.2), two measurements were obtained by our analysis, one of high quality (quality=4) (event 2009/09/05, Figure 3-33), but the other of low quality=1 (event 2009/09/30, Figure 3-34a,b).

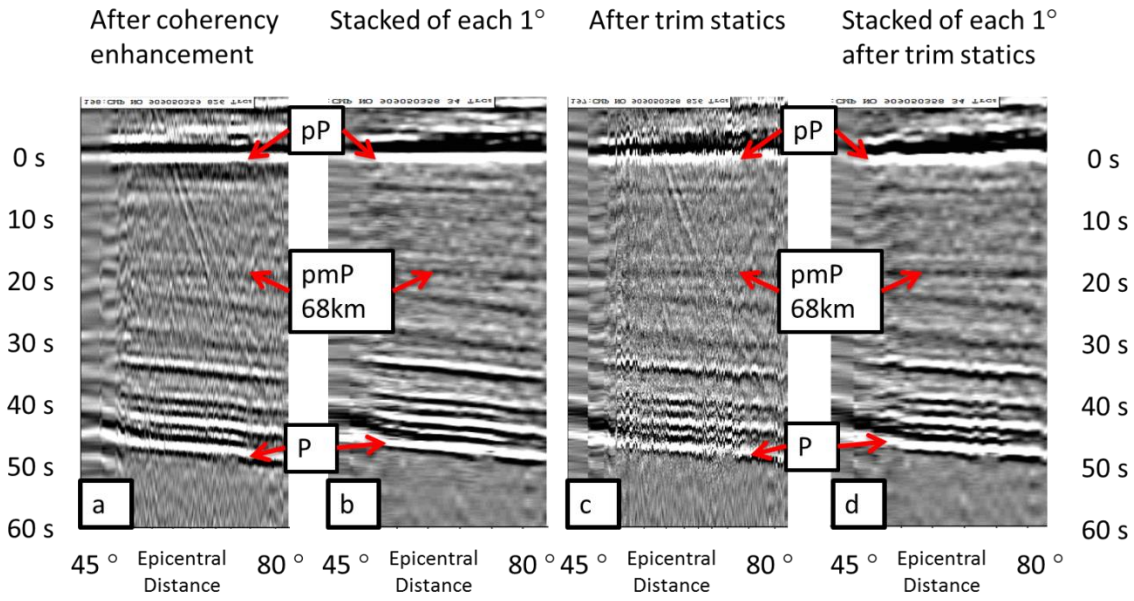

Figure 3-33 Event on 2009/09/05, M=5.8, Depth=210km (b.2). Data are filtered with window: 0.2-0.4-2-4Hz. (a) signal enhanced version (b) stacking of traces every 1° of epicentral distance of the signal enhanced version (c) trim static corrected version of pmP arrival at around 20s (d) stacking of traces every 1° of trim static corrected version. pmP shows moveout distinguishable from direct P. pmP was enhanced by trim static corrections on the time window of 16-22s.

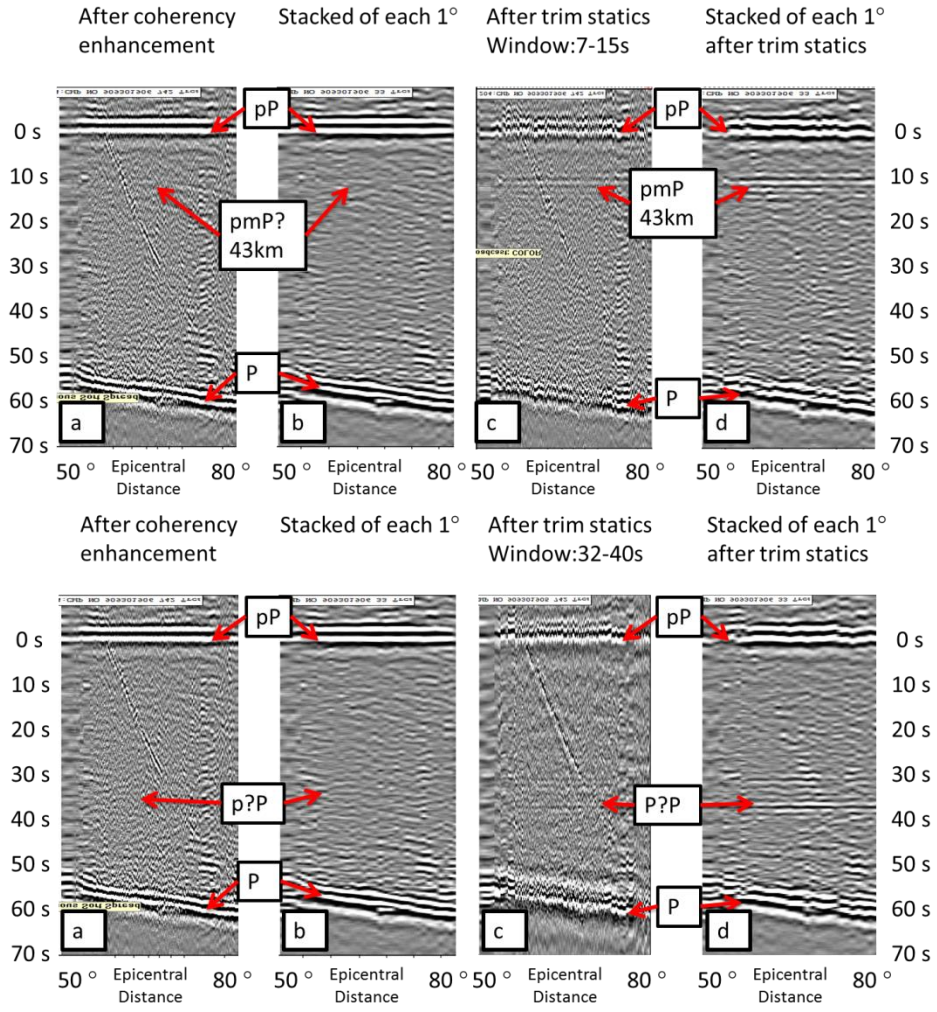

Figure 3-34 Event on 2009/09/30, M=5.9, Depth=255km (b.2). Data are filtered with window: 0.2-0.4-2-4Hz. Upper panel: (a) signal enhanced version (b) stacking of traces every 1° of epicentral distance of the signal enhanced version (c) trim static corrected version of pmP arrival at around 12s (d) stack of 1° of trim static corrected version. pmP enhanced by trim static corrections derived from the time window of 7-15s. Lower panel: the same as upper panel except the time window of 32-40s was used to compute a the trim static correction.

The 2009/09/05 earthquake shows a clear arrival around 20s before pP (Figure 3-33). It dips slightly to the side of smaller epicentral distance. The moveout is distinguishable from the direct P arrival. The differential moveout is best seen after

trim static correction computed over a time window including this arrival (Figure 3-33c, d). After this trim static correction, the precursor appears as a flat arrival, and the pP phase is almost flat while the P is still dipping significantly. Thus this precursor arrival is very likely to be the reflection from source side Moho. If so, this indicates the Moho at about 68 km depth to the south, shallowing about 3-5km to the north. The crust thus thins t away from the plateau over about 100km horizontal distance. This 68km thick crust is consistent with estimates of 70 km from a seismic refraction study by Ocola and Meyer (1972) in this region.

The 2009/09/30 earthquake (Figure 3-34) also shows a very subtle arrival 12.8s earlier than pP, which may correspond to a Moho at 43km. After trim static correction, this arrival becomes broader and more coherent. In order to assess whether this event might be an artifacts of the trim statics, we recomputed the statics using a different time window (32-40s) where no significant arrival is observed. Yet after the new trim static corrections, two "coherent arrivals" at 30s and 37s appeared along with an undulation of the pP arrival. We interpret this to indicate artificial alignment of noise in this case, and discount the pmP picks form this event entirely. Thus trim statics has to be applied with careful quality check and only arrivals that were visible before trim statics were accepted here for interface depth calculation.

For northern Bolivia at 12°S (a.3), significant Moho topography was imaged by a single event. The earthquake on 2011/11/22 has an arrival starting at 10.7s at an epicentral distance of 45° and extending to 12.1s at 67°(Figure 3-35 to Figure 3-37). Because of the large spread of the bounce points in this case, a distinctive dip can clearly be seen for this arrival. If this arrival is a reflection from the underside of the

Moho, that Moho is shallowing from about 41 km depth in the south to about 37 km in the north at depth. This 4-km depth difference of Moho along 150 km lateral distance yields a dip angle of about 1.5 degrees.

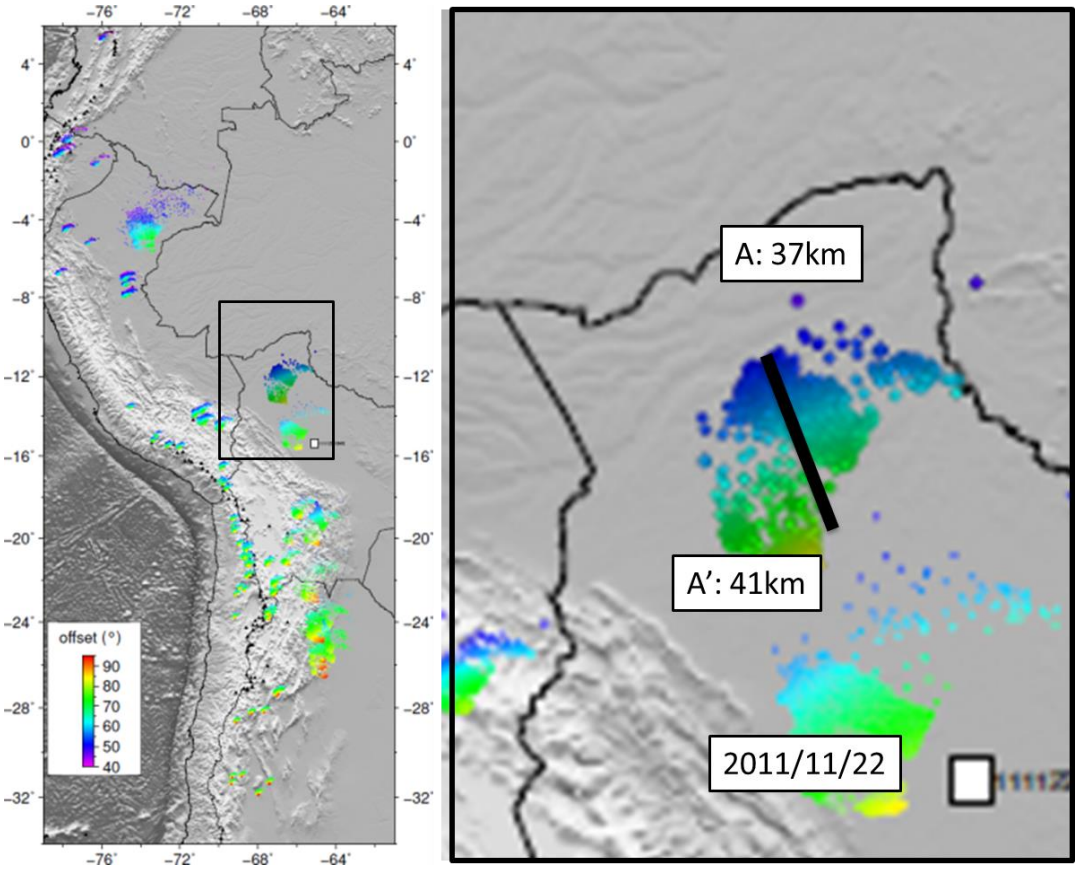

Figure 3-35 Map showing bounce points for event on 2011/11/22, M=6.6, Depth=549 km (c.3) colored by epicentral distances (offset). Notice the closer the earthquake to the recording stations (smaller epicentral distance), the further the bouncepoints are away from the earthquake, a result of ray path geometry. Bouncepoints span about 200 km horizontally.

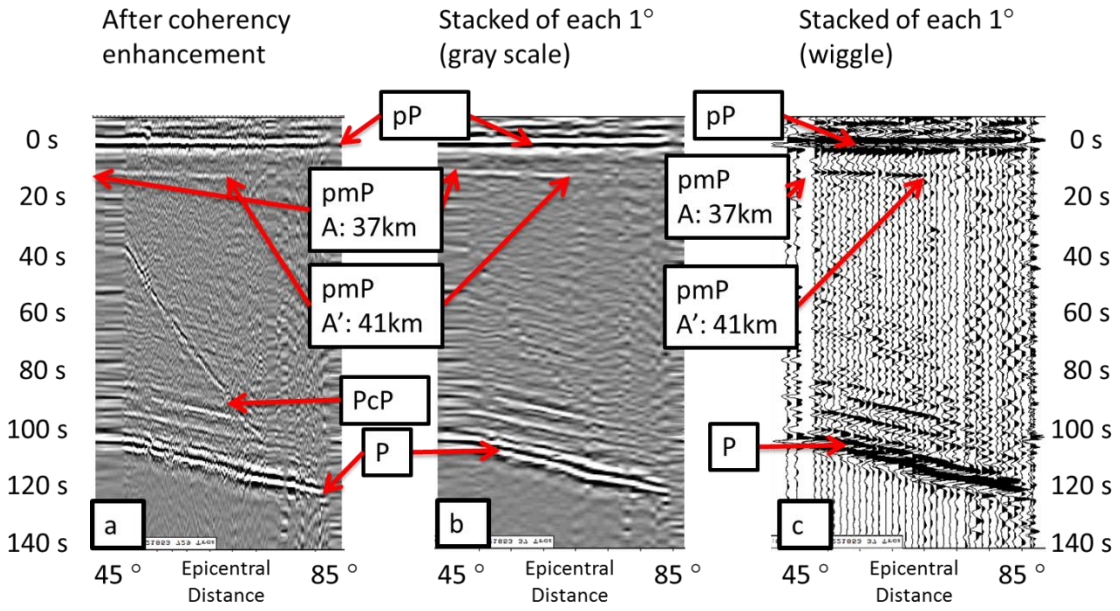

Figure 3-36 Event on 2011/11/22, M=6.6, Depth=549 km (c.3). Data are filtered with window: 0.1-0.2-0.4-0.8 Hz. (a) data aligned at pP phase at 0s with coherency enhancement (gray scale display). (b) stacking of traces every 1° of epicentral distance. (c) stacking of traces every 1° of epicentral distance (wiggle display).

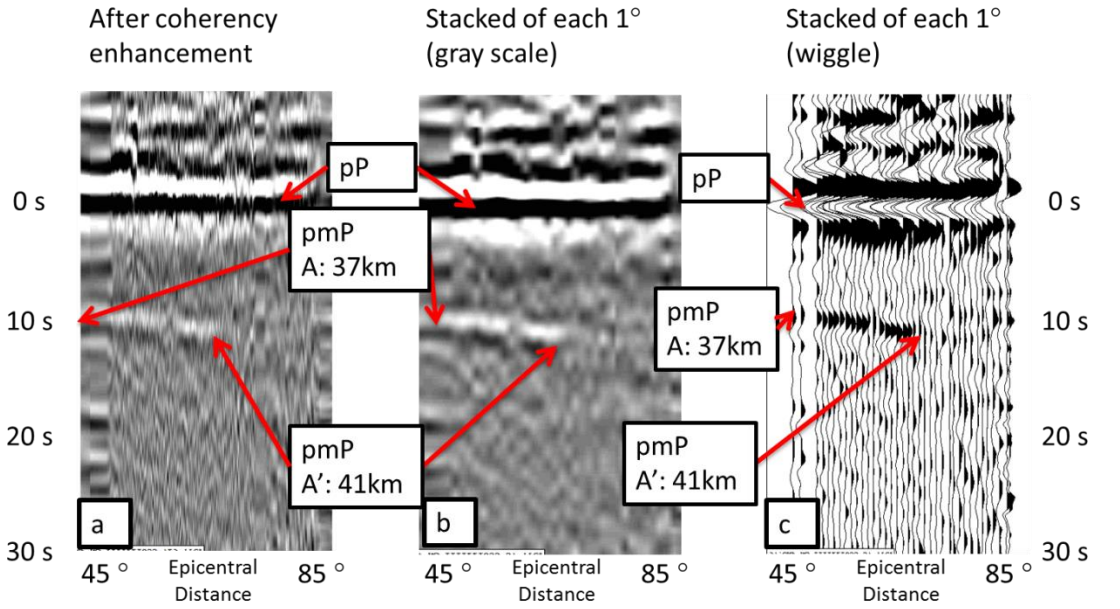

Figure 3-37 A detail of Figure 3-36, showing shallowing of Moho from 41 km (to the SE) to (A' in Figure 4-35) to 37 km to the NW (A in Figure 4-35.)

In northern Peru at 0-5°S (a.1), the pmP phases are well recorded from a few

earthquakes, yielding depths clustering between 37-42km, (e.g. event 2007/07/21 in Figure 3-38 and Figure 3-39). Geophysical measurements are lacking in this part of South America because of its inaccessibility. These Moho depth estimates measurements are the first for this region.

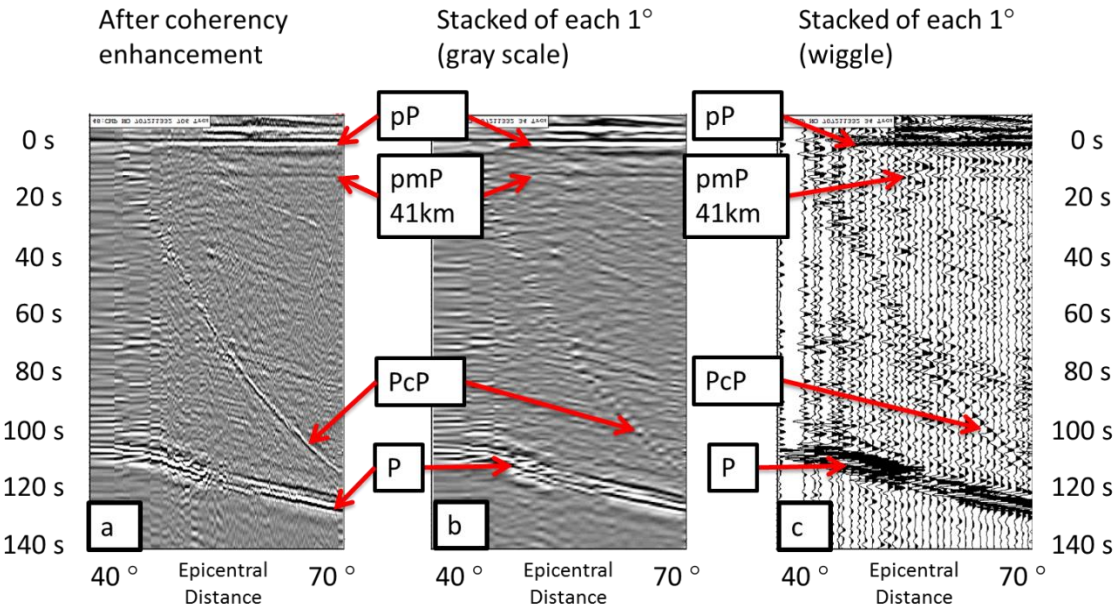

Figure 3-38 Event on 2007/07/21, M=6.1, Depth=644 km (a.1). Data are filtered with window: 0.1-0.2-0.4-0.8 Hz. (a) data aligned at pP phase at 0s with a series of coherency enhancement (gray scale display). (b) stacking of traces every 1° of epicentral distance. (c) stacking of traces every 1° of epicentral distance (wiggle display). Geophysical measurements are lacking here because of inaccessibility. These Moho measurements are the first constraints on crustal thickness for of this region.

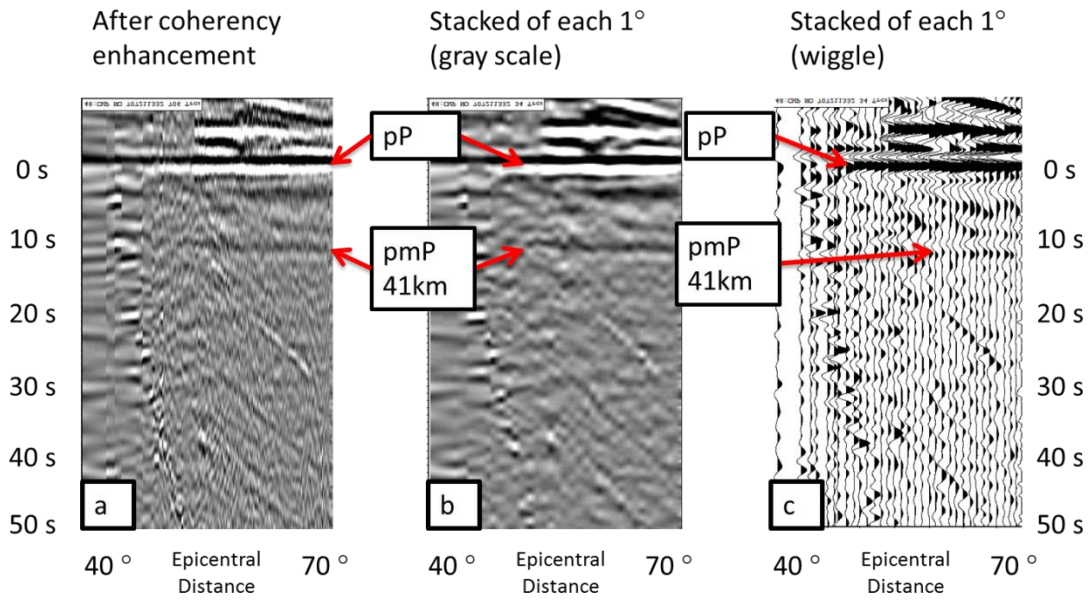

Figure 3-39 A detail version of Figure 3-38.

In the southern part of central Andes (30°S-33°S) (a.6), our data indicate crustal thicknesses are about 59-67 km, examples of which are shown in Figure 3-40 and Figure 3-41. The previous receiver function studies by Gilbert et al. (2006) and Gans et al. (2011) indicate crustal thickness of 60-65 km in this region while the Moho depths derived from pP precursor study by McGlashan et al. (2008) yielded estimates of 50-61km. Moho depths from a Pn apparent phase velocity study (Fromm et al., 2004) also ranged from 50-60 km. However isostatic equilibrium would suggest a crustal thickness of 44-51 km (Figure 3-31) for the average elevation of 800-2300m. All of the crustal thickness estimates thus suggest the area is out of equilibrium, perhaps due to flat slab effects (Kay and Abbruzzi, 1996).

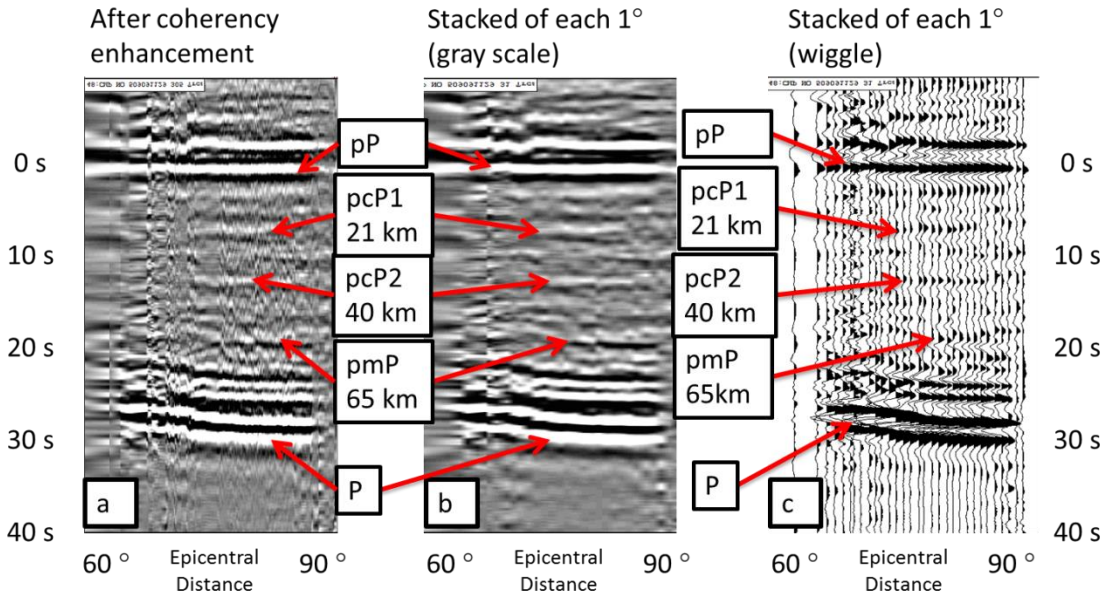

Figure 3-40 Event on 2005/09/09, M=5.8, Depth=112 km (a.6). Data are filtered with window: 0.2-0.4-2-4 Hz. (a) data aligned at pP phase at 0s with a series of coherency enhancement (gray scale display). (b) stacking of traces every 1° of epicentral distance. (c) stacking of traces every 1° of epicentral distance (wiggle display).

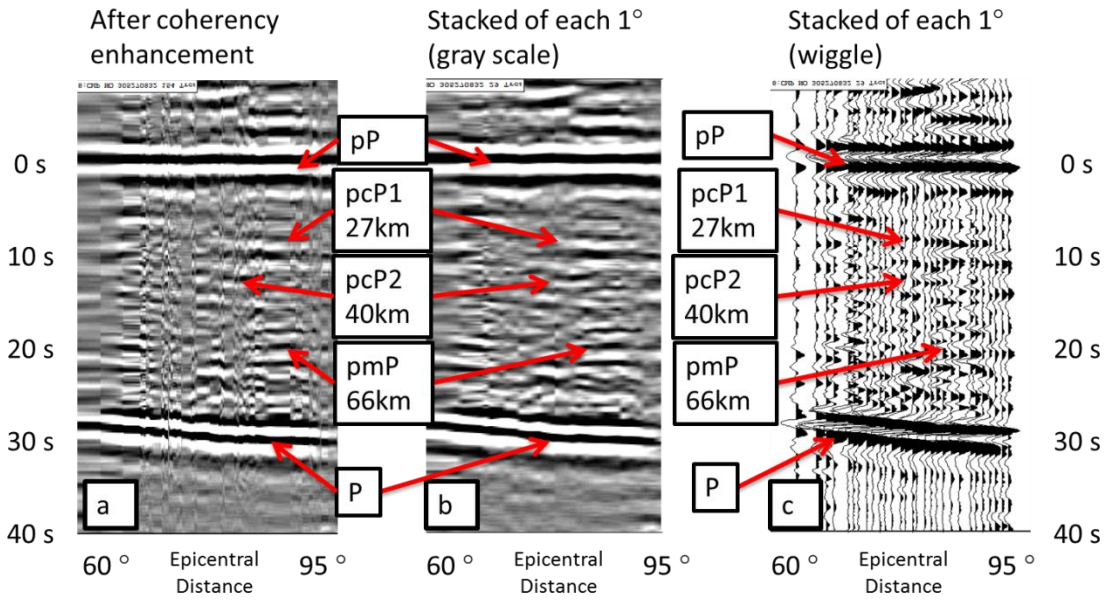

Figure 3-41 Event on 2003/05/27, M=5.7, Depth=118 km (a.6). Data are filtered with window: 0.2-0.4-2-4 Hz. (a) data aligned at pP phase at 0s with coherency enhancement (gray scale display). (b) stacking of traces every 1° of epicentral distance. (c) stacking of traces every 1° of epicentral distance (wiggle display).

For the central part of central Andes (20°S-24°S) (c.5), a few of our Moho depth estimates are shallower what would be consistent with Airy isostasy. These measurements (Figure 3-19 to Figure 3-21) are concentrated beneath the volcanic arc. It has already been mentioned that our Moho depth measurements there are less than the those from the receiver functions study of Yuan et al. (2002). Their crustal thickness of 67km fits the isostatic equilibrium estimate 60-65 km. This would suggest that the interface in our measurements may be from the lower crust rather than the top of the mantle.

In central Peru (7°S-8°S) (a.2), pmP from four earthquakes are observed. Three are well imaged. Two events show clearly the Moho depth in the range of 28-29km, one of which is shown in Figure 3-6 and Figure 3-7. Two other events indicate a Moho depth about 38km (Figure 3-10a, the 2008/08/26 event). James and Snoke (1994) derived crustal and sedimentary layer thicknesses using converted phases from regional intermediate-depth earthquakes in the region between 7°S-9°S (Figure 3-1). Their study showed a 4-4.5 km thick sedimentary layer and 33.5-35 km thick crust in the region of our bounce points. Atherton et al. (1983) also showed the crust in this region is about 30 km thick from gravity modeling.

Sedimentary basins often have a relatively low seismic P wave velocity compared to underlying basement, which can significantly affect the average crustal P wave velocity used to convert time to depth. If there were no sedimentary cover at the bounce points of the 2007/07/12 event, then the pmP would suggest a crust of 30 km thickness assuming an average crustal Vp=6.5km/s. However, if we assume 10 km of sedimentary cover at the bounce points of the 2008/08/26 event, then the crustal

thickness implied by the pmP time would be 33 km for the corresponding average crustal Vp of 5.5 km/s. Thus a large part of the apparent discrepancy of crustal thickness estimates between the 2007/07/12 event and 2008/08/26 event might be simply be due to variations in sedimentary cover. The alternatives are that these two pmP phases reflect real change of the Moho topography or that these two pmP phases are not both reflected from the Moho. It is possible that either the shallow one is from an intracrustal interface or the deep one from an upper mantle interface beneath the Moho. The expected isostatic Moho should lie around 40 km for this region. Isostatic equilibrium would certainly be a reasonable assumption for this region as it is part of the Brazilian craton. If the strong pmP event here is the reflection from a lower crustal interface at 28 km, the question arises as to why a prominent reflection from the underlying Moho is not also evident. It is possible that the Moho is non-reflective to our underside reflection technique if there is no large impedance contrasts between the crust and mantle, or if the distance over which the impedance changes is large with respect to the wavelength of pmP.

3.3.2 Non-reflective Moho

Non-reflective Mohos are not an unusual observation for deep seismic reflection surveys, which have sampled large portions of the continental crust since the inception of the COCORP (Consortium for Continental Reflection Profiling) in the US in the 70s. The Moho imaged by seismic reflection profiles has been variously characterized as a single reflector, double reflector, spatial termination of a reflective crust, the termination of strong laminated lower crust or simply indistinct (Oliver, 1988). Thus it is quite possible the lack of an observed underside reflection from a

deep earthquake is telling us something significant about the nature of the Moho at those bounce points. In particular, they may be diagnostic if more gradational crust-mantle transition zones are the case.

The white squares marked in Figure 3-24 indicate regions where intracrustal reflectors are observed by our study but no clear pmP precursors are seen (compare with intracrustal reflector map Figure 3-42 and detailed map of central Andes Figure 3-43).

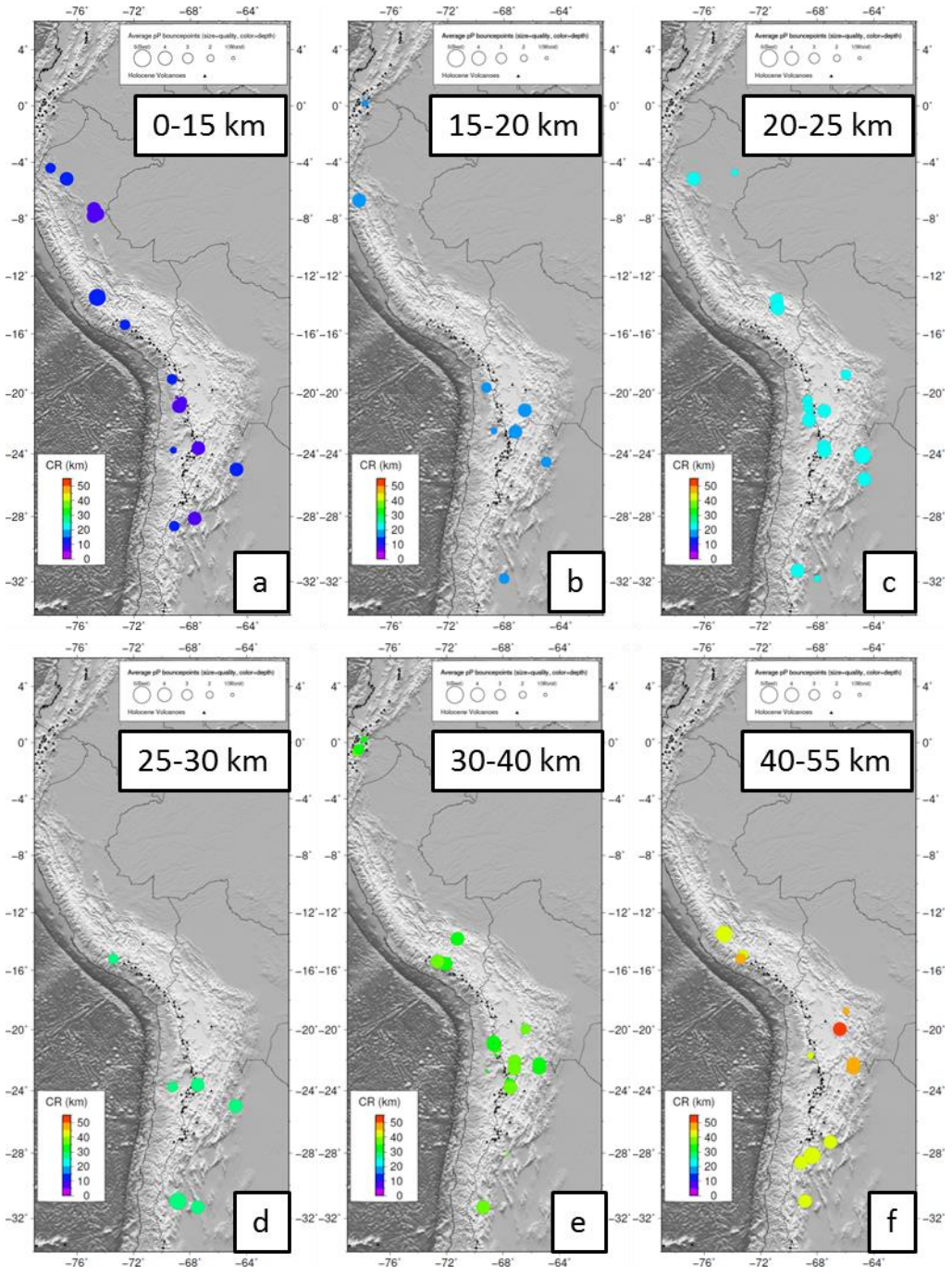

Figure 3-42 Intra-crustal reflector depth map (from pcP phase): (a) 0-15 km, (b) 15-20 km, (c) 20-25 km, (d) 25-30 km, (e) 30-40 km, (f) 40-55 km.

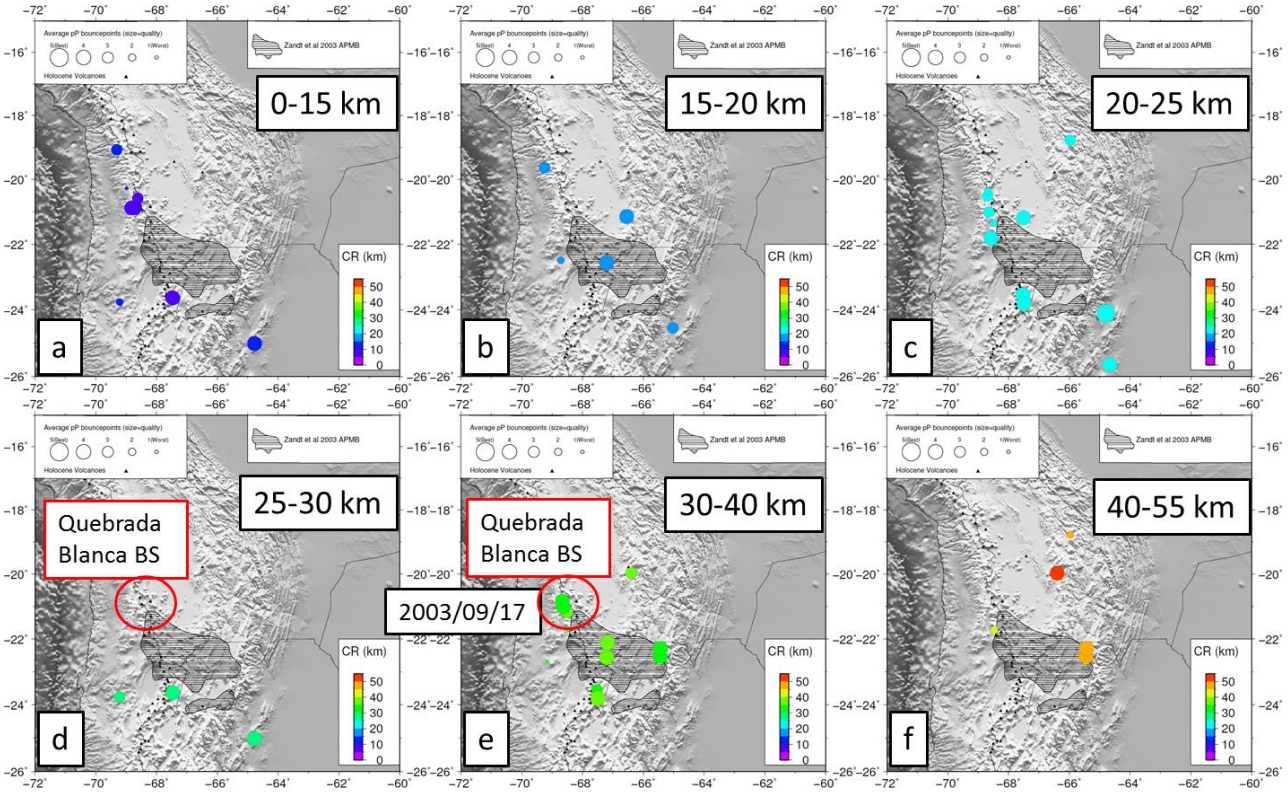

Figure 3-43 Intra-crustal reflectors from our study in the central Andes,. The position of the Altiplano-Puna magma body (APMB) discovered from receiver functions study (Zandt et al., 2003) is shaded (a) 0-15 km, (b) 15-20 km, (c) 20-25 km, (d) 25-30 km, (e) 30-40 km, (f) 40-55 km. Quebrada Blanca BS (bright spot) and nearby event in our study (Figure 3-20) are plotted.

These regions are mainly active volcanic arcs (c.2, c.3, c.4). Even though there are measurements of Moho depths from previous precursor study by McGlashan et al. (2008) in the southern Peru (c.3), the ambiguity still exists that those arrivals are from receiver side multiples or converted phases as we discussed before. Since intracrustal reflectors are detected for these areas, it is unlikely that the earthquakes simply lacked sufficient energy to illuminate Moho (Figure 3-2). Therefore the best explanation is that the Moho is truly non reflective. This could be interpreted to indicated that the Moho is too irregular to give rise to a coherent reflection but instead scatters seismic energy to various directions. Alternatively, the Moho is represented by a gradational change in impedance that is too gradational to be detected at the frequencies of the pP

phase. Thirdly, these areas may be represented by lower crust that is seismically indistinguishable from upper mantle. A mafic lower crust that has been converted to eclogite would be one example of a means of "erasing"" the seismic Moho.

3.3.3 Intracrustal Reflectors

One of the most interesting findings of this study are the presence of reflecting interfaces within the crust at some locales. The locations of intracrustal reflectors found during this survey are shown in Figure 3-42 and Figure 3-43.

As discussed above, some of the deeper reflectors that were first assumed to be from the Moho actually correspond to deep intracrustal interfaces in thick crust. These include the data from southern Peru (c.3), central Altiplano-Puna Plateau (b.3), southern edge of Puna plateau 28S-32S (a.5, a.6).

In the southern Peru (c.3), five events in the region are shown in Figure 3-26 to Figure 3-30. Clear reflections are observed at 10km, 25 km and depth of 34-49 km. None of these reflectors are thought to represent the Moho because they are not consistent with the 70 km crustal thickness expected beneath this part of the Altiplano plateau (Ocola and Meyer, 1972). For those apparent reflectors at 34-49km depth, we cannot totally rule out the possibility of their being generated at the receiver side because their moveout is indistinguishable from the direct P arrival which is also similar to the receiver side multiples and conversions from the direct P wave. Moreover, the time separations between P and pP are all less than 30s. Thus underside reflection above the source from any interface deeper than 50 km will occur at the travel time range of receiver side multiples or converted phases.

The seismic refraction study in this region by Ocola and Meyer (1972) showed

two low velocity zones, one around 10 km and the other at 36-46 km in Peru. It is very likely that our 34-49 km reflectors represent the interfaces of this low velocity zone, with high velocity zone above and below. This low velocity zone was interpreted by Ocola and Meyer (1972) as basaltic (intrusive and volcanic) material at depth and produced by overheated material (partial melt?).

Beneath the central Altiplano-Puna plateau and the Southern Andes at 28°S-32°S (a.5, a.6, b3), there are also reflectors in the 30-40 km depth range (Figure 3-16, Figure 3-17, Figure 3-32, Figure 3-40, Figure 3-41 and Figure 3-44). We interpret these phases as possible reflections from the top of an eclogitized lower crust. Such a boundary would be expected to give rise to a strong reflection because of the large velocity and density (impedance) contrast associated with a boundary between eclogite and intermediate composition rocks. Eclogitization might also explain the discrepancy between the calculated isostatic Moho depth and our observation. An eclogitized lower crust in this region might function as a sinker and pull the crust down. Delamination of eclogitized lower crust has been attributed to the rapid, large scale (~2.5km rise) surface uplift of central Andes during late Miocene (Garzione et al., 2006; Ghosh et al., 2006; Molnar and Garzione, 2007; Garzione et al., 2008; Hoke and Garzione, 2008). Moreover, an eclogite sinker has been also used to explain for the low elevation (0.9-1.2 km) of the southern Ural mountains in central Russia, where a presence of a thick, mafic, seismically fast eclogitic root in the crust has been confirmed by active-source deep seismic reflection studies (Carbonell et al., 1996; Knapp et al., 1996; Steer et al., 1998).

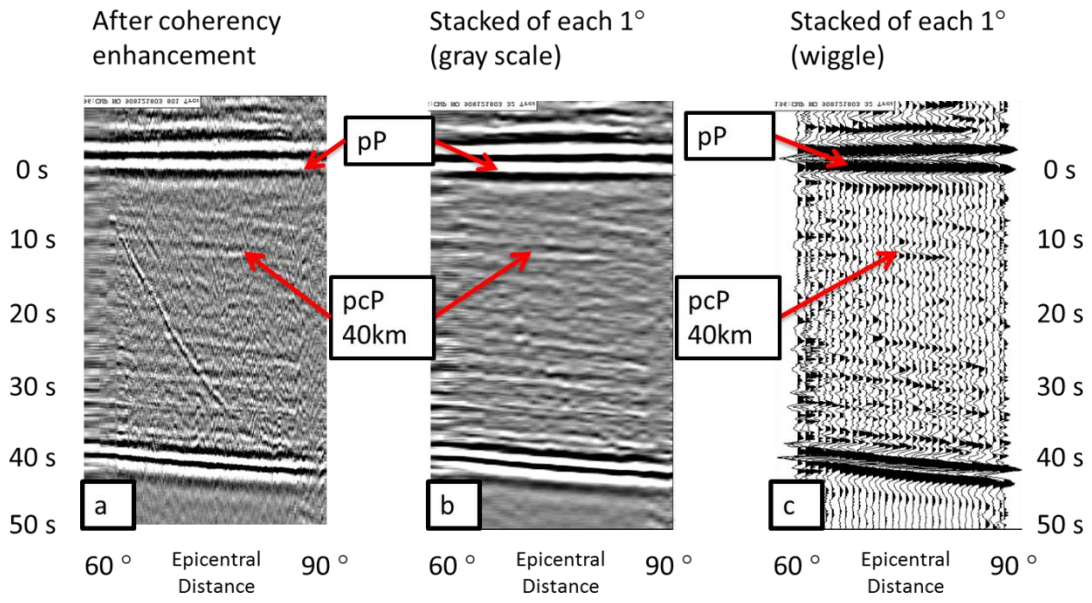

Figure 3-44 Event on 2009/08/12, M=5.5, Depth=173 km (a.5). Data are filtered with window: 0.2-0.4-2-4 Hz. (a) data aligned at pP phase at 0s with coherency enhancement (gray scale display). (b) stacking of traces every 1° of epicentral distance. (c) stacking of traces every 1° of epicentral distance (wiggle display).

If the concept of a non-reflective Moho marking a boundary between eclogitized lower crust and mantle peridotite is valid, these deep crustal underside reflectors would correspond to the top of a high velocity lower crustal layer. We note that all of these examples occur within the Andean forearc or nearby region, which suggest a common crustal evolution for this region along strike.

There is another possible interpretation of reflectors in the depth range from 30-50 km in other parts of the Andean system. There are few reflectors observed at depth of 30-50 km beneath the southeastern edge of the Puna plateau (a.4). Two reflectors are evident from the event 2005/03/21 at 33-km-depth (pcP1) and 47-km-depth (pcP2) (Figure 3-16 and Figure 3-17). Allmendinger and Zapata (2000) have argued from conventional seismic reflection data that a subAndean decollement exists at a depth of 32-41 km on the eastern flank of the Altiplano-Puna plateau. Bounce

points from event 2005/03/21 are very close (<100km) to their seismic reflection survey. Therefore it is reasonable to infer that our reflectors here may be a manifestation of such a megathrust or decollement at depth.

However, these deep (ca. 40-55km) interfaces are not the only strong crustal interfaces that we observe. A number of the records with bounce points beneath the Altiplano-Puna region exhibit strong reflectors at depths of about 15-35 km (Figure 3-15 to Figure 3-17, Figure 3-19, Figure 3-20 and Figure 3-45). For example, a clear arrival 9-10s before pP is observed from event 2003/09/17, which corresponds to a crustal reflector at depth of 30 km (using Vp=6.2km/s) (Figure 3-20). This reflector is very coherent and strong and may possibly indicate a large impedance contrast across the reflector. The location of this reflection and it depth are consistent of Quebrada Blanca bright spot discovered by ANCORP project (ANCORP Working Group, 1999, 2003). This bright spot was interpreted as small, localized bodies or a noninterconnected network of melts or fluids due to its negative polarity and existing MT data (ANCORP Working Group, 2003).

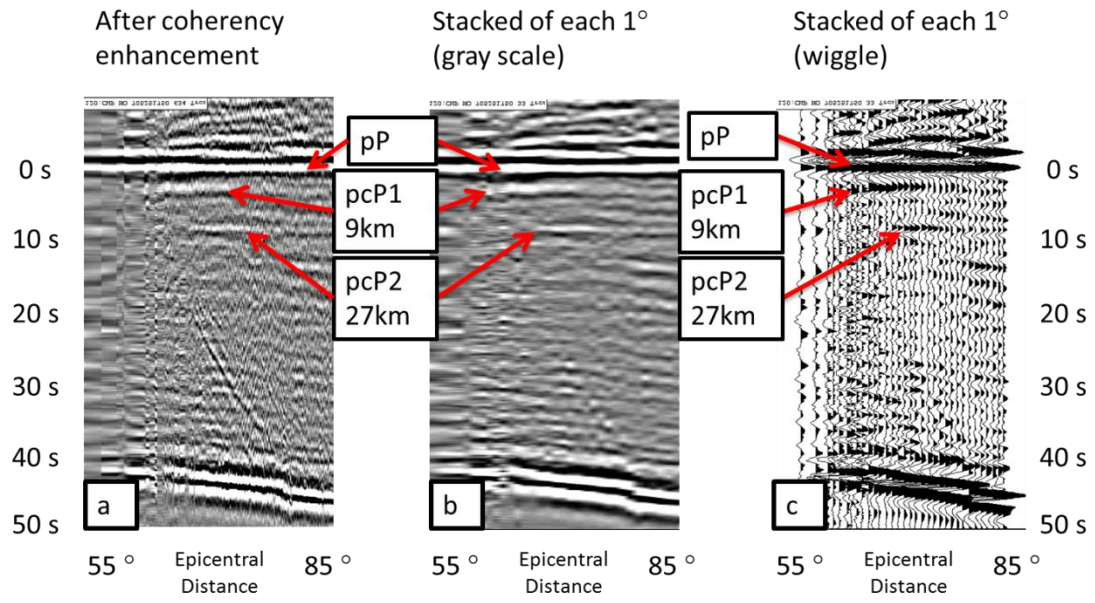

Figure 3-45 Event on 2007/05/25, M=5.9, Depth=180 km (b.3). Data are filtered with window: 0.2-0.4-2-4 Hz. (a) data aligned at pP phase at 0s with a series of coherency enhancement (gray scale display). (b) stacking of traces every 1° of epicentral distance. (c) stacking of traces every 1° of epicentral distance (wiggle display).

Previous teleseismic and local receiver function study by Zandt et al (2003) delineated a region characterized by a pervasive ~20-km-deep, very low-velocity layer, which they termed the Altiplano-Puna magma body (APMB). It has been associated with the Altiplano-Puna Volcanic Complex (APVC) in the central Andes (De Silva, 1989). Our observations are plotted on top of the APMB (Figure 3-43). Only one of our events, lying at a depth of 15-20 km, lies within the APMB zone. Many of reflectors we find in the 15-25 km depth are in areas surrounding the APMB zone. Others indicated intracrustal reflectors but at greater depths, 30-40 km than the APMB. These suggest the mid-crustal melting may be more extensive, but less continuous, than implied by the receiver function results. It is also certainly possible that some of the intracrustal reflections found in this area do not correspond to modern magmas like the APMB but represent older intrusions at various depths.

Interestingly, we also observe some prominent shallow (6-14 km) intracrustal reflectors in regions such as southern Peru (a.2, Figure 3-26 and Figure 3-46),and Northern Chile (c.4, c.5, Figure 3-19 and Figure 3-21). Since there is no complementary geophysical data to constrain the nature of these events, it is speculative but possible to suggest that magma sills may underlie these regions as well. A shallow magma body beneath the Coropuna and Andahua-Orcopampa volcanoes in southern Peru and Irruputuncu and Olca-Paruma volcano in northern Chile would certainly not be unlikely

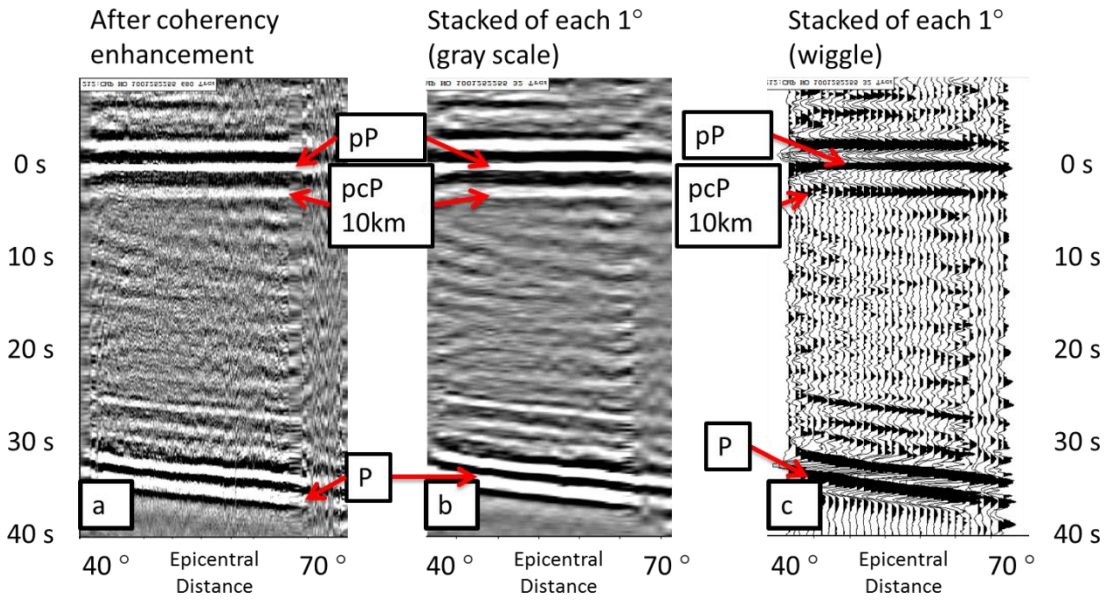

Figure 3-46 Event on 2010/01/25, M=5.9, Depth=146 km (a.2). Data are filtered with window: 0.1-0.2-0.4-0.8 Hz. (a) data aligned at pP phase at 0s with a series of coherency enhancement (gray scale display). (b) stacking of traces every 1° of epicentral distance. (c) stacking of traces every 1° of epicentral distance (wiggle display).

The relatively strong shallow crustal reflections in central Peru (a.2), within the Santa Barbara system (a.4), and under the southern Puna plateau (a.5) may have other explanations. Intracrustal reflectors at 9-10km event from two events (Figure 3-45 and Figure 3-46), less than 100 km east of the Subandean thrust and fold belt (STFB). This

region is known for its substantial sedimentary basin e.g. the Ucayali Basin (Mathalone, 1995). Megard (1984) argued that the STFB had a width of about 100-150 km containing a sedimentary prism consisting of 8 km of Mesozoic-Cenozoic strata overlying >1 km strata of Paleozoic. Pardo (1982) inferred the existence of a decollement at around 9 km depth because the steeply dipping upthrust observed from seismic profiling seems to flatten at depth. Recomputing the depth of the intracrustal events in our study using the lower velocities appropriate for a sedimentary basin (e.g. 4km/s or 5 km/s) suggest that they could well be from the sedimentary-basement contact or an associated decollement. The shallow reflectors at 13 km depth beneath the Santa Barbara system (a.4, Figure 3-47), at 12 km depth beneath southern edge of Puna plateau (a.5, Figure 3-48) may likewise arise from structural decollements in those region. Reflectors at 20-27 km beneath southern Andes at 32°S are also candidates for a decollement at depth (**Error! Reference source not found.**Figure 3-40 and Figure 3-41).

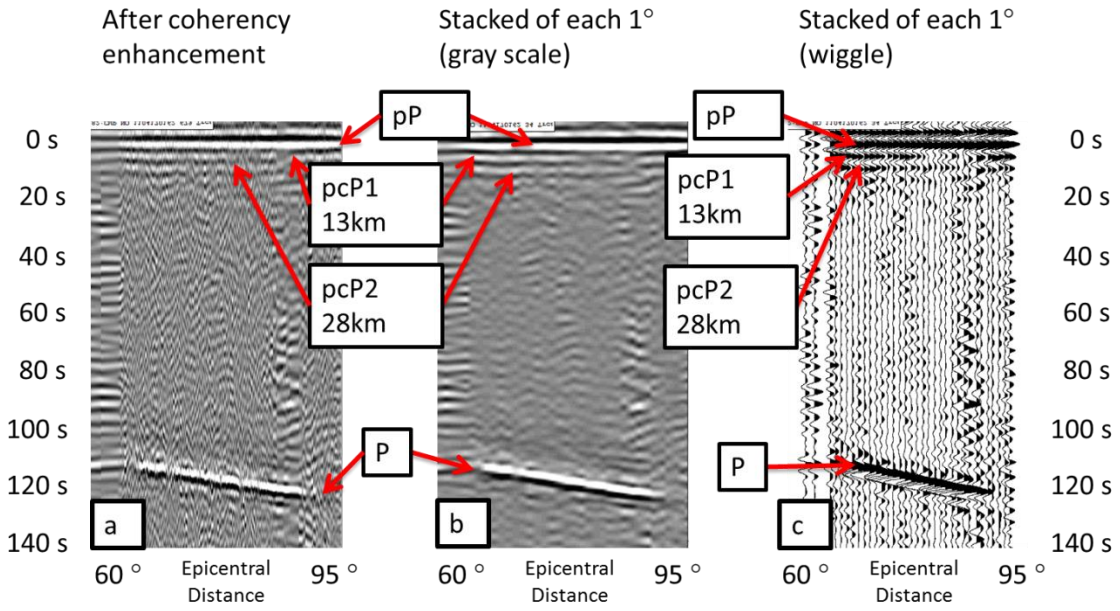

Figure 3-47 Event on 2011/04/17, M=5.7, Depth=556 km (a.4). Data are filtered with window: 0.1-0.2-0.4-0.8 Hz. (a) data aligned at pP phase at 0s with coherency enhancement (gray scale display). (b) stacking of traces every 1° of epicentral distance. (c) stacking of traces every 1° of epicentral distance (wiggle display).

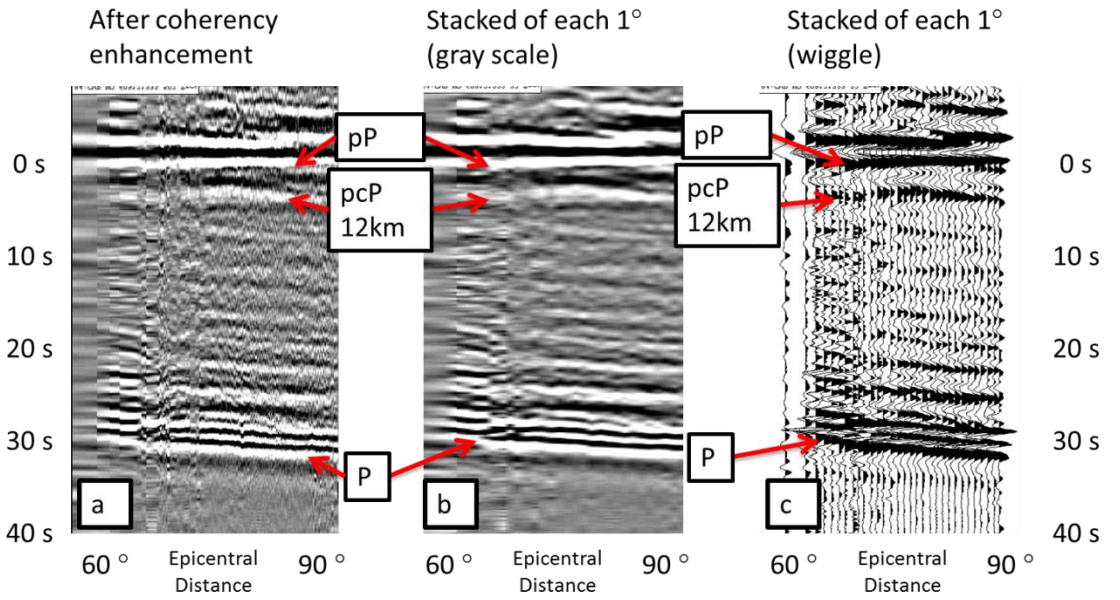

Figure 3-48 Event on 2006/09/12, M=6.0, Depth=114 km (a.5). Data are filtered with window: 0.2-0.4-2-4 Hz. (a) data aligned at pP phase at 0s with a series of coherency enhancement (gray scale display). (b) stacking of traces every 1° of epicentral distance. (c) stacking of traces every 1° of epicentral distance (wiggle display).

3.3.4 Upper mantle discontinuities

The lithospheric mantle is generally considered to be more homogeneous than the crust. However, both deep seismic reflection profiling (Steer et al., 1998) and receiver function studies (Kind et al., 2012) have found numerous instances of seismic discontinuities at depths that suggest they lie within the lithospheric mantle. In addition, there is considerable current debate over the nature of the lithosphere-asthenosphere boundary, and whether it is mappable by reflected or converted seismic waves or tomography (e.g. (Fischer et al., 2010; Yuan and Romanowicz, 2010)).

However, we have failed to identify any arrivals that we can conclusively associate with the LAB. McGlashan (thesis draft) reported arrivals on their single trace records that they suggest could correspond to the LAB beneath eastern edge of central Altiplano-Puna plateau at a depth of 120-180 km. We identify a possible 105 km deep intracrustal near their LAB detecting locations (Figure 3-16 and Figure 3-49). But our puP phase and their LAB phase show at very different time (ours: 30s, theirs: >50s). Depths of upper mantle interfaces indicated by our study are about 90-105 km beneath central Altiplano-Puna plateau, which are much shallower than McGlashan's (thesis draft) of 120-180 km in the same region. Also, only two of such reflections are observed in our study while several have been observed on McGlashan's single stack result. The difference between the single trace and array methods that have been discussed above may also apply in this case.

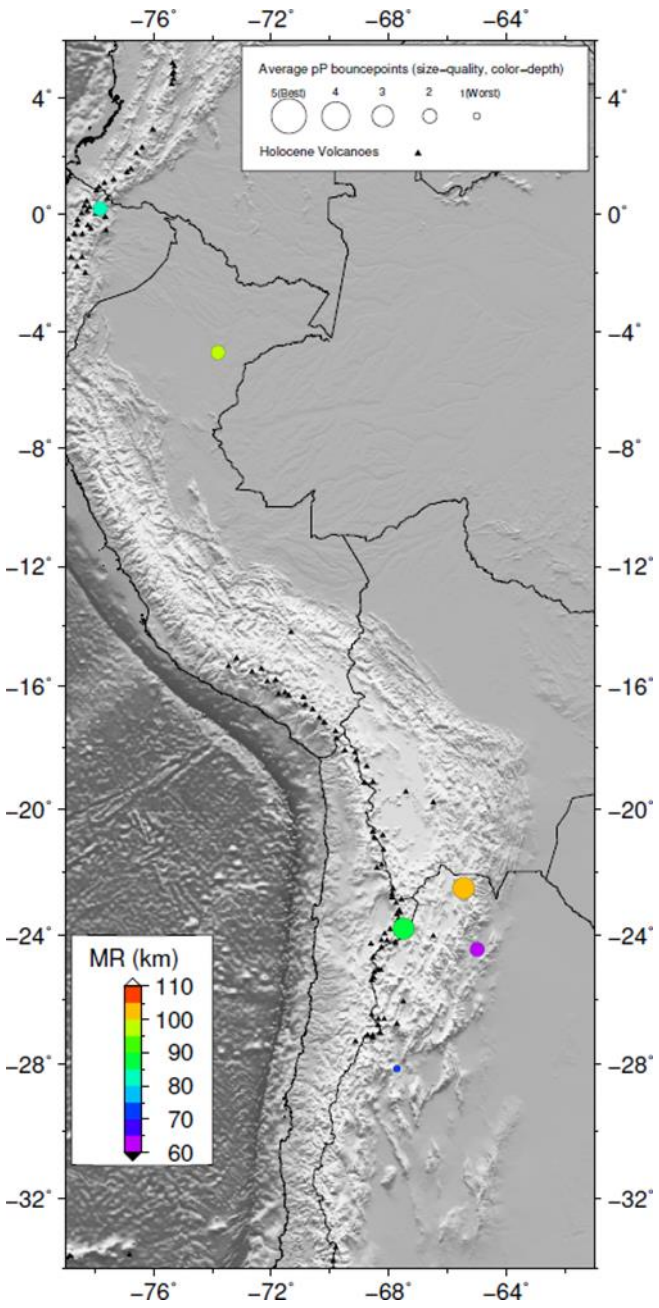

Figure 3-49 Upper mantle reflectors map, circles=average pP surface bounce points. Colors of circles indicate upper mantle reflector depths derived from puP time, using average Vp=7km/s.

There is another possible mantle reflector at 88 km depth from our new recordings as shown in (Figure 3-50). This depth has been associated in conventional refraction work with a change in velocity that has become known as the Hales discontinuity (*Hales*, 1969; Levin and Park, 2000). The Hales discontinuity has been

interpreted as phase transition from spinel to garnet in Iherzolitic peridotite (Bostock, 1997).

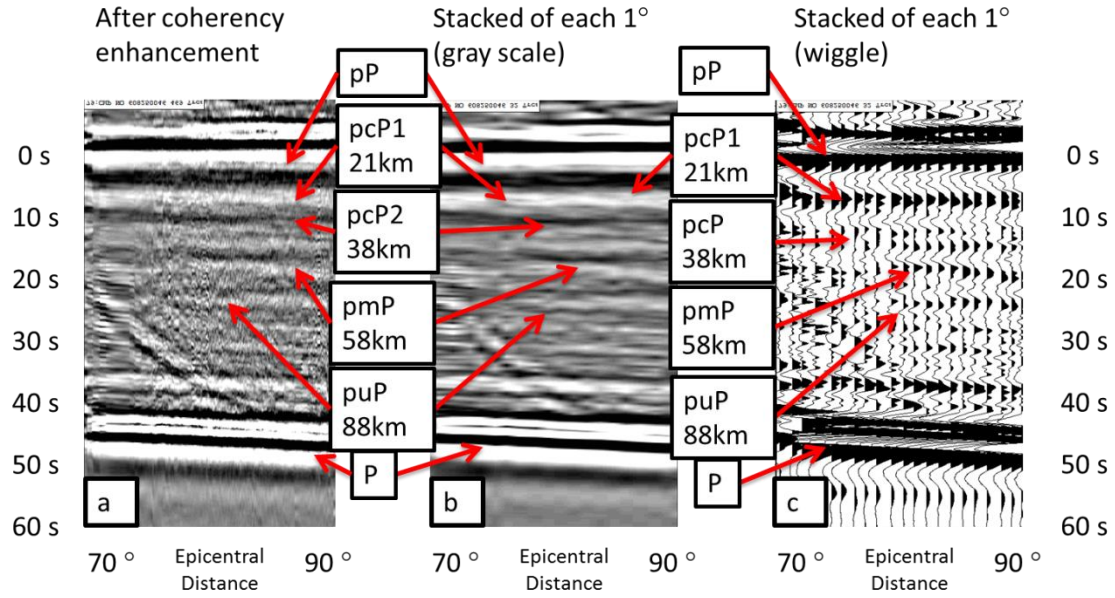

Figure 3-50 Event on 2006/08/25, M=6.6, Depth=184 km (b.3). Data are filtered with window: 0.1-0.2-1-2 Hz. (a) data aligned at pP phase at 0s with a series of coherency enhancement (gray scale display). (b) stacking of traces every 1° of epicentral distance. (c) stacking of traces every 1° of epicentral distance (wiggle display).

3.4 SUMMARY

Analysis of seismograms recorded by USArray in the US for deep earthquakes in South America has been used to detect and map key lithospheric structure within the Andean Mountain Belt. Key findings of this study include:

1. Demonstrating that array analysis allows detection and mapping of lithospheric structure using precursors to pP for events as small as 5.5, as well as discrimination of true underside reflections from arrivals from other ray interactions at both the source and receiver locations.

2. Confirmation of previous estimates of crustal thickness while providing new estimates in previous unsurveyed areas. Among the new estimates are values for

Andean foreland such as northern Peru and northern Bolivia.

3. Mapping of prominent intracrustal reflectors, some of which correspond to previously inferred magma layers e.g. in the central Andes. Others indicate the presence of previously unrecognized deep magma in southern Peru and northern Chile.

4. Detection of intracrustal reflectors that may be related to the top of eclogitization of the lower crust depth (e.g. southern Peru, central Altiplano-Puna plateau).

5. Detection of reflections that may mark major intracrustal detachments along the eastern edge of the Puna plateau and the base of sedimentary basins in central Peru.

6. One sub-Moho reflection that may correspond to the Hales discontinuity I the upper mangle.

7. No unambiguous evidence of underside reflections from the LAB (lithosphere-asthenosphere boundary).

REFERENCES

Allmendinger, R.W., Jordan, T.E., Kay, S.M., Isacks, B.L., 1997. The evolution of the Altiplano-Puna plateau of the Central Andes. Annu. Rev. Earth Planet. Sci. 25, 139–174.

Allmendinger, R.W., Nelson, K.D., Potter, C.J., Barazangi, M., Brown, L.D., Oliver, J. t, 1987. Deep seismic reflection characteristics of the continental crust. Geology 15, 304–310.

Allmendinger, R.W., Zapata, T.R., 2000. The footwall ramp of the Subandean decollement, northernmost Argentina, from extended correlation of seismic reflection data. Tectonophysics 321, 37–55.

ANCORP Working Group, 1999. Seismic reflection image revealing offset of Andean subduction-zone earthquake locations into oceanic mantle. Nature 397, 341–344.

ANCORP Working Group, 2003. Seismic imaging of a convergent continental margin and plateau in the central Andes (Andean Continental Research Project 1996 (ANCORP'96)). J. Geophys. Res. Solid Earth 108, n/a–n/a. doi:10.1029/2002JB001771

Atherton, M.P., Pitcher, W.S., Warden, V., 1983. The Mesozoic marginal basin of central Peru. Nature 305, 303–306. doi:10.1038/305303a0

Babeyko, A.Y., Sobolev, S.V., Vietor, T., Trumbull, R.B., Oncken, O., 2006. Weakening of the upper plate during tectonic shortening: Thermo-mechanical causes and consequences. Front. Earth Sci. 1, 495–512.

Bamford, D., Prodehl, C., 1977. Explosion seismology and the continental crust-mantle boundary. J. Geol. Soc. 134, 139–151. doi:10.1144/gsjgs.134.2.0139

Beck, S.L., Zandt, G., 2002. The nature of orogenic crust in the central Andes. J. Geophys. Res. 107, 2230.

Bianchi, M., Heit, B., Jakovlev, A., Yuan, X., Kay, S.M., Sandvol, E., Alonso, R.N., Coira, B., Brown, L., Kind, R., others, 2013. Teleseismic tomography of the southern Puna plateau in Argentina and adjacent regions. Tectonophysics 586, 65–83.

Bostock, M.G., 1997. Anisotropic upper-mantle stratigraphy and architecture of the Slave craton. Nature 390, 392–395. doi:10.1038/37102

Brocher, T.M., 2005. Empirical Relations between Elastic Wavespeeds and Density in the Earth's Crust. Bull. Seismol. Soc. Am. 95, 2081–2092. doi:10.1785/0120050077

Calixto, F.J., Robinson, D., Sandvol, E., Kay, S., Abt, D., Fischer, K., Heit, B., Yuan, X., Comte, D., Alvarado, P., 2014. Shear wave splitting and shear wave splitting tomography of the southern Puna plateau. Geophys. J. Int. 199, 688–699.

Calixto, F.J., Sandvol, E., Kay, S., Mulcahy, P., Heit, B., Yuan, X., Coira, B., Comte, D., Alvarado, P., 2013. Velocity structure beneath the southern Puna plateau: Evidence for delamination. Geochem. Geophys. Geosystems 14, 4292–4305.

Canales, L.L., 1984. Random noise reduction, in: 1984 SEG Annual Meeting.

Carbonell, R., Pérez-Estaún, A., Gallart, J., Diaz, J., Kashubin, S., Mechie, J., Stadtlander, R., Schulze, A., Knapp, J.H., Morozov, A., 1996. Crustal root beneath the Urals: Wide-angle seismic evidence. Science 274, 222–224.
Chmielowski, J., Zandt, G., Haberland, C., 1999. The Central Andean Altiplano-Puna magma body. Geophys. Res. Lett. 26, 783–786. doi:10.1029/1999GL900078
Christensen, N.I., Mooney, W.D., 1995. Seismic velocity structure and composition of the continental crust: A global view. J. Geophys. Res. Solid Earth 1978–2012 100, 9761–9788.
Clague, D.A., Straley, P.F., 1977. Petrologic nature of the oceanic Moho. Geology 5, 133–136.
Cook, F.A., 1995. The reflection Moho beneath the southern Canadian Cordillera. Can. J. Earth Sci. 32, 1520–1530.
Crotwell, H.P., Owens, T.J., Ritsema, J., 1999. The TauP Toolkit: Flexible seismic travel-time and ray-path utilities. Seismol. Res. Lett. 70, 154.
De Silva, S.L., 1989. Altiplano-Puna volcanic complex of the central Andes. Geology 17, 1102–1106.
Dorbath, C., 1996. Velocity structure of the Andes of central Peru from locally recorded earthquakes. Geophys. Res. Lett. 23, 205–208. doi:10.1029/95GL03778
Dorbath, C., Granet, M., Poupinet, G., Martinez, C., 1993. A teleseismic study of the Altiplano and the eastern Cordillera in northern Bolivia: New constraints on a lithospheric model. J. Geophys. Res. Solid Earth 98, 9825–9844. doi:10.1029/92JB02406
Fischer, K.M., Ford, H.A., Abt, D.L., Rychert, C.A., 2010. The lithosphere-asthenosphere boundary. Annu. Rev. Earth Planet. Sci. 38, 551–575.
Flanagan, M.P., Shearer, P.M., 1998. Topography on the 410-km seismic velocity discontinuity near subduction zones from stacking of sS, sP, and pP precursors. J. Geophys. Res. 103, 182.
Flanagan, M.P., Shearer, P.M., 1999. A map of topography on the 410-km discontinuity from PP precursors. Geophys. Res. Lett. 26, 549–552.
Fromm, R., Zandt, G., Beck, S.L., 2004. Crustal thickness beneath the Andes and Sierras Pampeanas at 30 S inferred from Pn apparent phase velocities. Geophys. Res. Lett. 31, L06625.
Gans, C.R., Beck, S.L., Zandt, G., Gilbert, H., Alvarado, P., Anderson, M., Linkimer, L., 2011. Continental and oceanic crustal structure of the Pampean flat slab region, western Argentina, using receiver function analysis: new high-resolution results. Geophys. J. Int.
Garzione, C.N., Hoke, G.D., Libarkin, J.C., Withers, S., MacFadden, B., Eiler, J., Ghosh, P., Mulch, A., 2008. Rise of the Andes. science 320, 1304–1307.
Garzione, C.N., Molnar, P., Libarkin, J.C., MacFadden, B.J., 2006. Rapid late Miocene rise of the Bolivian Altiplano: Evidence for removal of mantle lithosphere. Earth Planet. Sci. Lett. 241, 543–556.
Gerbault, M., Martinod, J., Hérail, G., 2005. Possible orogeny-parallel lower crustal flow and thickening in the Central Andes. Tectonophysics 399, 59–72.

Ghosh, P., Garzione, C.N., Eiler, J.M., 2006. Rapid uplift of the Altiplano revealed through 13C-18O bonds in paleosol carbonates. Science 311, 511–515.
Gilbert, H., Beck, S., Zandt, G., 2006. Lithospheric and upper mantle structure of central Chile and Argentina. Geophys. J. Int. 165, 383–398.
Graeber, F.M., Asch, G., 1999. Three-dimensional models of P wave velocity and P-to-S velocity ratio in the southern central Andes by simultaneous inversion of local earthquake data. J. Geophys. Res. Solid Earth 1978–2012 104, 20237–20256.
Gulunay, N., 1986. FXDECON and complex Wiener prediction filter, in: 1986 SEG Annual Meeting.
Hales, A.L., 1969. A seismic discontinuity in the lithosphere. Earth Planet. Sci. Lett. 7, 44–46. doi:10.1016/0012-821X(69)90009-0
Heit, B., Bianchi, M., Yuan, X., Kay, S.M., Sandvol, E., Kumar, P., Kind, R., Alonso, R.N., Brown, L.D., Comte, D., 2014. Structure of the crust and the lithosphere beneath the southern Puna plateau from teleseismic receiver functions. Earth Planet. Sci. Lett. 385, 1–11.
Heit, B., Sodoudi, F., Yuan, X., Bianchi, M., Kind, R., 2007. An S receiver function analysis of the lithospheric structure in South America. Geophys. Res. Lett. 34, L14307.
Hess, H.H., 1959. The AMSOC hole to the earth's mantle. Trans. Am. Geophys. Union 40, 340–345.
Hess, H.H., 1962. History of ocean basins.
Hirn, A., Jobert, G., Wittlinger, G., ZHONG-XIN, X., GAO, E.N.Y., 1984. Main features of the upper lithosphere in the unit between the High Himalayas and the Yarlung Zangbo Jiang suture. pp. 113–117.
Hirn, A., Nercessian, A., Sapin, M., Jobert, G., Xin, X.Z., Yuan, G.E., Yuan, L.D., Wen, T.J., 1984. Lhasa block and bordering sutures[mdash] a continuation of a 500-km Moho traverse through Tibet. Nature 307, 25–27. doi:10.1038/307025a0
Hoke, G.D., Garzione, C.N., 2008. Paleosurfaces, paleoelevation, and the mechanisms for the late Miocene topographic development of the Altiplano plateau. Earth Planet. Sci. Lett. 271, 192–201.
Isacks, B.L., 1988. Uplift of the central Andean plateau and bending of the Bolivian orocline. J. Geophys. Res. 93, 3211–3231.
James, D.E., Snoke, J.A., 1994. Structure and tectonics in the region of flat subduction beneath central Peru: Crust and uppermost mantle. J. Geophys. Res. Solid Earth 99, 6899–6912. doi:10.1029/93JB03112
Jarchow, C.M., Thompson, G.A., 1989. The nature of the Mohorovicic discontinuity. Annu. Rev. Earth Planet. Sci. 17, 475.
Kay, R.W., Kay, S.M., 1993. Delamination and delamination magmatism. Tectonophysics 219, 177–189.
Kay, S.M., Abbruzzi, J.M., 1996. Magmatic evidence for Neogene lithospheric evolution of the central Andean "flat-slab" between 30 S and 32 S. Tectonophysics 259, 15–28.

Kay, S.M., Coira, B.L., 2009. Shallowing and steepening subduction zones, continental lithospheric loss, magmatism, and crustalflow under the Central Andean Altiplano-Puna Plateau. Backbone Am. Shallow Subduction Plateau Uplift Ridge Terrane Collis. 204, 229.

Kay, S.M., Mpodozis, C., Gardeweg, M., 2014. Magma sources and tectonic setting of Central Andean andesites (25.5–28 °S) related to crustal thickening, forearc subduction erosion and delamination. Geol. Soc. Lond. Spec. Publ. 385, 303–334. doi:10.1144/SP385.11

Kennedy, G.C., 1959. The origin of continents, mountain ranges, and ocean basins. Am. Sci. 47, 491–504.

Kennett, B.L.N., Engdahl, E.R., Buland, R., 1995. Constraints on seismic velocities in the Earth from traveltimes. Geophys. J. Int. 122, 108–124.

Kind, R., Yuan, X., Kumar, P., 2012. Seismic receiver functions and the lithosphere–asthenosphere boundary. Tectonophysics 536–537, 25–43. doi:10.1016/j.tecto.2012.03.005

Klemperer, S.L., Hauge, T.A., Hauser, E.C., Oliver, J.E., Potter, C.J., 1986. The Moho in the northern Basin and Range province, Nevada, along the COCORP 40 N seismic-reflection transect. Geol. Soc. Am. Bull. 97, 603–618.

Knapp, J.H., Steer, D.N., Brown, L.D., Berzin, R., Suleimanov, A., Stiller, M., Lüschen, E., Brown, D.L., Bulgakov, R., Kashubin, S.N., 1996. Lithosphere-scale seismic image of the southern Urals from explosion-source reflection profiling. Science 274, 226–228.

Liang, X., Sandvol, E., Kay, S., Heit, B., Yuan, X., Mulcahy, P., Chen, C., Brown, L., Comte, D., Alvarado, P., 2014. Delamination of southern Puna lithosphere revealed by body wave attenuation tomography. J. Geophys. Res. Solid Earth 119, 549–566.

Lovering, J. [ohn] F., 1958. The nature of the Mohorovicic discontinuity. Trans. Am. Geophys. Union 39, 947–955.

Mathalone, J.M., 1995. Petroleum geology of the sub-Andean basins of Peru.

McGlashan, N., Brown, L., Kay, S., 2008. Crustal thickness in the Central Andes from teleseismically recorded depth phase precursors. Geophys. J. Int. 175, 1013–1022.

Mégard, F., 1984. The Andean orogenic period and its major structures in central and northern Peru. J. Geol. Soc. 141, 893–900. doi:10.1144/gsjgs.141.5.0893

Mohorovičić, A., 1909. Das Beben vom 8. Oktober 1910. Jahrb Meteorol Obs. Zagreb Für.

Molnar, P., Garzione, C.N., 2007. Bounds on the viscosity coefficient of continental lithosphere from removal of mantle lithosphere beneath the Altiplano and Eastern Cordillera. Tectonics 26.

Moores, E.M., Jackson, E.D., 1974. Ophiolites and oceanic crust.

Mulcahy, P., Chen, C., Kay, S.M., Brown, L.D., Isacks, B.L., Sandvol, E., Heit, B., Yuan, X., Coira, B.L., 2014. Central Andean mantle and crustal seismicity beneath the Southern Puna plateau and the northern margin of the Chilean-Pampean flat slab. Tectonics 33, 1636–1658.

Ocola, L.C., Meyer, R.P., 1972. Crustal Low-Velocity Zones Under the Peru-Bolivia Altiplano. Geophys. J. Int. 30, 199–208. doi:10.1111/j.1365-246X.1972.tb02353.x

O'Connell, R.J., Wasserburg, G.J., 1967. Dynamics of the motion of a phase change boundary to changes in pressure. Rev. Geophys. 5, 329–410.

Oliver, J., 1988. Moho. Geology 16, 291.

Oncken, O., Hindle, D., Kley, J., Elger, K., Victor, P., Schemmann, K., 2006. Deformation of the central Andean upper plate system—Facts, fiction, and constraints for plateau models, in: The Andes. Springer, pp. 3–27.

Owens, T.J., Taylor, S.R., Zandt, G., 1987. Crustal structure at Regional Seismic Test Network stations determined from inversion of broadband teleseismic P waveforms. Bull. Seismol. Soc. Am. 77, 631–662.

Pardo, A., 1982. Caracteristicas Estructurales de la Faja Subandina del Norte del Peru [PAPER IN SPANISH] Structural characteristics of the Sub-Andean Belt of Northern Peru.

Schmerr, N., Garnero, E., 2006. Investigation of upper mantle discontinuity structure beneath the central Pacific using SS precursors. J Geophys Res 111.

Schmitz, M., Lessel, K., Giese, P., Wigger, P., Araneda, M., Bribach, J., Graeber, F., Grunewald, S., Haberland, C., Lüth, S., Röwer, P., Ryberg, T., Schulze, A., 1999. The crustal structure beneath the Central Andean forearc and magmatic arc as derived from seismic studies — the PISCO 94 experiment in northern Chile (21°–23°S). J. South Am. Earth Sci. 12, 237–260. doi:10.1016/S0895-9811(99)00017-6

Steer, D.N., Knapp, J.H., Brown, L.D., 1998. Super-deep reflection profiling: exploring the continental mantle lid. Tectonophysics 286, 111–121.

Suárez, G., Molnar, P., Burchfiel, B.C., 1983. Seismicity, fault plane solutions, depth of faulting, and active tectonics of the Andes of Peru, Ecuador, and southern Colombia. J. Geophys. Res. Solid Earth 1978–2012 88, 10403–10428.

Swenson, J.L., Beck, S.L., Zandt, G., 2000. Crustal structure of the Altiplano from broadband regional waveform modeling: implications for the composition of thick continental crust. J. Geophys. Res. Solid Earth 1978–2012 105, 607–621.

Vermeer, G.J., 1999. Factors affecting spatial resolution. Geophysics 64, 942–953.

Wang, R., 1999. A simple orthonormalization method for stable and efficient computation of Green's functions. Bull. Seismol. Soc. Am. 89, 733–741.

Wölbern, I., Heit, B., Yuan, X., Asch, G., Kind, R., Viramonte, J., Tawackoli, S., Wilke, H., 2009. Receiver function images from the Moho and the slab beneath the Altiplano and Puna plateaus in the Central Andes. Geophys. J. Int. 177, 296–308. doi:10.1111/j.1365-246X.2008.04075.x

Yilmaz, Ö., 2001. Seismic data analysis: processing, inversion, and interpretation of seismic data. SEG Books.

Yuan, H., Romanowicz, B., 2010. Lithospheric layering in the North American craton. Nature 466, 1063–1068. doi:10.1038/nature09332

Yuan, X., Sobolev, S., Kind, R., 2002. Moho topography in the central Andes and its geodynamic implications. Earth Planet. Sci. Lett. 199, 389–402.

Yuan, X., Sobolev, S., Kind, R., Oncken, O., Bock, G., Asch, G., Schurr, B., Graeber, F., Rudloff, A., Hanka, W., others, 2000. Subduction and collision processes in the Central Andes constrained by converted seismic phases. Nature 408, 958–961.

Zandt, G., Beck, S.L., Ruppert, S.R., Ammon, C.J., Rock, D., Minaya, E., Wallace, T.C., Silver, P.G., 1996. Anomalous crust of the Bolivian Altiplano, central Andes: Constraints from broadband regional seismic waveforms. Geophys. Res. Lett. 23, 1159–1162. doi:10.1029/96GL00967

Zandt, G., Leidig, M., Chmielowski, J., Baumont, D., Yuan, X., 2003. Seismic detection and characterization of the Altiplano-Puna magma body, central Andes. Pure Appl. Geophys. 160, 789–807.

Zandt, G., Velasco, A.A., Beck, S.J., 1994. Composition and thickness of the southern Altiplano crust, Bolivia. Geol.-BOULDER- 22, 1003–1003.

Zhang, Z., Lay, T., 1993. Investigation of upper mantle discontinuities near northwestern Pacific subduction zones using precursors to sSH. J. Geophys. Res. 98, 4389–4405.

Zheng, Y., Lay, T., Flanagan, M.P., Williams, Q., 2007. Pervasive seismic wave reflectivity and metasomatism of the Tonga mantle wedge. science 316, 855.

Zoeppritz, K., 1919. Joachim Ritter & Johannes Schweitzer. Part C Biogr. Angenheister Geiger Wiechert's Bibliogr. Biogr. Notes 34.

APPENDIX

APPENDIX I EARTHQUAKE CATALOG

Table 1 Earthquake locations in Chapter 3.

Earthquake (yymmddhhmm)	Magnitude	Earthquake Longitude	Earthquake Latitude	Earthquake Depth, km
0304272257	6.0	-071.592	-08.195	559
0305182110	5.5	-069.094	-31.396	114
0305270829	5.7	-068.596	-31.365	118
0306200619	7.1	-071.722	-07.606	558
0309172134	5.8	-068.325	-21.467	127
0311260742	5.5	-075.723	-01.908	183
0403170321	6.1	-065.586	-21.118	289
0406170116	5.7	-068.372	-21.246	115
0411120636	6.1	-063.319	-26.705	568
0503211223	6.9	-063.470	-24.983	579
0503211243	6.4	-063.507	-24.725	570
0504111454	6.0	-077.886	-07.293	129
0504162241	5.8	-069.663	-17.647	118
0506021056	6.1	-067.003	-24.221	196
0507261411	5.9	-072.962	-15.345	110
0508140239	5.8	-068.980	-19.780	113
0509091126	5.8	-069.136	-31.680	112
0509260155	7.5	-076.398	-05.678	115
0510171923	5.7	-069.486	-17.775	123
0511091133	5.9	-076.943	-01.024	248
0512232147	6.1	-077.517	-01.386	192
0606270207	5.5	-068.695	-22.762	115
0606271124	5.5	-068.516	-21.287	122
0607080913	5.5	-067.389	-28.562	140
0608250044	6.6	-067.028	-24.403	184
0609121330	6.0	-068.898	-28.944	114
0609170934	6.2	-067.145	-31.733	137
0609220232	6.0	-063.149	-26.868	598
0609242108	5.7	-067.687	-32.228	141
0609301626	6.0	-073.160	-15.588	107
0610070820	5.7	-068.980	-24.087	104

0610170402	5.9	-068.276	-21.042	140
0611071325	5.8	-068.204	-21.729	121
0702131456	5.6	-077.778	-01.424	174
0705010352	5.5	-068.412	-21.327	120
0705251747	5.9	-067.027	-24.222	180
0706141041	5.5	-068.915	-23.027	105
0707120523	6.1	-074.379	-07.933	152
0707211327	6.1	-071.272	-08.133	644
0707211534	6.4	-065.777	-22.151	289
0708291618	5.5	-068.360	-20.948	134
0710250835	5.6	-068.754	-20.602	100
0712251620	5.8	-069.048	-19.445	112
0801050729	5.7	-068.484	-22.820	103
0802161445	6.1	-068.385	-21.346	130
0803242039	6.2	-068.963	-20.043	120
0807080913	6.2	-071.748	-15.986	123
0808262100	6.4	-074.377	-07.641	154
0809031125	6.3	-063.225	-26.736	569
0809130932	5.7	-075.517	004.790	132
0810122055	6.2	-064.971	-20.123	352
0812041647	5.5	-068.288	-21.389	115
0903150819	5.7	-070.365	-14.452	189
0904031754	5.7	-066.593	-27.842	174
0907120612	6.1	-070.445	-15.041	198
0907141838	5.7	-067.087	-21.822	175
0908121800	5.5	-066.672	-27.893	173
0909050358	5.8	-070.248	-15.121	210
0909301903	5.9	-069.293	-15.551	255
0911130727	5.8	-064.095	-17.917	608
0911141944	6.2	-066.641	-22.965	220
1001252252	5.9	-074.466	-08.498	146
1001280804	5.9	-066.712	-23.357	208
1003042239	6.3	-068.328	-22.227	114
1004092223	5.8	-068.124	-28.559	117
1005190415	6.0	-077.541	-05.083	132
1005232246	6.1	-074.352	-13.928	101
1005241618	6.5	-071.558	-08.087	581
1007120011	6.3	-068.216	-22.146	115
1009130715	5.9	-070.777	-14.612	179
1010221931	5.8	-068.372	-20.878	132

1101010956	7.0	-063.136	-26.803	576
1103061231	6.3	-069.362	-18.021	118
1104170158	5.7	-063.201	-27.596	556
1106080306	5.9	-069.518	-17.083	145
1106201636	6.4	-068.228	-21.701	128
1108241746	7.0	-074.525	-07.641	147
1109021347	6.7	-063.029	-28.398	578
1111221848	6.6	-065.089	-15.364	549
1205141000	6.2	-069.591	-17.678	105
1205280507	6.7	-063.094	-28.043	586
1206020752	5.9	-063.555	-22.059	527
1206071603	6.1	-072.413	-15.877	110
1208020938	6.1	-074.259	-08.414	144

APPENDIX II pP PRECURSOR BOUNCEPOINT LOCATION

Table 2 Station locations (average) and calculated pP surface bouncepoint locations in Chapter 3.

Earthquake (yymmddhhmm)	Station Longitude (Average)	Station Latitude (Average)	Station Elevation (Average), meter	pP bouncepoint Longitude	pP bouncepoint Latitude
0304272257	-105.768	037.521	00662	-073.816	-04.724
0305182110	-108.687	036.950	00731	-069.353	-31.032
0305270829	-105.484	037.556	00704	-068.851	-30.974
0306200619	-104.543	037.267	00681	-073.958	-04.037
0309172134	-107.538	037.442	00790	-068.638	-21.007
0311260742	-105.489	037.448	00736	-076.312	-00.965
0403170321	-106.542	037.460	00752	-066.396	-19.970
0406170116	-109.828	037.026	00741	-068.662	-20.846
0411120636	-109.595	037.118	00731	-065.209	-24.340
0503211223	-110.473	037.157	00772	-065.449	-22.533
0503211243	-109.662	037.273	00742	-065.434	-22.287
0504111454	-110.172	037.399	00779	-078.251	-06.706
0504162241	-109.902	037.374	00747	-069.968	-17.214
0506021056	-111.406	037.486	00752	-067.520	-23.548
0507261411	-112.597	037.425	00843	-073.251	-14.933
0508140239	-112.424	037.424	00904	-069.270	-19.395
0509091126	-112.052	037.880	00916	-069.392	-31.344
0509260155	-111.853	037.817	00943	-076.737	-05.181
0510171923	-112.334	038.240	01004	-069.804	-17.340
0511091133	-111.909	038.254	00936	-077.828	000.216
0512232147	-112.479	038.348	00923	-078.167	-00.466
0606270207	-113.225	038.632	00948	-068.975	-22.388
0606271124	-113.171	038.607	00946	-068.820	-20.882
0607080913	-112.688	038.584	00940	-067.724	-28.131
0608250044	-114.272	039.817	00909	-067.486	-23.809
0609121330	-113.772	040.166	00881	-069.151	-28.604
0609170934	-114.006	040.195	00883	-067.454	-31.343
0609220232	-113.686	040.439	00871	-065.021	-24.544
0609242108	-113.915	040.433	00874	-068.001	-31.824
0609301626	-114.007	040.535	00899	-073.417	-15.199
0610070820	-113.708	040.654	00895	-069.213	-23.761
0610170402	-114.128	040.569	00881	-068.614	-20.579
0611071325	-114.306	040.722	00893	-068.488	-21.340

0702131456	-113.290	041.021	00911	-078.312	-00.606
0705010352	-112.912	040.554	00943	-068.693	-20.931
0705251747	-113.340	040.583	00963	-067.462	-23.635
0706141041	-114.594	040.794	01008	-069.154	-22.698
0707120523	-113.906	040.645	01013	-074.801	-07.303
0707211327	-114.276	040.778	01029	-073.894	-04.455
0707211534	-114.101	040.703	01032	-066.543	-21.147
0708291618	-114.233	040.639	01057	-068.681	-20.507
0710250835	-113.546	041.100	01028	-068.982	-20.279
0712251620	-113.208	041.266	01066	-069.307	-19.070
0801050729	-113.193	041.253	01090	-068.713	-22.494
0802161445	-113.336	040.986	01090	-068.689	-20.916
0803242039	-112.691	040.646	01101	-069.246	-19.637
0807080913	-112.170	040.064	01154	-072.050	-15.529
0808262100	-111.088	040.060	01214	-074.805	-06.973
0809031125	-111.160	039.997	01227	-064.980	-24.464
0809130932	-111.119	040.202	01225	-075.982	005.405
0810122055	-111.006	040.044	01272	-065.967	-18.774
0812041647	-109.919	040.393	01258	-068.551	-20.996
0903150819	-109.953	040.173	01223	-070.859	-13.691
0904031754	-109.261	040.179	01193	-066.993	-27.270
0907120612	-107.838	039.992	01203	-070.952	-14.218
0907141838	-107.887	040.009	01199	-067.506	-21.187
0908121800	-107.105	039.900	01185	-067.063	-27.306
0909050358	-106.885	039.878	01162	-070.786	-14.232
0909301903	-105.596	039.542	01109	-069.966	-14.437
0911130727	-104.942	039.353	00946	-066.182	-14.780
0911141944	-105.163	039.314	00963	-067.175	-22.123
1001252252	-104.820	039.341	00886	-074.838	-07.814
1001280804	-104.460	039.380	00867	-067.205	-22.563
1003042239	-104.641	039.339	00854	-068.578	-21.810
1004092223	-104.434	039.452	00824	-068.365	-28.161
1005190415	-103.767	039.232	00753	-077.871	-04.418
1005232246	-103.895	039.309	00763	-074.570	-13.496
1005241618	-103.537	039.282	00755	-073.720	-04.297
1007120011	-103.570	039.036	00751	-068.468	-21.718
1009130715	-103.288	038.938	00690	-071.217	-13.821
1010221931	-102.262	039.083	00656	-068.663	-20.362
1101010956	-100.963	039.499	00591	-064.791	-24.102
1103061231	-101.280	039.384	00587	-069.617	-17.541

1104170158	-100.136	039.033	00535	-064.769	-25.013
1106080306	-100.412	038.779	00525	-069.844	-16.462
1106201636	-100.309	038.754	00527	-068.500	-21.195
1108241746	-099.233	038.405	00501	-074.874	-06.890
1109021347	-098.869	038.465	00496	-064.672	-25.644
1111221848	-098.230	039.540	00485	-066.802	-12.240
1205141000	-096.967	038.799	00485	-069.799	-17.231
1205280507	-097.851	038.895	00488	-064.724	-25.191
1206020752	-096.824	038.770	00472	-065.044	-19.341
1206071603	-097.023	038.761	00482	-072.623	-15.381
1208020938	-096.411	038.450	00475	-074.569	-07.664

APPENDIX III pP PRECURSOR ARRIVAL TIME

Table 3 pP precursor arrival time relative to pP in Chapter 3.

Earthquake (yymmddhhmm)	pP-pmP (s)	pP-p1P (s)	pP-p2P (s)	pP-p3P(s)
0304272257	11.30	05.95	00.00	25.15
0305182110	19.15	00.00	00.00	00.00
0305270829	20.40	12.80	08.30	00.00
0306200619	10.95	00.00	00.00	00.00
0309172134	14.60	06.70	09.35	00.00
0311260742	12.00	00.00	00.00	00.00
0403170321	21.40	11.80	15.35	00.00
0406170116	13.90	02.65	09.10	00.00
0411120636	13.50	00.00	00.00	00.00
0503211223	19.70	10.00	14.40	27.70
0503211243	20.50	10.45	14.65	00.00
0504111454	17.55	04.45	00.00	00.00
0504162241	00.00	00.00	00.00	00.00
0506021056	00.00	07.10	10.00	00.00
0507261411	00.00	12.95	00.00	00.00
0508140239	00.00	00.00	00.00	00.00
0509091126	20.10	06.50	12.20	00.00
0509260155	14.35	02.95	06.40	00.00
0510171923	00.00	00.00	00.00	00.00
0511091133	15.30	05.25	10.15	21.10
0512232147	00.00	00.00	10.15	00.00
0606270207	17.80	00.00	00.00	00.00
0606271124	14.50	01.85	00.00	00.00
0607080913	19.25	02.35	10.90	19.25
0608250044	17.75	06.35	11.65	23.40
0609121330	16.85	03.65	12.35	00.00
0609170934	18.10	07.90	00.00	00.00
0609220232	00.00	05.40	00.00	00.00
0609242108	00.00	04.80	07.45	00.00
0609301626	00.00	14.70	07.54	00.00
0610070820	00.00	04.15	08.20	00.00
0610170402	00.00	02.70	00.00	00.00
0611071325	00.00	06.35	00.00	00.00
0702131456	00.00	11.05	00.00	00.00
0705010352	00.00	02.65	09.85	00.00

0705251747	17.35	02.70	08.25	00.00
0706141041	13.60	00.00	09.25	00.00
0707120523	08.45	02.75	00.00	00.00
0707211327	12.10	00.00	00.00	00.00
0707211534	19.85	05.15	00.00	00.00
0708291618	00.00	06.60	00.00	00.00
0710250835	00.00	02.70	00.00	00.00
0712251620	00.00	04.55	00.00	00.00
0801050729	00.00	05.45	00.00	00.00
0802161445	00.00	11.50	00.00	00.00
0803242039	00.00	04.95	00.00	00.00
0807080913	00.00	10.35	00.00	00.00
0808262100	11.25	00.00	00.00	00.00
0809031125	12.80	00.00	00.00	16.60
0809130932	10.60	00.00	00.00	00.00
0810122055	00.00	06.50	13.75	00.00
0812041647	15.80	00.00	00.00	00.00
0903150819	00.00	06.50	00.00	00.00
0904031754	15.25	00.00	00.00	00.00
0907120612	00.00	06.85	00.00	00.00
0907141838	19.50	06.75	00.00	00.00
0908121800	00.00	12.35	00.00	00.00
0909050358	20.50	06.90	00.00	00.00
0909301903	12.80	00.00	00.00	00.00
0911130727	12.90	00.00	00.00	00.00
0911141944	00.00	11.10	00.00	00.00
1001252252	00.00	02.85	00.00	00.00
1001280804	18.75	06.00	12.10	00.00
1003042239	16.10	06.95	00.00	00.00
1004092223	17.65	12.85	00.00	00.00
1005190415	00.00	03.90	00.00	00.00
1005232246	00.00	03.00	12.10	00.00
1005241618	11.75	00.00	00.00	00.00
1007120011	00.00	10.45	12.65	00.00
1009130715	00.00	09.25	00.00	00.00
1010221931	00.00	06.15	00.00	00.00
1101010956	14.40	06.40	00.00	00.00
1103061231	00.00	00.00	00.00	00.00
1104170158	12.80	08.40	03.85	00.00
1106080306	00.00	00.00	00.00	00.00

1106201636	00.00	10.60	00.00	00.00
1108241746	08.75	00.00	00.00	00.00
1109021347	11.75	06.20	00.00	00.00
1111221848	11.45	00.00	00.00	00.00
1205141000	00.00	00.00	00.00	00.00
1205280507	11.80	00.00	00.00	00.00
1206020752	16.15	00.00	00.00	43.15
1206071603	00.00	10.95	00.00	00.00
1208020938	10.80	02.50	00.00	00.00

APPENDIX IV pP PRECURSOR QUALITY

Table 4 pP precursor quality (1: worst, 5: best, 0: no precursor) in Chapter 3.

Earthquake (yymmddhhmm)	pmP quality	p1P quality	p2P quality	p3P quality
0304272257	2	2	0	2
0305182110	3	0	0	0
0305270829	4	4	5	0
0306200619	2	0	0	0
0309172134	3	3	4	0
0311260742	4	0	0	0
0403170321	3	3	4	0
0406170116	4	3	4	0
0411120636	4	0	0	0
0503211223	5	4	4	3
0503211243	5	4	4	0
0504111454	4	4	0	0
0504162241	0	0	0	0
0506021056	0	4	3	0
0507261411	0	3	0	0
0508140239	0	0	0	0
0509091126	5	4	4	0
0509260155	2	4	4	0
0510171923	0	0	0	0
0511091133	2	2	2	2
0512232147	0	0	3	0
0606270207	4	0	0	0
0606271124	3	4	0	0
0607080913	1	4	1	1
0608250044	4	4	4	3
0609121330	3	3	4	0
0609170934	3	4	0	0
0609220232	0	3	0	0
0609242108	0	3	2	0
0609301626	0	3	3	0
0610070820	0	2	3	0
0610170402	0	3	0	0
0611071325	0	2	0	0

0702131456	0	3	0	0
0705010352	0	3	1	0
0705251747	3	4	4	0
0706141041	3	0	1	0
0707120523	5	4	0	0
0707211327	5	0	0	0
0707211534	4	4	0	0
0708291618	0	3	0	0
0710250835	0	1	0	0
0712251620	0	3	0	0
0801050729	0	2	0	0
0802161445	0	3	0	0
0803242039	0	3	0	0
0807080913	0	4	0	0
0808262100	5	0	0	0
0809031125	3	0	0	2
0809130932	3	0	0	0
0810122055	0	3	2	0
0812041647	4	0	0	0
0903150819	0	4	0	0
0904031754	3	0	0	0
0907120612	0	3	0	0
0907141838	4	4	0	0
0908121800	0	4	0	0
0909050358	4	4	0	0
0909301903	1	0	0	0
0911130727	1	0	0	0
0911141944	0	4	0	0
1001252252	0	4	0	0
1001280804	4	4	4	0
1003042239	3	4	0	0
1004092223	5	5	0	0
1005190415	0	3	0	0
1005232246	0	5	5	0
1005241618	4	0	0	0
1007120011	0	1	2	0
1009130715	0	4	0	0
1010221931	0	2	0	0
1101010956	3	5	0	0
1103061231	0	0	0	0

1104170158	4	4	4	0
1106080306	0	0	0	0
1106201636	0	3	0	0
1108241746	4	0	0	0
1109021347	3	4	0	0
1111221848	4	0	0	0
1205141000	0	0	0	0
1205280507	2	0	0	0
1206020752	3	0	0	1
1206071603	0	4	0	0
1208020938	2	4	0	0

APPENDIX V INTERFACE DEPTHS INDICATED BY pP PRECURSOR

Table 5 Interface depth indicated by pP precursors, Vp = 6.2 km/s is used in calculation for pmP, p1P, p2P (Moho, layer 1, layer 2); and Vp = 7 is used in calculation for p3P(layer 3) in Chapter 3.

Earthquake (yymmddhhmm)	pmP Moho depth (km)	layer1 depth (km)	layer2 depth (km)	layer3 depth (km)
0304272257	38.56	20.30	00.00	099.84
0305182110	62.51	00.00	00.00	000.00
0305270829	66.66	41.83	27.12	000.00
0306200619	37.48	00.00	00.00	000.00
0309172134	48.27	22.15	30.91	000.00
0311260742	41.36	00.00	00.00	000.00
0403170321	70.78	39.03	50.77	000.00
0406170116	45.91	08.75	30.05	000.00
0411120636	44.26	00.00	00.00	000.00
0503211223	64.70	32.84	47.29	104.49
0503211243	67.38	34.35	48.16	000.00
0504111454	59.70	15.14	00.00	000.00
0504162241	00.00	00.00	00.00	000.00
0506021056	00.00	23.30	32.82	000.00
0507261411	00.00	43.17	00.00	000.00
0508140239	00.00	00.00	00.00	000.00
0509091126	65.37	21.14	39.68	000.00
0509260155	48.74	10.02	21.74	000.00
0510171923	00.00	00.00	00.00	000.00
0511091133	52.47	18.00	34.81	084.33
0512232147	00.00	00.00	34.75	000.00
0606270207	58.41	00.00	00.00	000.00
0606271124	47.67	06.08	00.00	000.00
0607080913	62.70	07.65	35.50	071.82
0608250044	57.96	20.73	38.04	087.59
0609121330	54.77	11.86	40.14	000.00
0609170934	58.57	25.56	00.00	000.00
0609220232	00.00	17.58	00.00	000.00
0609242108	00.00	15.53	24.10	000.00
0609301626	00.00	48.74	25.01	000.00
0610070820	00.00	13.56	26.80	000.00
0610170402	00.00	08.85	00.00	000.00
0611071325	00.00	20.79	00.00	000.00
0702131456	00.00	37.65	00.00	000.00

0705010352	00.00	08.69	32.31	000.00
0705251747	56.65	08.82	26.94	000.00
0706141041	44.46	00.00	30.24	000.00
0707120523	28.38	09.23	00.00	000.00
0707211327	40.75	00.00	00.00	000.00
0707211534	64.92	16.84	00.00	000.00
0708291618	00.00	21.64	00.00	000.00
0710250835	00.00	08.86	00.00	000.00
0712251620	00.00	14.95	00.00	000.00
0801050729	00.00	17.83	00.00	000.00
0802161445	00.00	37.70	00.00	000.00
0803242039	00.00	16.27	00.00	000.00
0807080913	00.00	34.33	00.00	000.00
0808262100	37.93	00.00	00.00	000.00
0809031125	41.77	00.00	00.00	062.09
0809130932	36.53	00.00	00.00	000.00
0810122055	00.00	21.38	45.23	000.00
0812041647	51.95	00.00	00.00	000.00
0903150819	00.00	21.63	00.00	000.00
0904031754	49.73	00.00	00.00	000.00
0907120612	00.00	22.83	00.00	000.00
0907141838	64.18	22.22	00.00	000.00
0908121800	00.00	40.34	00.00	000.00
0909050358	68.38	23.02	00.00	000.00
0909301903	42.72	00.00	00.00	000.00
0911130727	42.93	00.00	00.00	000.00
0911141944	00.00	36.58	00.00	000.00
1001252252	00.00	07.54	00.00	000.00
1001280804	61.79	19.77	39.87	000.00
1003042239	53.16	22.95	00.00	000.00
1004092223	57.77	42.06	00.00	000.00
1005190415	00.00	13.36	00.00	000.00
1005232246	00.00	10.08	40.67	000.00
1005241618	40.11	00.00	00.00	000.00
1007120011	00.00	34.54	41.82	000.00
1009130715	00.00	31.02	00.00	000.00
1010221931	00.00	20.39	00.00	000.00
1101010956	47.38	21.06	00.00	000.00
1103061231	00.00	00.00	00.00	000.00
1104170158	42.11	27.64	12.67	000.00

1106080306	00.00	00.00	00.00	000.00
1106201636	00.00	35.16	00.00	000.00
1108241746	29.92	00.00	00.00	000.00
1109021347	38.68	20.41	00.00	000.00
1111221848	38.48	00.00	00.00	000.00
1205141000	00.00	00.00	00.00	000.00
1205280507	38.88	00.00	00.00	000.00
1206020752	53.72	00.00	00.00	165.54
1206071603	00.00	36.85	00.00	000.00
1208020938	36.95	06.65	00.00	000.00